NANO · MICRO small
www.small-journal.com

Identification of Catalytic Active Sites for Durable Proton Exchange Membrane Fuel Cell: Catalytic Degradation and Poisoning Perspectives

Syed Shoaib Ahmad Shah, Tayyaba Najam, Muhammad Sohail Bashir, Muhammad Sufyan Javed, Aziz-ur Rahman, Rafael Luque,* and Shu-Juan Bao**

Recent progress in synthetic strategies, analysis techniques, and computational modeling assist researchers to develop more active catalysts including metallic clusters to single-atom active sites (SACs). Metal coordinated N-doped carbons (M-N-C) are the most auspicious, with a large number of atomic sites, markedly performing for a series of electrochemical reactions. This perspective sums up the latest innovative and computational comprehension, while giving credit to earlier/pioneering work in carbonaceous assembly materials towards robust electrocatalytic activity for proton exchange membrane fuel cells via inclusive performance assessment of the oxygen reduction reaction (ORR). M-N_x-C_y are exclusively defined active sites for ORR, so there is a unique possibility to intellectually design the relatively new catalysts with much improved activity, selectivity, and durability. Moreover, some SACs structures provide better performance in fuel cells testing with long-term durability. The efforts to understand the connection in SACs based M-N_x-C_y moieties and how these relate to catalytic ORR performance are also conveyed. Owing to comprehensive practical application in the field, this study has covered very encouraging aspects to the current durability status of M-N-C based catalysts for fuel cells followed by degradation mechanisms such as macro-, microdegradation, catalytic poisoning, and future challenges.

1. Introduction

Confronted with the energy dilemma, the fast depletion of fossil fuels, environmental deteriorations speed up the human race to seek futuristic technologies for renewable energy from nonhazardous sources.[1] These technologies belong to clean energy generation with more sustainability, such as, polymer electrolyte membrane fuel cells and metal–air batteries (MABs) have gained importance due to high power densities and zero-carbon emission.[2–6] Among them, the proton exchange membrane fuel cells (PEMFCs) are weighed as an emerging technology for a sustainable future.

Greater energy densities, improved efficiencies, fast oxidation kinetics, and less impact of hydrogen fuel on the environment make PEMFC one of the emerging technologies related to energy conversion systems.[7–9] Nevertheless, the inclusion of the PEMFC into automotive and fixed energy applications needs to reduce the total cost of fuel cell and long-term

S. S. A. Shah, S.-J. Bao
Key Laboratory of Luminescence Analysis and Molecular Sensing
Ministry of Education, School of Materials and Energy
Southwest University
Chongqing 400715, P. R. China
E-mail: baoshj@swu.edu.cn

T. Najam
College of Chemistry and Environmental Engineering
Shenzhen University
Shenzhen 518060, P. R. China
E-mail: tayyabanajam@outlook.com

The ORCID identification number(s) for the author(s) of this article can be found under https://doi.org/10.1002/smll.202106279.

DOI: 10.1002/smll.202106279

M. S. Bashir
Hefei National Laboratory for Physical Sciences at the Microscale
CAS Key Laboratory of Soft Matter Chemistry
Department of Polymer Science and Engineering
University of Science and Technology of China
Hefei, Anhui 230026, P. R. China

M. S. Javed
School of Physical Science and Technology
Lanzhou University
Lanzhou 730000, P. R. China

A.-u. Rahman
Institute of Chemistry
The Islamia University of Bahawalpur
Bahawalpur 63100, Pakistan

R. Luque
Departamento de Química Orgánica Universidad de Córdoba
Edificio Marie Curie (C-3)
Campus de Rabanales
Ctra. Nnal. IV-A
Km 396, Cordoba E14014, Spain
E-mail: q62alsor@uco.es

durability, primarily attributed to platinum (Pt)-based catalysts required for relevant electrochemical reactions, i.e., the cathodic and anodic reactions. Conversely, the overall cost and energy performance of a fuel cell is determined by the slow kinetics of electrochemical reduction of oxygen, which is six orders less speedy than that of hydrogen oxidation reaction (HOR).[10,11] Thus, ORR is one of the main barriers to the extensive use of PEMFC due to the decelerated ORR along with the utilization of costly Pt-based catalysts. It is therefore critically important to create active but cost-effective catalytic materials to replace platinum catalysts. To decrease Pt consumption, electrocatalysts with economic loading of Pt have been developed.[12–14] For example, the Pt_3Ni nanoframes/C and FePt/C with Pt-skin[13,15] and jagged Pt nanowires[16] are synthesized, which demonstrated a better activity with minimum Pt stuffing as compared to the traditional Pt/C.[8,17,18] However, this lowest Pt stuffs are leaning to accumulate or collapse during ORR progression due to their high energy, leading to deactivation of catalysts.[19,20] Combined with low stability, the slightly complex synthesis process and the insertion of toxic reagents have collectively withdrawn the considerable interest to use these low or extremely low Pt catalysts for oxygen reduction reaction (ORR) in PEMFCs. To overcome these bottleneck issues, recent research has aimed to rationally design the non-noble/ Pt-free electrocatalysts to substitute commercial Pt/C. Regarding this, carbon-based heterogeneous materials are often studied due to their lower cost, simple features, and ease of processing capabilities.

In recent decades, outstanding advancement has been carried out in PGM-free catalysts through material innovation, nano-engineering, and the effect of advanced tools for acquiring scientific understanding.[21–33] Among the various catalysts studied, the metal-N-doped carbons (M-N-C) are categorically active catalysts for ORR for PEM fuel cells (PEMFCs).[34,35] New unanimity in this arena is that ORR active sites must be made up of fully exposed N-coordinated transition metal centers with an improved density of dispersed active sites.[36–39] The constitution of undesired agglomerated metal clusters thus remains the main barrier to further improve the ORR performance. Suitable precursor materials indicate a high surface area, porosity, molecular level integration of M-N-C along with harmonized morphology.[7,40,41] Today, the power density of PGM-free catalysts assembled in the membrane electrode assembly (MEA) is approaching nearly half of commercial PGM-based ones.[42,43] However, countless challenges still remain with PGM-free catalysts to become viable for acidic fuel cells, though the catalytic instability seems to be the major problem. The catalytic poisoning is another drawback of catalysts that is usually ignored. To recognize the capability of carbon-based electrocatalysts in fuel cell applications, it is important to figure out the long-term chemical and structural stability of the catalytic materials under the harsh electrochemical environment present in fuel cell cathodes. Despite increasing interest in M-N-C electrocatalysts, few studies reported the long-term sustainability while most of the reports focus only on the initial performance.[44] The initial progress is almost and/or relatively better than that of commercially available Pt/C. By using the M-N-C cathodes in PEMFCs, it was observed that micropores (<2 nm in diameter) have a major role in the activity and as well as in degradation at an initial stage. The surface area having a large number of micropores often led to both high primary performance and a quick rate of degradation.[45] Because the active sites, for example, $M\text{-}N_4$, are most likely appealing with micro- and mesopores in the carbon.[43,46,47] The performance of a fuel cell with PGM-free cathodes representatively degrades from 40 to 80% in the first 100 h of testing. The PGM-free catalysts with higher initial activity usually degrade faster.[43] Therefore, studying the degradation mechanisms of PGM-free catalysts/ cathodes has become critically essential.

The instability and activity problems can be resolved by identification/ quantification of active sites and tuning the intrinsic/ extrinsic performance of the catalysts. Double or triple doping of heteroatoms in carbon with metal-N_x regulates the electrical properties,[48] and improves the inherent features of the active sites.[49] In the meantime, the physical characteristics, for example, conductivity, density/ distribution of active sites, specific surface area, porosity, and morphology, have a high impact on their ORR performance. Several new strategies, such as the construction of electron pathways, single-atom catalysts, and hierarchical structures with different stencils or fine precursors, remain advantageous to exploit the activity of catalysts.

On the basis of above mention data, we present a brief summary of the latest advances of efficient M-N-C catalysts for ORR in PEMFC while giving credit to the previous pioneering works. First, the identification and quantification of active sites are discussed at the atomic level via spectroscopic, experimental (probing), and theoretical evidences. Then, the emphasis is given on the mechanism of ORR on M-N-C catalysts, followed by recent efforts in manipulating the electronic structures of M-N-C catalysts. Ensuing, novel, exciting concepts of design and preparation methods to adapt the structure, density/dispersion and conductivity of M-N-C catalysts are summarized. Important progress of M-N-C electrocatalysts for PEMFCs is also summarized based on their high power densities and more extended stability for real applications. Furthermore, a thorough discussion based on understanding the current instability mechanisms of PGM-free ORR catalysts in an acidic environment is presented. Finally, a brief clarification of the ultimatum and future prospects of carbon-based heterogeneous catalysts are explored.

2. Structure of M-N-C Active Sites and ORR Mechanism

A low-cost, excellent electronic conductivity, structural flexibility on the atomic scale, high specific surface area, and stability throughout the entire pH range with several unique advantages of carbon-based nonprecious nanomaterials have emerged as a replacement of precious-metal-based electrocatalysts. Heteroatom (e.g., N, S, B, P, etc.) doped carbon with transition metal (M = Fe, Co, Ni, Mn, etc.), such as single atom M-N-C catalysts, M-based particles with carbon materials (e.g., core@shell M@C) are extensively investigated for ORR electrocatalysis. However, M-N-C materials synthesized by the

R. Luque
Peoples Friendship University of Russia (RUDN University)
6 Miklukho Maklaya str, Moscow 117198, Russian Federation

high-temperature treatment of different precursors (metal source + N source + C source) and/or one precursor, e.g., metal organic frameworks (MOFs), are regarded as auspicious candidates for ORR. During the pyrolysis process, the C and N atoms reorganized to transform into N-doped conductive matrix with the simultaneous existence of atomically dispersed M-N-C active sites; however, alteration in pyrolysis conditions (temperature, time, and atmosphere) can provide metallic nanoparticles and/or metal oxides/carbides decorated on N-C (N-doped carbon) surface.[50–52] It is anticipated that the attached metal species altered the electronic properties of N-C, leading to the improvement in ORR activity. Therefore, it is now a firmed belief that M-N_xC_y sites in catalysts are mainly responsible for the enhanced ORR catalysis. Further, M-N_xC_y moieties are now spotted by atomic resolution (scanning transmission electron microscopy (STEM) and electron energy loss spectroscopy (EELS)), which is in line with previous evidence identified by a secondary ion mass spectrometry, X-ray absorption spectroscopy (XAS), and Mossbauer spectroscopy. In addition, M-N-C catalysts have recently been reported, which only contain active M-N_xC_y sites, giving an attractive way-out to solve this puzzle through combined XAS and[57] Fe Mossbauer spectroscopy.[53–55] Advanced in situ methods, and theoretical calculations have been used to propose new directions of active sites, which shows that the level of development of these catalysts is slowly shifting from traditional hit and trial methods to accurate design for production of catalysts at the molecular or atomic level.

2.1. Identification and Location of Atomically Dispersed M-N_x-C_y Active Site

The sluggish ORR is dependent on the specific active sites in the catalyst; however, the configuration of the active site in case of pyrolyzed M-N-C catalysts remains unclear.[56] From theoretical and experimental results, several types of active sites are proposed (**Figure 1**). The majority of the results suggest that metal-coordinated pyridinic N are the main active sites. However, some alternate coordination structures for active sites have also been suggested, including; M-N_4/C species, M-N_2/C-edge, macrocyclic M-N_4/C species, and graphitic nitrogen N-C species. Nonetheless, the current data could not provide sufficient evidence for the overall picture.[57] Additionally, Jia et al.[58] designed 3 types of active sites containing Fe-N_4/C moieties (**Figure 2**) and proposed that during ORR in acidic media there were different switching behaviors of Fe-N_4 and were associated with a dynamic structure of Fe^{III}/Fe^{II} redox transition.[59] The higher ORR performance of pyrolyzed Fe-N_4/C may be related to electron-deficient environment around the Fe–N coordination structure, resulting in a positive displacement of the Fe^{III}/Fe^{II} redox potential.

Recently, spectroscopic technologies based on synchrotron radiation light spectroscopy technologies, such as synchrotron radiation (SR) methods, SR-X-ray photoelectron spectroscopy (XPS), and XAS usually incorporated to look into the atomic structures of catalysts. More specifically, a lot of interests have been committed to the use of XAS in characterizing the atomic/electronic structure of catalysts for understanding the structure–activity relationship via joining with first-principle simulations.

2.1.1. Structure of Active Sites

Several structures of active sites in the M-N-C based catalysts have been proposed; however, M-N_xC_y moieties have two commonly accepted structures such as, metal ion interconnected by 4 pyridinic-N (containing two C atoms defect inside a single graphene sheet M-N_4C_{10})[60–64] or combining two phenanthroline groups (M-$N_{2+2}C_{4+4}$) placed on two armchair borders of two different graphene planes.[46,65] These active sites (M-N_4C_{10} and M-$N_{2+2}C_{4+4}$) are further confirmed by density functional theory (DFT) studies for stability and chemisorption of oxygen.[65–70]

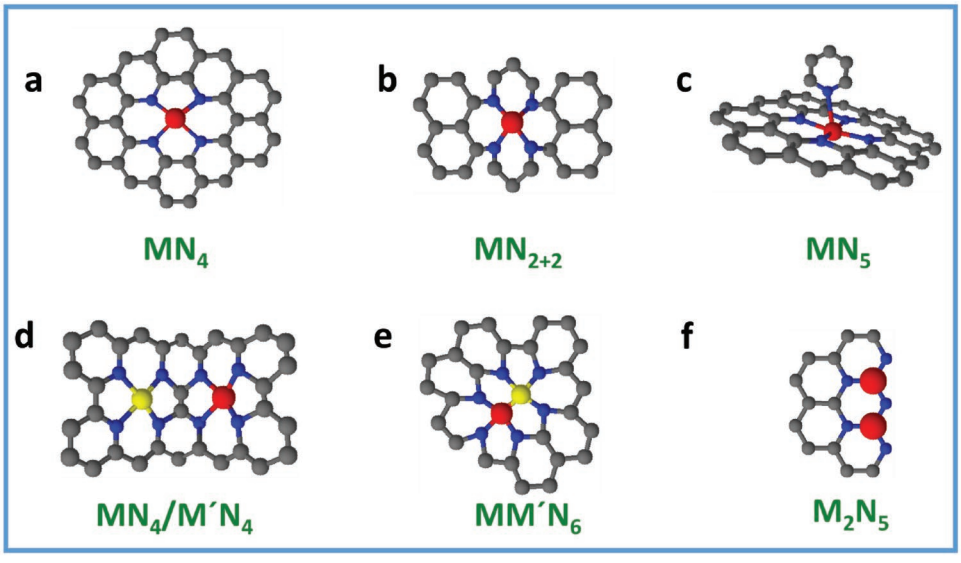

Figure 1. Schematic presentation of various reported metal-based active sites for ORR.

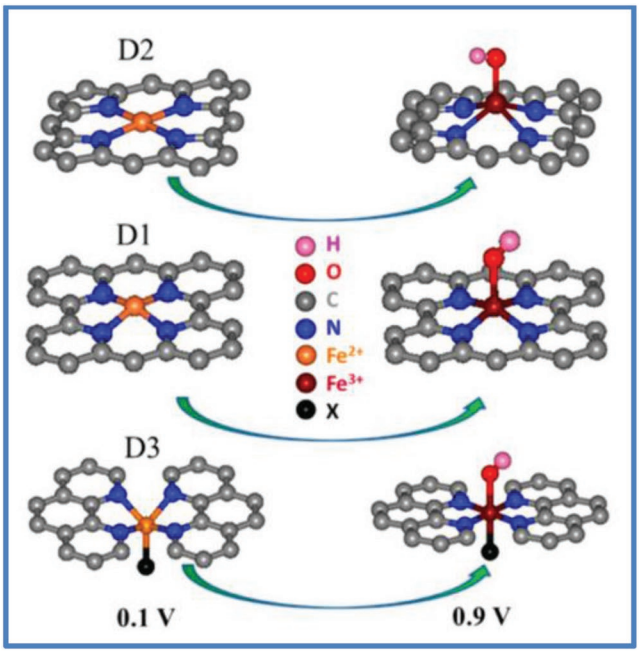

Figure 2. Three different $Fe^{II}N_4$ and $Fe^{III}N_4$ structures of Fe-N-C-based catalysts. Reproduced with permission.[58] Copyright 2015, Elsevier.

Until now, numerous M-N-C-based (M = Fe, Co, Mn, Ni, Zn, etc.) electrocatalysts have been prepared with these types of active sites. For example, Huang and co-workers experimentally reproduced the simulated XANES spectra of M-N_4C_{10} moieties in a 2D graphene lattice and further verified these M-N_4C_{10} sites by STEM images.[71] In contrast, some studies on M-N-C (M = Fe, Co) materials concluded that experimental XANES spectra of M-N_xC_y moieties could be further prepared with porphyrinic M-N_4C_{12} or M-$N_{2+2}C_{12}$ clusters.[72] Such porphyrinic moieties can be placed at in-plane defects or the zig-zag borders, consisting of highly perplexed fraction of 5 membered and higher rings.[62] This phenomenon is normally observed in disorder carbon matrix and recently also confirmed by STEM images in Fe-N-C and Co-N-C catalysts.[73] It is also further observed that amorphous carbons have a higher ability to host the sufficient number of Fe-N_xC_y active sites.

Recently, the ORR activities of Fe-N_4,[74,75] Co-N_4,[76,77] and Mn-N_4 sites[78,79] to approach the PGM level have been significantly improved.[80] Yet, volcano relation explains the dependency of ORR activities on the linking capabilities of reaction intermediates with numerous M-N_x sites suggested by Zagal's group,[59] Mn-N_4 and Fe-N_4 with the strong joining site give water, Co-N_4 with weak joining site gives hydrogen peroxide, following 2-electron ORR-pathway. Precisely, Fe-N-C displays good enactment for ORR as compared to other transition metals. Hence, Fe-N-C has been widely studied in advanced in-situ experiments along with several theoretical calculations to investigate the actual active sites and their structure in Fe-N-C catalysts. Dodelet and co-workers studied an efficient Fe-based electrocatalyst, encapsulated iron cations inter-connected with pyridinic-N (Fe-N_4).[46] Further, studied by Wang's group via DFT calculations and reported *OOH linked with Fe-N_4 sites same as that of Pt.[69] In combination with theoretical studies, the N-FeN_4C_{10} moiety is proved as a major active site for ORR. Moreover, the potential-relevant dynamic cycles of both geometric structure and electronic configuration of single-Fe-atom sites are evidenced via capturing the peroxide ($^*O^{2-}$) and hydroxyl ($^*OH^-$) intermediates under in situ ORR conditions.[81] As of Fe-N_4, the Mn-N_4 sites give firmer bonding to oxygen and sluggish O–O affinity during the oxygen dissociation step,[82] which may take to a complete tract of four electrons and improved efficiency for ORR catalysis.[70,83] Although, there present significant performance, such as Mn-N_4 based catalysts and the Fe-N_4 sites[84] or the traditional Pt/C catalysts. Orellana[85] reported that Mn-N_4 grafted into graphitic defects gives declined activation barriers in the dissociation step of oxygen. Apart from that, the poor ORR catalysis may be further ascribed to two major factors: first is the less conduction ability of electron[85] to molecules based on Mn-N_4 and the other is the hassle in defecting and omitting of strongly adhered *OH intermediate[59,86,87] from the resulting metal sites.[88] However, the current experimental and theoretical studies toward ORR performance of the Mn-N_4 site remain challenging due to the absence of systematic investigation of different effects of coordination of N, C structure toward ORR performance and the working mechanism behind the various Mn-N_x sites. We can conclude that STEM is a good tool for visualizing atomically (single) dispersed atoms and XANES analysis can identify the M-N_xC_y cluster in the nitrogen-doped carbon matrix. However, it is not an easy task to explain the structure–activity relationship in M-N-C catalyst based on sole M-N_xC_y moieties.

2.1.2. Site Location

The exact location of M-N_xC_y active sites in the M-N-C catalysts is debatable, whether these are settled in-plane or edge defects; in this aspect, different views have been reported. Usually, the knowledge of active sites' position would give beneficial perceptions for the rational synthesis of the many active catalysts. First, it was described by DFT studies that the iron-atoms favorably joined with pyridinic nitrogen located at the borders.[89] This expectation was experimentally confirmed by Dai's[90] and Zelenay's group[47]; they found that in Fe-N-C catalyst, iron-atoms are bounded at the borders of graphene sheets with a highly graphitized matrix. In contrast, Workman et al.[91] reported the in-plane location of M-N_xC_y moieties and further described the negative relation between the kinetic activity of Fe-N-C catalyst and the number of graphitic sheets. If the mainstream of M-N_xC_y moieties exists at the border, the number of available electrochemical sites per unit weight of the catalyst may be augmented by decreasing the adjacent size of the graphene sheets, although the vertically aligned graphene sheets will not show any participation in this case. In contrast, if more active sites are situated in-plane of graphene sheets, then the electrochemically reachable active sites could be maximized by improving the defects and reducing the mean number of stacked graphene sheets (**Figure 3**a).[91]

Several M-N-C electrocatalysts were synthesized with different techniques, including pyrolysis of metal porphyrine support on carbon, by using MOFs as sacrificial precursors and hard-templating (SiO_2) approach. These materials were

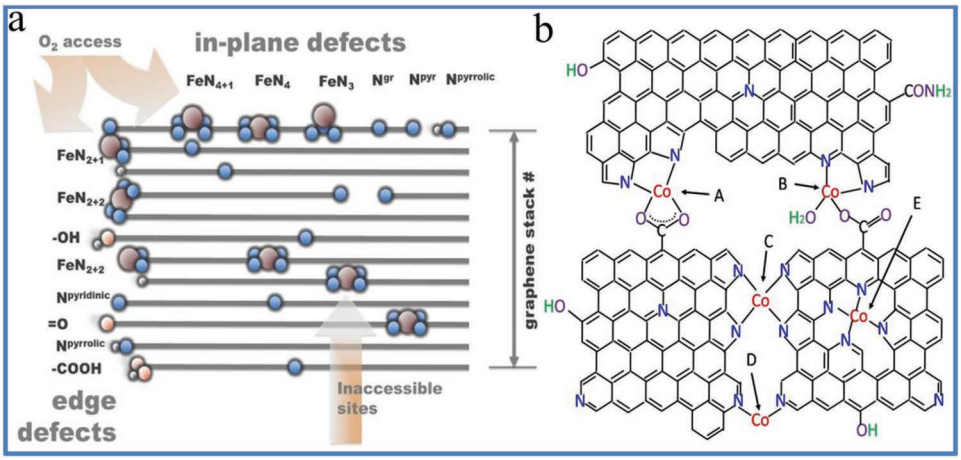

Figure 3. a) The graphitic crystallites showing the several positions of active sites, particular Fe-N_{2+2} or Fe-N_{2+1} edge structures. Reproduced with permission.[91] Copyright 2017, ACS. b) Possible catalytic active sites on Co-N-rGO catalyst. Reproduced with permission.[92] Copyright 2019, Elsevier.

examined for M-N_xC_y active sites through joined[57] Fe Mossbauer and XAS spectroscopy. Noticeably, the same quadrupole doublets (D1 and D2) have been seen in Fe-N-C, with different ratios.[72,93,94] Li et al.[93] showed the morphology of active sites in such catalysts (measured ex situ) drastically varies from that in operando conditions. The proposed active sites for ORR are the Fe-N_4 moieties with nonplanar configuration implanted in the defective carbon host, which was therefore analyzed by the high redox potential of $Fe^{2+/3+}$, which is contrary to what has previously been proposed by ex situ characterizations. The active site is indirectly changed to the in-plane Fe-N_4 ferric site in redox transition, which was poisoned by oxygen adsorbates, and redox potential ($Fe^{2+/3+}$) controls the number of active sites. The reversible structural alterations in M-N_xC_y active sites identified by XAS are caused by the removal/addition of oxygen-containing species and/or electrochemical potentials.[93] XANES characterization of Fe-N_xC_y moieties demonstrated minute but a tangible difference in these catalysts. As a result of both techniques, it was confirmed that the pyridinic and prophyridinic Fe-N_4 (active sites) are present. However, it was observed that Fe-N-C catalysts with almost the same XANES and Mossbauer spectra did not show the same ORR performance. For example, the Fe-N-C catalysts synthesized from the same materials (iron acetate, phenanthroline, and ZIF-8) but in different pyrolysis treatments, i.e., precursors were first pyrolyzed at 1050 °C in Ar for 1 h and named as $Fe_{0.5}$.[72] The second catalyst of $Fe_{0.5}$ was prepared by pyrolysis at 950 °C under NH_3 atmosphere for 5 min and named as $Fe_{0.5}$-950. The XANES and[57] Fe Mossbauer spectra of both catalysts were almost identical. Still, the ORR performance of $Fe_{0.5}$ was 30 times lower than $Fe_{0.5}$-950 in PEMFC at 0.9 V. The twice the surface area of $Fe_{0.5}$-950 is not enough to ultimately justify the performance difference in both catalysts. There must be an effect of chemical state in the nitrogen-doped carbon matrix, which increased the turn-over frequency (TOF) of Fe-N_xC_y active sites in $Fe_{0.5}$-950.[72] The supply of ammonia gas during pyrolysis is famous for introducing the N-group, leading to enhanced the basicity of the catalysts. However, the DFT studies revealed that the p*Ka* < 5 value of pyridinic-N could not create considerable alteration with augmented cluster size.[95] Therefore, the higher p*Ka* value > 8 can be justified because of other existing groups such as amide/amine with high p*Ka* in ammonia-treated samples; however, the manifestation of such functional groups after heat treatment is also debatable. By disturbing the π-electrons of graphene sheets, these highly basic nitrogen groups may alter the electron density at iron centers.[96] This concept was disclosed through experimental parameters confirming the straight relation between the ORR performance of Fe-N_4 on carbon and the Levis alkalinity of the carbon support. From the above discussion, we can conclude that Fe-N-C catalysts may have different ORR performance while having similar spectroscopic signatures for Fe. Thus ORR performance depends not only on the TOF of Fe centers but also long-distance consequences from the nitrogen-doped carbon, suggesting the vital role of basicity in nitrogen-doped carbon structure. Nevertheless, the lower stability of these ammonia-treated Fe-N-C catalysts was unexpected, normally 50% reduction in power enactment after 10–20 h of operation.[43,72] Zhai et al.[92] reported cobalt and nitrogen co-doping on the reduced graphene oxide (Co-N-rGO) with enhanced ORR performance. They explored some possible active sites in Co-N-rGO through DFT calculations, comprising Co-N_2/C, Co-N_4/C with edge plane, and some basal plane macrocyclic Co-N_4/C (Figure 3b). Very recently, Wu et al.[97] reported the in situ XAS analysis, which evidenced the conversion of inactive Co-OH and Co-O species into preferable active Co-N_4 sites for ORR.

2.1.3. Operando/In Situ Identification of M-N_xC_y Active Sites

The key advancement in exposing the local geometry of M-N_xC_y centers by using ex situ techniques swapped to the formation of reaction intermediates and tempted in exploration with real-time measurements. In this regard, in situ spectroscopy is being used to explore the M-N-C catalysts.[93,94,98,99] For example, XANES analysis carried out for ZIF-8 derived Fe-N-C and Co-N-C samples demonstrated that the Fe-N-C presented a possible-dependent shift of porphyrin clusters in Fe K-edge XANES spectrum, while the XANES Co-Edge spectrum stayed unchanged throughout the dynamic ORR potential range.

These results are achieved by repetitive $Fe^{2+/3+}$ switching at approximately 0.7–0.8 V versus RHE, but this phenomenon was not observed in cobalt,[99] further emphasizing that the active sites may be changed during the reaction, and in situ characterization are important tool to elucidate the active sites. There may be some drawbacks due to the bulkiness of XAS; however, these disadvantages would be controlled via Δμ XANES analysis. Li et al.[93] reported that in situ morphology of Fe-N-C catalysts is different as compared to ex situ measurements; a non-planar ferrous Fe-N_4 active site with out-of-plane shift with a stretched bond length of Fe-N was allocated as the operando active site. Further, operando Fe K-edge XANES measurements also revealed the possible dependent shift of $Fe^{3+/2+}$ transition of the redox potential traced by square-wave voltammetry.[93,98,99] Along with cyanide probe, this transition proved the direct contribution of Fe in ORR. In contrast, Co-N-C catalyst did not show this type of Co K-edge shift or Co-N_4 structural variation in operando XANES measurement, might be accredited to the varying redox potential of $Fe^{3+/2+}$N and $Co^{3+/2+}$N. The redox potential of $M^{3+/2+}$ and M–O binding energy has the inverse relation. Via regulating d-electrons of metal ions, the M–N bond distance and obviously the redox potential can be modified.[59,62,100,101]

Recently, Huang and co-workers[81] developed operando Mossbauer spectroscopy to recognize the actual composition (structure/spin state) of atomically dispersed Fe active sites and further studied by linking the operando Raman and X-ray absorption spectroscopy (XAS) measurements (**Figure 4**) with DFT calculations. The researchers proved the electronic and structural dynamics of single-Fe-atom moieties under in situ ORR conditions via directly capturing the $*O^{2-}$ and $*OH^{-}$ intermediates. This study may open new doors for the application of operando techniques to study the reaction kinetics directly.

In short, ORR performance of Fe-N-C catalyst with extraordinary M–O binding energy (low redox potential) is restricted by the TOF of Fe ion at relatively less potential. In contrast, the Co-N-C catalysts with less M–O binding energy (high redox potential) are restricted by less TOF.

2.2. Quantification of Active Sites

The turnover frequency (TOF) is used to measure the intrinsic activity and also used for comparison between different active sites.[102] The measurement of active sites is considered as the key of TOF calculations; however, the widely used methods for precious-metal-based catalysts,[103,104,] i.e., titration by under potential deposition (UPD) of Cu, H_2, and/ or CO stripping are inactive for M-N-C based catalysts. Though, some important

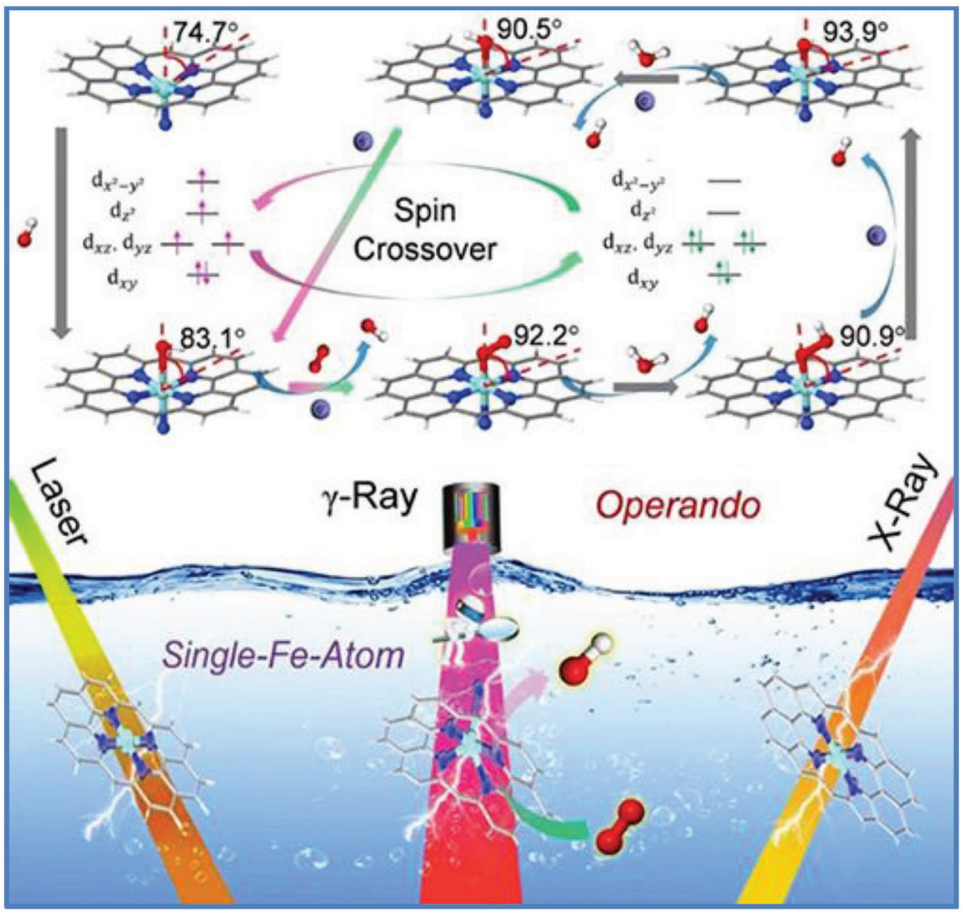

Figure 4. Structural and dynamics of N-FeN_4C_{10} moiety in ORR with optimized geometries and application of operando spectroscopy for identification of active sites. Reproduced with permission.[81] Copyright 2020, Elsevier Inc.

developments were reported for the quantification of Fe-N-C based active sites, assembling it as an example for future development and rational design of M-N-C based materials. TOF of a single site is considered as a ratio between the kinetic current density (I_k) of electrocatalyst at the specific potential to the site density (SD).[105]

$$I_k\left(Ag^{-1}\right) = F\left(C\,mol^{-1}\right) \times TOF\left(\left(electrons/site\right)/s\right) \times SD\left(mol\,g^{-1}\right) \quad (1)$$

More importantly, an exact understanding of SD values of the M-N-C materials is necessary for conveying the entire ORR process into SD and TOF. Evidence could assist in promoting exertions to develop the catalysts with enhanced performance. The density of perfect M-N_x-C_y moieties in materials can be quantified by updating M or N amounts. Therefore, XPS and EXAFS are widely used to determine the ratio of M and N, thus justified the active site density. For the very low M concentrations, inductively coupled plasma optical emission spectroscopy (ICP-OES) is used by digesting the M-N-C sample in nitric acid and hydrochloric acid (5:1). Moreover, the total reflective X-ray fluorescence spectroscopy (TXRF) is a trustworthy source anticipated for determining the elemental level in M-N-C catalysts.

Kramm et al.[106] also used neutron activation analysis (NAA) for the determination of mononuclear Fe-N_4 moieties. Furthermore,[57] Fe Mossbauer, along with XAS, are the dominant tools to survey the volume of active sites. Nevertheless, it is not a wise decision to consider all the metal contents as active sites for ORR within M-N-C-based catalysts. Therefore, in-depth understanding can be achieved by using some molecular probe to precisely occupied the ORR active sites (M-N_xC_y) on the surface of catalysts. Though CO electrochemical stripping and/ or chemisorption is considered as an effective probe for the quantification of Pt-based active sites,[107,108] on the other hand certainly not or fragile CO poisoning was detected on the surface of Fe-N-C catalysts during ORR.[109,110] In addition, DFT calculations showed that many Fe-N_xC_y moieties attach strongly to O_2 than CO, unlike in the case of Pt sites. Furthermore, the temperature-programmed desorption (TPD) technique was used to study the chemisorption of CO, to explore the add up of gas-phase nearby sites in M-N-C catalysts.[111,112] The TOF value can be obtained through SD information and the number of active sites by less-temperature adsorption of carbon monooxide based on the statement that sites with CO-adsorption resemble to O_2-adsorption sites.[112] Nevertheless, few CO-adsorption sites perhaps are less active for ORR; conversely, various sites that are active for ORR cannot link CO. As a result, there may be a difference between the actual SD of the metal contents for the ORR and the SD estimated through adsorption of carbon monoxide at low temperature. However, the confirmatory connection of CO consumption and ORR performance was found in acidic electrolytes. Further, $NO_{(g)}$ was studied as a probing agent for the detection of ORR-active sites through strong Fe-NO formation, which appeals to a variety of oxygen-activating systems.[113,114] The Mössbauer spectrum was drawn before and after the reduction of ferric in Fe-N_xC_y at -0.1 V RHE and confirmed the spectroscopic changes in some duplicates (referred as D2, D3, and D4), but not in the components of sextet (iron clusters). At the next stage, the reduced catalyst came into contact with $NO_{(g)}$ and found that certain doublet (D4) changed dramatically, with isomer swing varying from 1.54 to 0.60 mm s^{-1} and quadrupole splitting varying from 2.72 to 0.56 mm s^{-1}.[93,94,106,115,116]

In short, for CO, yet there exists no guarantee that the binding ability of CO moiety is the same as that of O_2. However, for NO, experimental and theoretical links between SD calculation from the adsorbed NO(g) and ORR activity in acid medium for numerous M-N-C catalysts, are required. Other anionic probes sturdily combine to M-N_xC_y, such as; thio/-cyanides, are considered promising poisons for M-N_xC_y moieties, mostly reported for Fe-N_xC_y sites.[117] Very recently, in situ SD quantification method is proposed by using cyanide anion as a probe molecule. The adsorption of cyanides on the active sites was determined by spectrophotometry and correlated with Fe-N-C active sites. The linear correlation verifies the surface-sensitive and metal-specific adsorption of cyanide on Fe-N_x sites, based on which the values of SD and TOF can be determined.[118] Interestingly, nitrite ions (NO_2^-) can strongly interact with Fe-N_xC_y active sites, but the poisoned active sites can successfully get back by reductive nitrite stripping.[105] In adsorbed NO_2^-, the stripping charge was used to evaluate the number of reactive sites, but the capability of this probe is questionable since NO_2^- anions only specifically decrease the activity of the ORR catalysts. This indicates that a few Fe-N_xC_y sites that are ORR active may not be fully linked to NO_2^- or these anions and O_2 absorb on the surface. In the first hypothesis, based on the charge stripping the calculated value of absorbed NO_2 would be less than that of the actual SD value of the active ORR sites in Fe-N-C catalysts and vice versa in the second case. Further, Zhang et al.[119] determined the SD of Fe-N-C electrocatalysts by measuring the FeN_x component at 399.7 eV in the N1s XPS spectrum of the catalyst via assuming that Fe-N_x are the only active sites. In summary, recent research reports in this area are attractive but must be gone through some practical phases for the wide range implementation of M-N-C materials. Because, there is no exact and accurate method to quantify the SD values, the achieved values, via different methods, should be compared to each other and with the ORR activity of other materials.

2.3. Mechanism of ORR on M-N-C Catalysts

To define the reduction of oxygen molecule and water formation by atomic active sites (M-N_xC_y) in ORR catalysis, three mechanisms have been suggested, such as; dissociation of 1) oxygen, 2) peroxyl, and 3) hydrogen peroxide, where dissociation of peroxyl is a potential mechanism with the least energy path to depict ORR.[120,121] Inside a pure thermodynamic model, Nørskov et al.[122] determined the reaction free energy (ΔG) with the expression: $\Delta G = \Delta E + \Delta_{ZPE} - T\Delta S + \Delta E_{solvation}$, where ΔE is the reaction energy of basic chemical reaction and can be calculated by the DFT, Δ_{ZPE} is the change in the zero-point energy, ΔS is a difference in entropy and $\Delta E_{solvation}$ is associated to the energy of solvation. Here, the zero-point energy derives from the vibration frequency analysis (**Figure 5**a). Fe-N-C catalysts with atomically dispersed Fe-N_x-C_y active sites have higher activity for ORR than others. Nevertheless, it stays debatable how the active sites facilitate catalysis and deviations

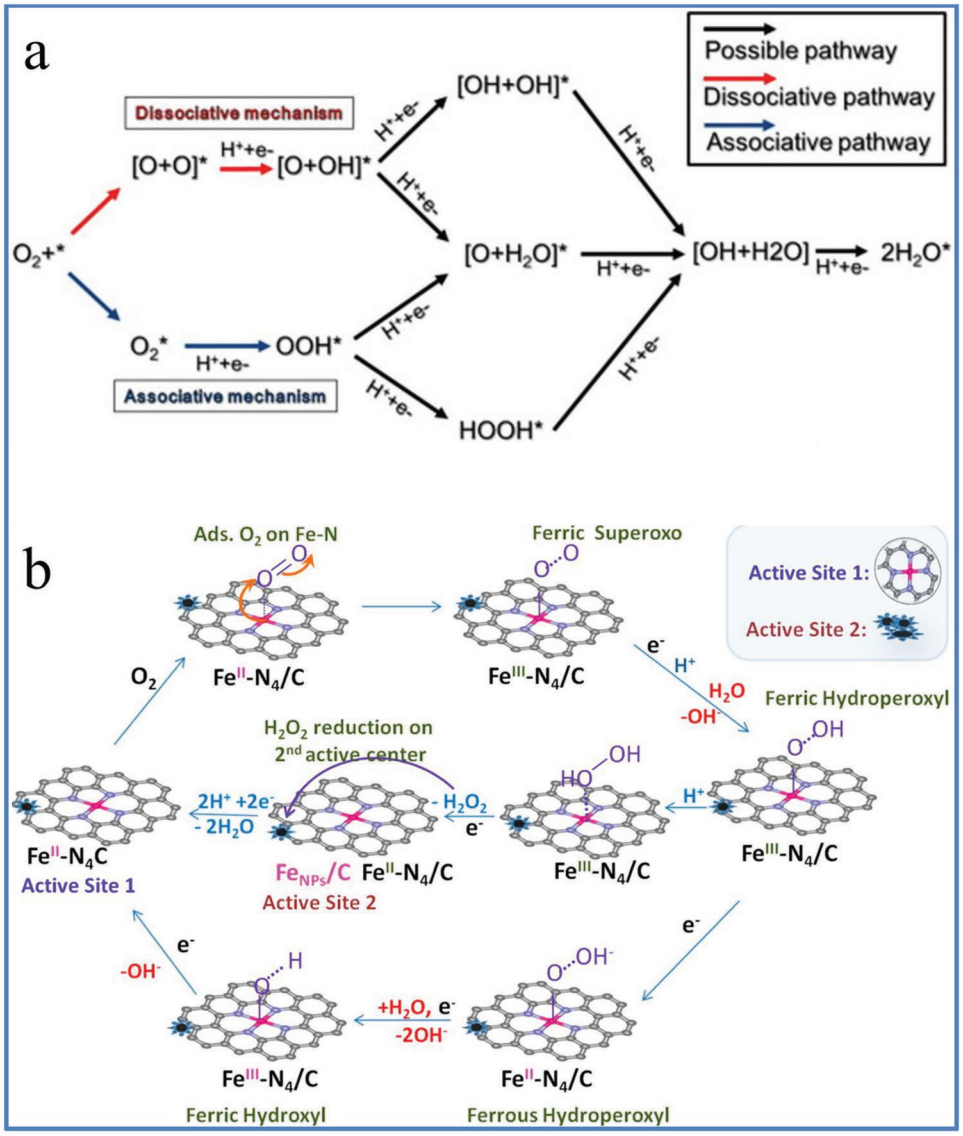

Figure 5. a) The proposed ORR mechanism, Reproduced with permission.[127] Copyright 2014, Elsevier. b) Reaction mechanism on Fe-N_4/C active sites in acidic and alkaline media, Reproduced with permission.[123] Copyright 2014, ACS.

of the expected possibility in observed results, which hinders the development of ultimate catalysts. For example, Mukerjee and co-workers proposed dual active sites (Fe-N/C and Fe_{NPs}/C) that synergistically enhanced the ORR performance on the surface-bound metallic nanoparticles with faradaic reduction of peroxide intermediate (2 e′ + 2e′ mechanism) in an acidic electrolyte (Figure 5b).[123] Further, it was claimed that Fe-N_4 having -N_4 would tightly adsorb O* at the high potential to achieve one electron deficient penta-coordinated Ox-Fe^{3+}-N_4 site to complete molecular oxygen adsorption on this site.[124] The similar phenomenon was further explored by DFT calculations, and they presented a four-electron OOH* separation corridor linked with Fe-N_4 sites same as of Pt.[69] Further, Wang et al.[125] used first principal calculations to create a microkinetic model on iron-based single-atom electrocatalysts, and results showed the actual active site of Fe-N-C atom are the Fe(OH)N_4 group instead of the inactive center Fe-N_4, since it is contained in the central OH*, which is associated to the active substance, and the values of the ΔG along the linked path of Fe(OH)N_4 active sites are more advantageous for catalysis as compared to that of the Fe-N_4 center. This conclusion was used to interpret the process of ORR catalyzed by a single Fe-N-C atom, and the result was endemic to previous experimental results. Holby et al.[126] studied Fe-atoms positioned on the terminal N and found that the structure of the Fe-N_3 cluster (Fe_2N_5 sites) able to create a barrier for small distribution of O–O bonds over the dissociative ORR path, preventing the formation of H_2O_2.

In the case of Co-N_x-C catalysts, numerous research reports have demonstrated two regions (Co-N_4, Co-N_2), and both regions have perfect catalytic performance to ORR, while Co-N_4 may be transformed to Co-N_2, which has a stronger interaction with hydrogen peroxide at elevated temperature, evidently supporting the 4 e^- ORR pathway.[92,120,128–130] Xiao et al.[120] testified a new binary active structure of the Co_2N_5 range with

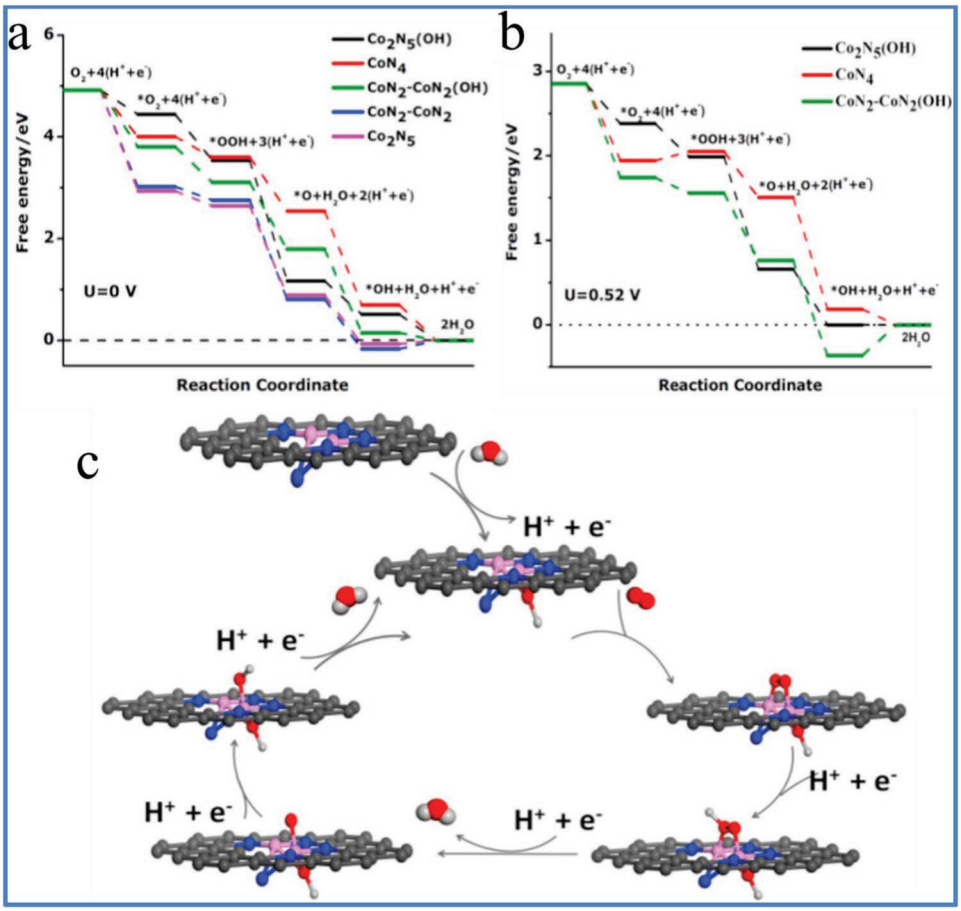

Figure 6. a,b) ORR energy pathway profiles on various Co_xN_y moieties in acidic electrolyte. c) Anticipated reaction scheme of associative mechanism on the Co_2N_5. Reproduced with permission.[120] Copyright 2018, Elsevier.

a binuclear distance of 2.1–2.2 Å (Co–Co), confirming the formation of binuclear sites. The proposed ORR mechanism on the Co_2N_5 active sites is shown in **Figure 6**a,b; Co_2N_5 activity is reported to be higher than CoN_4 activity, which open new doors for the production of highly efficient ORR electrocatalysts.

The DFT calculations were further applied at two binary metallic structures, such as Co_2N_5, CoN_2–CoN_2, and conventional CoN_4 structures. The minimum energy pathways (MEPs) for ORR for these metallic clusters were computed as; $O_2 \rightarrow *O_2 \rightarrow *OOH \rightarrow *O \rightarrow *OH \rightarrow H_2O$. The Co_2N_5 and CoN_2-CoN_2 structures, i.e., $*OH + H^+ + e^- \rightarrow H_2O$, exhibits positive reaction free energies even at a potential of 0.0 V (Figure 6c). The free energy profiles were estimated for the MEP at the $Co_2N_5(OH)$ and CoN_2-$CoN_2(OH)$ structures, i.e., the Co_2N_5 and CoN_2–CoN_2 structures each bearing a *OH, respectively. The $Co_2N_5(OH)$ exhibits a free energy profile with no uphill step in the MEP at the potential of 0.52 V; whereas both CoN_4 and CoN_2–$CoN_2(OH)$ structures represent one uphill step at the same potential (Figure 6d). While the step $*O_2 + H^+ + e^- \rightarrow *OOH$ becomes up-hilled for the CoN_4 structure, the $*OH + H^+ + e^- \rightarrow * + H_2O$ step requires a substantial thermodynamic obstacle for CoN_2–$CoN_2(OH)$ structure. The DFT calculation results suggest that the $Co_2N_5(OH)$ sites act better for ORR between different structures, endorsing the experiential results.[120] The process of ORR on the binuclear active site was concise in Figure 6.[120]

3. Strategies for Structural Design of ORR Electrocatalysts

Electrocatalysis is a surface-dominated multistep process; there are several factors that may affect the performance of ORR electrocatalysts. The activity of the catalyst is mostly controlled by the adsorption/ desorption capacity of the key reaction intermediates at the active sites.[131] Therefore, the activity of the catalysts can be increased by controlling the adsorption/ desorption capacity of these reactive species. And the surface chemical properties will influence the adsorption and desorption capacity of the active sites towards different molecules, affecting the selectivity and stability of the electrocatalyst.[132] The crucial components to design high-efficiency electrocatalysts are the structure and the density of the active sites, the pore structure and surface chemical properties of the catalyst. Which surface structure has the best electrocatalytic activity or what is the active site; are the most concerned issues. The adsorption behavior of the reactants and the catalytic activity

of catalysts can be modulated by modifying the electronic properties. Undoubtedly, abundant active sites are essential for high-performance electrocatalysts.[133] Thus, a highly active electrocatalyst can be obtained by constructing a suitable electronic structure (or charge state) and a physical structure, by which the activity of a single active site and the number of active sites can be increased.[134,135]

The scientists have been able to accurately tune the electronic structure (including charge status, spin density, and coordination state) of carbon via various approaches, such as precisely double/trinary-doping of reasonably selected heteroatoms in carbon, the introduction of new forms of nitrogen atoms in certain carbon regions, and the coordination of key metal atoms other than Fe and Co in the M-N-C structure.[39] These strategies lead to boost the specific activity of carbon sites (**Figure 7**). In addition to the intrinsic activity and density of active sites, the ORR performance of carbon-based catalysts can be improved via tuning some crucial physical properties, such as the dispersion of active sites, conductivity, morphology, specific surface area, and porous structure. At present, several niches have been reported focusing on synthetic concepts, such as the production of catalysts with exposed single active sites, the synthesis of efficient electron pathways in catalysts, and the construction of hierarchically porous structures from different templates or subtle precursors. These synthetic strategies are helpful in maximizing the use of active sites for electrochemical reduction of oxygen in PEM fuel cells.

3.1. Improving Intrinsic Activity of M-N-C

The universal understanding of inherent ORR pathways is a basic step to get high-performance electrocatalysts. The output of catalysts is mainly linked with active sites and the activation of O_2 molecules by the active site. If we consider the example of Fe-N-C active site, the DFT measurements based on the

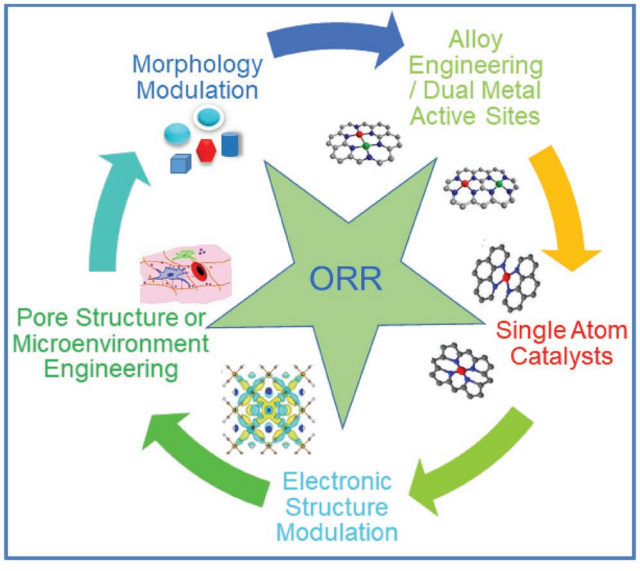

Figure 7. Recent approaches to increase the ORR performance of electrocatalysts.

spin-polarized demonstrated that the outer shells of oxygen (2p) are hybridized with 3d orbitals of Fe in both spin channels (up/down spin), the O_2–2p* function partly involved in the spin-down channel owing to the charge transfer from Fe-N-C monolayer to the oxygen.[136] The controlled d_z^2 orbital of iron by the engagement of functional groups may be subdivided into bonding and antibonding states before and after adsorption of oxygen. In comparison, d_z^2 (orbital) energy position to the Fermi level may generate a possible Fe-redox potential shift and perform an enhanced catalytic activity towards ORR.[137] Hence, the inherent activity of Fe-N-C relied on interconnecting environments with iron, such as N coordination number, the function of coordinated N, and microenvironment of metallic center. For example, the M-N_4, a stable structure with different N-coordination, shows varying performance for ORR, contingent on the different coordination configurations of active M-N_x sites besides the M-N_4, such as M-N_2 moieties.[138] Most specifically, present experimental and theoretical results have shown that individually dispersed M-N_2 moieties showed enhanced performance than M-N_4 and even better than Pt/C catalysts.[139–141] This outstanding performance has been attributed to the poor interfaces among the M-N_2 and *O_2/*OH byproducts compared to the M-N_4 moieties, which can increase the electron transport phenomena.[142] Further, according to DFT calculations, M-N_2 moieties also have stronger peroxide interactions compared to M-N_4,[73] which is firmly connected with better ORR performance. Moreover, DFT calculations also showed that Fe-N_2 moieties are comparatively more active for ORR than Co-N_2, having lower energy barriers for intermediates and products.[143]

Instead of M-N_x active sites, the location/geometry of these active sites in carbon support also played a vital role. By keeping the outermost electrons in d orbital (θ_d) and electronegativity together, Xu et al. correlated the solid bonding with observed ORR activity and suggested a corresponding descriptor (φ) to predict the activity of a catalyst.[144] Both experimental and theoretical validations gave a volcano relationship between descriptor φ and the ORR potential$_{(onset)}$,[145] thus demonstrated that the Fe-N_4-C_{10} (having four pyridinic-N) had better ORR performance than Fe-N_4-C_{12} (with four pyrrolic-N). Further, the DFT calculations performed on Fe-N_4-C_x moieties having four pyridinic-N atoms showed the lower activation energy (0.20 eV) for the breakage of O–O bonds in Fe-N_4-C_8 as compared to Fe-N_4-C_{10} (0.56 eV). This indicates that the Fe-N_4-C_8 has better intrinsic catalytic ORR activity than Fe-N_4-C_{10}.[58,146] However, $2e^-$ pathway with preferable H_2O_2 production exhibited by electrocatalyst consisting of iron coordinated two N and one C atoms (C-Fe-N_2 active site), and has minimal active as compared with in-plane Fe-N_4 site for ORR.[147,148] Moreover, linked to Fe-N_4, the border site Fe-N_2 (Fe is not straightly joined to C) had superb activity owing to lesser interaction with intermediates *O_2 and *OH and better transport of electrons.[142,143,149,150] However, Dodelet and co-workers also stressed that the simultaneous existence of the two active sites (Fe-N_2 and Fe-N_4) in carbon-supported materials with a certain ratio showed better ORR performance.[150,151]

In summary, the sequence of the inherent performance of various active sites on Fe-N-C follows as Fe-N_2 > Fe-N_4C_8 > Fe-N_4C_{10} > Fe-N_4C_{12} > C-Fe-N_2. Thus, a catalyst that constitutes

plentiful Fe-N-C sites with high activity is in demand; most specifically, this possesses some benefits to get enough Fe-N_2 species from the carbon support. For instance, by using a template casting strategy, a nominal catalyst based on Fe-N_2-based (Fe-N_2/NOMC) is prepared. Further, the [57]Fe Mössbauer spectroscopy proved that nitrogen atoms only interconnect with Fe, and K-edge X-ray absorption spectroscopy depicts that the average coordination number of Fe is 2.[74–77,82,83]

Recently, a dual-atomic catalyst with more active sites has been reported. To demonstrate greater intrinsic activity, many experimental and theoretical reports have shown that dual-metal catalysts declined the thermodynamic obstacles.[120] For instance, Holby et al.[126] examined that iron-atoms on the terminal edges having Fe-N_3 moieties (that may form Fe_2-N_5 dual sites) able to cross the energy barrier of O–O bond cleavage via a dissociative ORR pathway, thus restricting the production of hydrogen peroxide. Additionally, initial molecular dynamics showed that the process of solvation did not seem to put an impact on the impulsive reaction and stabilization of such N-coordinated edge defects in the C matrix.[126] Further, Xiao et al.[120] has formulated several possible configurations via DFT calculations for Co_2-N_x to identify potential structures of active sites, including Co_2N_5, CoN_4-CoN_3, CoN_2-CoN_2, and Co_2-N_6. The EXAFS fitting results identified that the distance of Co–Co (2.21Å) obtained from the binuclear structure (Co_2-N_5) was almost equal to 2.12 Å, and the new Co_2-N_5 binary sites had higher ORR activity, which was around 12 times higher as compared to conventional Co-N_4 sites. This can be ascribed to a significantly reduced thermodynamic energy barrier that comes from the binuclear active site.

Another kind of atomic dual metal catalysts (ADMC) comprised of two different isolated metal atoms on support[152–154] such as; binuclear Fe-Co, also proved as excellent ORR catalysts in acidic electrolytes.[120,155] However, the addition of another ligand or metal-doping further makes the situation complex. There are arguments related to the bonding types of the bimetallic compounds in bi-atomic catalysts; specifically, the bonds between metals, such as; M1-M1, M2-M2, or M1-M2 and in cases where the coordination of M-ligand bonding is strong keeping in view a general example of ADMC, FeCo-ISA/CN with individually distributed Fe and Co-atoms. Zhang et al.[153] described that the two main peaks at 1.5 and 1.4 Å were assigned to Fe-N and Co-N, respectively, in Fe K-edge and Co K-edge FT-EXAFS spectra. Moreover, the absence of other peaks at 2.2 Å eradicate the presence of Fe–Fe or Co–Co bonds. The enhanced ORR kinetics was due to the increased/ dispersed metallic active sites as well as dependent properties of the neighboring Fe and Co atomic sites. Instead of Fe, Lu et al.[152] explored Zn/Co-N_xC based catalysts, making Zn–Co biatomic active sites with a distance of 0.22 ± 0.04 nm and the coordination number of M-N (Co-N and Zn-N) was calculated about 3.5, indicating the presence of mixed-valence (M-N_3 and M-N_4). In addition, the second shell coordination number in both cases, i.e., either Co-M or Zn-M, was estimated to be 0.5 ± 0.1 nm, pointing to weak interactions in the form of ZnCo-N_6. DFT calculations further verified that Co–Zn bonding results in the lowest activation energy for ORR, confirming the formation of Co–Zn binuclear diatomic pair. Though the dual-atom approach may increase the overall catalytic active sites per specific surface area, coordination states are becoming more complex due to the fact that the preparation of pure dual-atomic sites is challenging. However, the possible coexistence of single-atom sites cannot be ignored.[156] Advanced and updated characterization techniques, for example, probe molecules, Mössbauer spectroscopy, nuclear resonance spectroscopy, etc., combined with theoretical calculations may be useful for analyzing the structural information.[114]

Heteroatom-doped carbon supports can also be utilized in addition to the above descriptors to further enhance the electronic structure of the metallic species in the M-N-C configuration.[157–161] For example, Zhao and co-workers[152,162] designed efficient Zn and Co dual doped dendritic carbon by modifying the adjacent Co-N_4 and Zn-N_3 active sites with sulfur. They performed DFT calculations and observed that doping of sulfur can increase the binding capacity of Co-N_4 by declining the variation in free energy of $*O_2$ to *OOH.

The dual-heteroatom doping further amends the electronic structure of catalysts and improves ORR performance. The N-, S-dual doping has widely explored for the improvement in catalytic performance. For example, S-, N-doped mesoporous carbon nanostructures with Fe-based active sites were prepared for ORR performance in acidic solutions. The optimized electrocatalyst performed well with a high peak power density (386 mW cm^{-2}) of PEMFC. The improved performance was attributed to the Fe-based active sites with dual-heteroatom doping and mesoporous structure.[163] The electropositive effect also occurs on Fe-N_4 via ammonia treatment, thus increases the density of doped N to improve the ORR activity.[72,164] Recently, Yuan et al.[53] synthesized nitrogen and phosphorus dual doped carbon nanosheets embedded with iron-active sites Fe-N/P-C. Both experimental and theoretical results indicated that the two-coordinated iron (N and P) were beneficial for adsorption/ desorption of oxygen intermediates, resulting in accelerated reaction kinetics and promising catalytic oxygen reduction activity. The combined results (experimental and theoretical) suggested that N/P organized Fe-active sites are beneficial for adsorption/desorption of O_2, accelerates the reaction kinetics, and ultimately increases the catalytic ORR performance. However, the ORR activity of Fe-N/P-C-700 in acidic medium was relatively lower ($E_{1/2}$ 0.72 V vs RHE) than that of reported Fe-based electrocatalysts for ORR in acid media.

This discussion could be summarized that electronic modifications for the structure of M-N-C catalysts by doping electronegative/-positive elements are important for enhancing the performance. However, the precise doping and identification of actual catalytic active sites may further support the rational design of new catalysts with better performance.

3.2. Improving Density and Dispersity of Active Sites

The ORR process in an acidic medium is sluggish and follows the $2e^-$/$4e^-$ transfer reaction; however, the $2e^-$ transfer reaction is considered as menacing due to high yield of H_2O_2 that can cause degradation of proton membrane in the fuel cell system. The overall four-electron reduction mechanism is promising owing to its evident efficacy advantages (four electrons per oxygen molecule), and because it escapes the creation of

hydrogen peroxide species in the electrode. For improving the electronic conductivity of ORR catalysts, the pyrolysis route is modified to prepare high degree of graphitization by increasing the pyrolysis temperature which lead to enhance the conductivity of derived materials.[29] Though the high-temperature pyrolysis enhanced the electron transfer efficiency to effectively boost the ORR performance, but relatively higher pyrolysis temperature also caused the agglomeration of metal species and reduction of heteroatom-contents leading to decay in ORR performance. A balanced and moderate pyrolysis temperature is required, and this may range from 700 to 1000 °C, depending on the nature of the precursors.

Despite the intrinsic activity, a dense and dispersed active site also significantly increases the ORR performance. The activity of catalysts is contingent on the M-N-C active sites available on the surface. Previous studies have shown that the ORR activity is directly related to the concentration of active sites.[142] Therefore, the high contents of active M-N_x-C_y sites are necessary to ensure high catalytic ORR activity. To date, state-of-the-art processes have been developed to enhance M-N_x-C_y sites, while the simplest technique for improving M-N_x-C_y sites is to increase the catalyst loading during testing. For example, Wang et al.[165] reported that H_2O_2 yield produced by Fe-N-C is proportional to the loading of catalyst. As the loading of catalyst increases from 0.06 to 0.6 mg cm^{-2}, the performance of the average H_2O_2 decreases (16 to 1%). The approximated rate according to the Wroblova model shows that at increased load density, the average H_2O_2 undergoes a further conversion into H_2O instead of adsorption, while a lower catalyst loading leads to a reduction of O_2 via the 2-electrons pathway.[166] Nevertheless, the increased catalyst loading takes to the denser modified layer and a further pronounced diffusion, specifically in 3D porous materials.[167] Alternatively, considerable struggles were made to enhance the active sites of M-N_x-C_y, either by increasing density or by improving the available area for catalysis. Here, we have concisely summarized the up-to-date approaches for improving the active sites through controlled synthetic methods.

3.2.1. Closed Pyrolysis Strategy

The carbon-based catalysts for ORR are usually produced by pyrolysis at a specific temperature that is 600–1000 °C in an open inert environment. In an open system, nitrogen and carbon precursors are affected by considerable weight loss due to the evaporation of several gases, lead to relatively low catalyst yield, thus ultimately decreases the abundant ORR active sites. Therefore, inhibiting the formation of carbides during heat treatment is an emerging way to increase the density of active sites in Fe-N-C catalysts.[106] To solve this problem, researchers are trying to crack down in the "closed" system, using the hard template method; the sample can produce porous structure after carbonization and retain its structure; however, the selected template is used to determine the surface area. For example, SiO_2 nanoparticles, arranged in mesoporous silica and montmorillonite, are being utilized as models to achieve mesoporous structures, indicating a strong relationship between specific surface area and activity.[168,169] At this stage, SiO_2 is mostly used to generate a controlled space, the general approach, supported by the silica layer, is designed to produce the best catalytically active sites of M-N_x-C_y in catalysts by inhibiting the production of large metal nanoparticles.[170–172] For example, Yang's group suggested a surfactant-assisted method to enhance the active site with Fe traces.[173] Expending a strategy based on semiembedded integration of the iron precursor on the template SBA-15 surface, the strong linkage of the template inhibits iron species from penetration and construction of the Fe (surface) species easily available for catalysis. By this method, different quantities of Fe-N_x-C_y sites are introduced simply by increasing the quantity of impregnated iron precursor.[174] Nevertheless, it's worth mentioning here that it is not possible to incessantly increase the content of M-N_x-C_y by adding higher amount of metal precursors. Because the transition metals, for example, Ni, Co, and Fe, are traditional catalysts for improving graphitic carbon,[175,176] results in reduced nitrogen contents and specific surface areas. Therefore, balancing invasive metal precursor and doped nitrogen in a controlled way is the basic key to optimize M-N-C materials. Recently, an interesting method named as "shape fixing via salt recrystallization" is introduced to prepare efficient catalyst by using NaCl crystals as sealed monoreactor, which facilitate the controlled incorporation of N with sufficient contents during pyrolysis even in the presence of Fe contents.[177,178]

3.2.2. Semiclosed Pyrolysis Strategy

The hard templates like silica follow the tedious acid leaching step with HF to remove the template, thus considered as a costly and environmentally hazardous process. Moreover, a pyrolysis strategy in the "semi-closed system" technique acquired the use of $ZnCl_2$/KCl eutectic salts to tune the precursor during carbonization and generates porosity.[179] In order to prevent fast decomposition, the eutectic salts in molten form produce an ionic liquid-confined space, decreases the possibility of sintering and cracking of precursors. During pyrolysis, this strategy also inhibits the huge weight loss and also significantly reduces the N-evaporation from the precursor. Thus performs its role in the formation of novel 3D graphene-like morphology with an improved specific surface area and a high degree of graphitization, apart from the greater density of the Fe-N-C sites. On the same lines, the as-synthesized Fe-N-C catalyst displays better performance with $E_{1/2}$ of 0.803 V and 0.918 V in both acid and basic media, respectively. Nevertheless, these strategies and methodologies are normally subjected to concise density of active sites. Being not stable in a strong acidic environment, the metallic nanoparticles, metal carbides, and metal oxides are usually removed through postsynthetic acid leaching step.[156,180] Many of these are time-taking and need state-of-the-art facilities, which are not suitable for large-scale synthesis of catalyst; however, the MOF-pyrolysis is a recent strategy to prepare a well-dispersed atomic active site (details in Section 3.4).

3.3. Pore-Structure Modulation

Likewise, in active sites, the mass/charge transfer ability of the catalyst is also a critical point in terms of determining ORR performance. Hence, the structural design of carbon-based

catalysts must be clearly arranged with uninterrupted species for mass/charge transfer from in or out of the active sites during the ORR pathway. For mass transfer, earlier studies have highlighted that microporous morphology having active sites can significantly boost the ORR activity. However, the nature of carbon and nitrogen precursors critically influences the formation of micropores.[181,182] Some studies also reported that the mesoporous structure and porosity of materials play a key role toward electrocatalytic behavior, particularly at high current densities where transport limitations dominate. Considerably, high porous morphology with packed active sites contributed to increase the ORR activity. Even so, it must be noticed that a lot of active sites in the microporous structure may not be exploited owing to the deficiency of mass transfer channels. The formation of macro and mesopores are also required for uplifting the considerable mass transport during ORR-pathway. Hence, making a hierarchical porous structure[183] equipped with well-organized structures of micro-, meso-, and macropores would be more desirable. Aiming at this point, a lot of elaborative pathways of utilizing templates such as; polystyrene, eutectic salt, silica, etc., have been prepared.[184] Wei and co-workers designed a method by mixing zinc salt with colloidal silica template for the preparation of hierarchically porous Co-N-C and Fe-N-C catalysts.[172,185] It was explored that zinc evaporation results in interconnected macroporous structure while leaching out silica leads to the formation of meso-/micropore. On the basis of this study, recently, the same group further proposed NaCl-ZnO joint-template method to prepare 3D hierarchical metal-free porous NC catalysts.[186] Although the better performance was achieved through templating methods but still comprised of shortcomings due to long time-consuming procedure and utilization of poisonous reagents. Regarding this, few convenient strategies for the template-free synthesis of 3D hierarchical pores in engineering have been reported. For example, the proposed in situ synthesis of Fe-N-C-Phen-PANI catalyst with 3D nanoporous sheet-like assembly, by utilizing binitrogen sources (PANI and Phen). Phenanthroline was used as a pore-forming agent to extend the outer shell of PANI during heat treatment, resulting in increased surface area of 1073 m^2 g^{-1} with exuberant meso/macropores generation in Fe-N-C-Phen-PANI. Recently, a phase-transition-assisted (PTA) technique was proposed by Wei et al.[187] to prepare hierarchically porous C-based materials. During the PTA process, a separation of liquid/gas combined with an interfacial reaction of gas and liquid leads to the formation of open macroporous channels with many active sites. Moreover, by controlling the interfacial rate of solidification, the channel size of the macropore can be tuned between 1.3 and 120 nm. Though few achievements are attained, it still counteracts some limitations during synthesis. Further, MOF-derived electrocatalysts are emerging for high mass transfer and well-dispersed active sites owing to the inherent features of MOFs (porosity and high surface area).[188,189] Due to the high applicability of MOF-derived electrocatalysts, the details of catalytic structure design are discussed in the following sub-section.

3.4. MOF-Derived Electrocatalysts

The correlation of electrocatalytic ORR performance and the structural features such as conductivity, surface area, highly dense/dispersed active sites with intrinsic activity is well established (in the above sections), leading to the conclusion that appropriate designing for catalysts is absolutely important. The researchers have introduced several methods; in recent years, MOFs, as new porous materials, have gained extensive attention for several applications because of the well-defined porous structure and highly ordered arrangement of organic linkers and metal nodes.[30,190–200]

MOF-derived porous compounds, with high surface area, high stability, and flexible structures, are very promising candidates for ORR catalysis due to their inherited porous structures with large surface area and identical active sites after rational pyrolysis.[195,201] More importantly, their periodic structures give rise to spatial separation of building units and thus inhibit potential agglomeration of metal sites during pyrolysis, enabling MOFs as ideal precursors to create atomically dispersed active sites. There are several reviews for MOF-derived ORR electrocatalysts and synthetic strategies.[54,192,193,202–205] Therefore, here we will summarize only recent and most promising studies to manipulate the MOF-derived catalysts for highly efficient ORR catalysis.

3.4.1. Strategies for Tuning Metallic Active Sites

Several methods were introduced for the design and synthesis of MOF-derived ORR electrocatalysts with high performance. The emerging approaches are not limited to chemical doping,[206] cage-encapsulation,[207] adsorptions,[173] core–shell confinement,[208] and multi-ligand strategy.[209] In this section, we will discuss the synthetic routes of MOF-derived M-N-C electrocatalysts and some perspectives to further improve this appealing research field.

MOF-Derived Single-Atom Catalysts (SACs): Mostly, MOFs have one type of metal in their network, which has more chances to agglomerate during the pyrolysis process. For this, the mixed metal strategy is being applied for homogeneous dispersion of metallic nodes in the MOF network. In mixed metal MOFs, the targeted metal is usually in low contents, and the second metal (having low boiling point) is used in high contents. The synthesis of nanoporous carbons by self-sacrificed precursor which consists of nitrogen-containing organic ligand and transition metal ions, mainly with the zeolitic imidazolate frameworks (ZIFs), such as ZIF-7[210] and ZIF-8.[28,207,211–213] In addition, different strategies are also employed to avoid the agglomerations of metals such as: a) Pre-doping of required metal-ions in ZIF-8 structure in the form of M-complex, b) Host–guest strategy to confine the required metal in the pores of MOF, c) Adsorption of targeted metals in the MOF-derived N-doped carbons. There are several reviews for MOFs-derived ORR electrocatalysts and synthetic strategies.[54,192,193,202,203] For example, Li et al. reported the single-atom Co-N-C catalysts with high loadings of Co (4 wt%) via high-temperature pyrolysis of mixed-metal MOF (Zn/Co-ZIF).[139] With regard to bimetallic-ZIF catalysts, researchers have extensively examined the link between composition, structure, and associated ORR performance by changing the Zn/Co ratio in the precursors (0–30 at%) and the heat treatment in the range of 700–1100 °C.[28,172,214–217]

The chemical doping strategy is applied for the production of Fe-N-C materials tracked by one-step pyrolysis. The accurate

and controllable modification of morphology and metal contents in derived carbons ultimately developed an encouraging connection between the assembly/configuration and ORR performance.[164,210,209] Despite the Fe contents, the ORR performance is also dependent on the particle size of MOF-derived carbons; it might be attributed to varying surface area, exposure of active sites, and morphologies. For instance, Zhang et al.[209] proposed the Fe-doped ZIF-8 nanocrystal precursors with controlled particle size (20–1000 nm) by altering the amount of solvent during synthesis of MOF precursors. This controllable approach of morphology (retention of morphology even after 1100 °C pyrolysis) and metal contents offered a chance to study the structure/activity connection for ORR. At a nanocrystal size of 50 nm, the $E_{1/2}$ was 0.85 V versus RHE in 0.5 M H_2SO_4, showing a half-wave potential ($E_{1/2}$) of 0.85 V versus RHE. Further, Li et al.[218] applied this two-step method to prepare the atomically dispersed Mn-N_4 sites (**Figure 8**a). The metal exchange strategy was applied to replace some Zn nodes from the MOF skeleton with targeted metal (Mn) following the pyrolysis of Mn-ZIF-8 precursors under N_2 atmosphere. In the second step, the host adsorption strategy was applied to adsorb more Mn in the N-doped carbons resulting from Mn-ZIF-8 precursors following the pyrolysis to produce high loading of Mn-N_4 active sites on graphitic carbons. The prepared catalyst exhibited enhanced ORR performance ($E_{1/2}$ = 0.80 V vs RHE) and high power density (0.46 W cm^{-2}) in MEA with superior stability. Further, a confinement strategy was applied to prepare Co-N-C core–shell structures for enhancing the catalytic ORR performance of Co-N_x-C active sites. He et al. produced a core–shell structure with atomically dispersed Co-N_x moieties via direct pyrolysis of surfactants coated Co-doped ZIF-8 crystals (Figure 8b).[208] During the pyrolysis, the interface contact between the MOF and surfactant (F127) formed the confinement effect preventing the breakdown of the microporous structure and agglomeration of Co.

Spatial confinement is another method widely used for the synthesis of MOF-derived electrocatalysts, which is based on the incorporation of metal salt into the pores of MOFs. Noticeably, the size of metal salts should be large enough than half of the pore size of MOFs so that the atomic dispersion of targeted metal can be achieved. This dispersion would be valuable for preventing the metal agglomeration during the pyrolysis.[38,219] Thus, metal salts with large ligands are used; for example, metal acetylacetonate (acac) and ferrocene are often employed. Li and co-workers trapped the Fe(acac)$_3$ molecule into the cage of ZIF-8 and after the pyrolysis, the Fe-N-C catalyst with atomically distributed Fe-N_x moieties was achieved towards enhanced ORR performance.[210] However, this strategy has a key issue for the selection of metal salts; only selective metal salts can be used according to the pore size of MOFs, excluding the

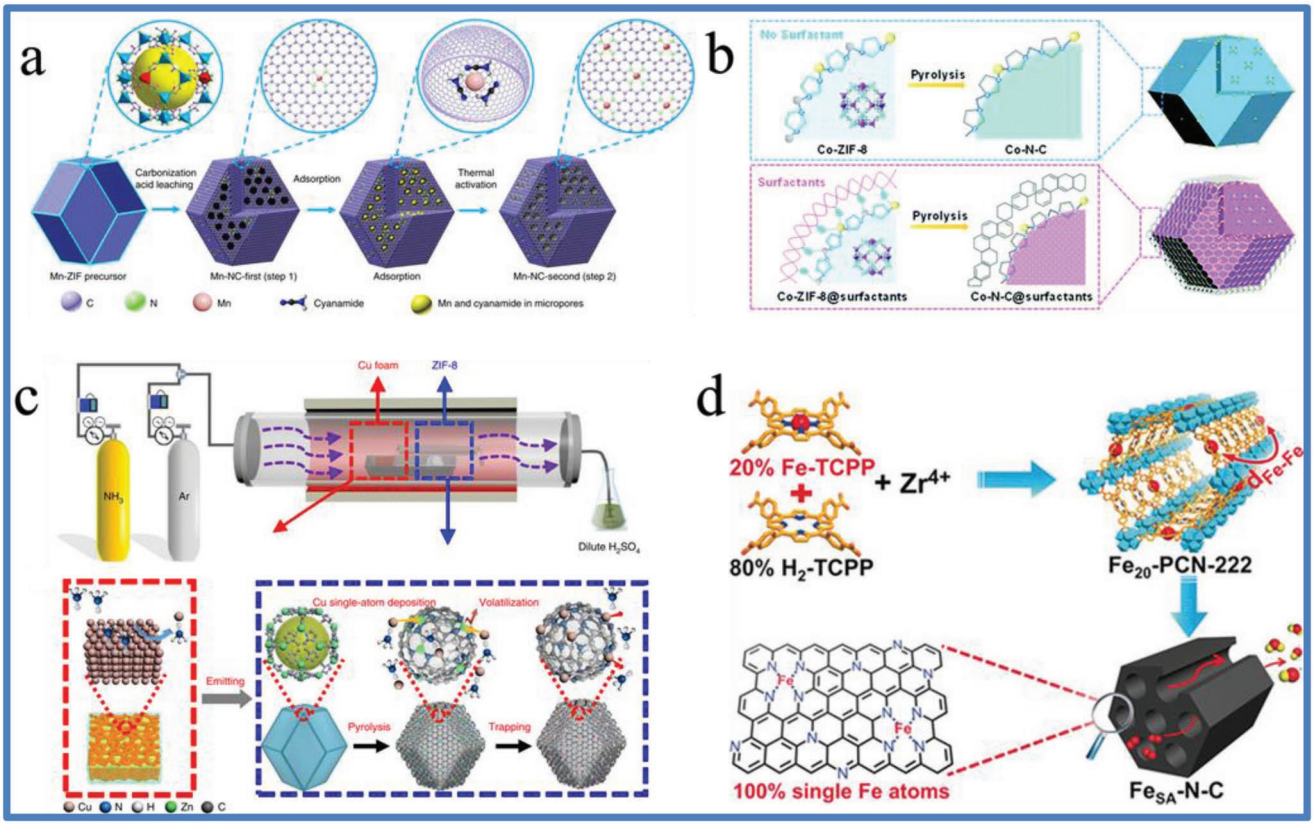

Figure 8. a) A two-step doping and adsorption approach to prepare MOF-derived Mn-N-C catalysts. Reproduced with permission.[218] Copyright 2018, Springer Nature. b) Synthesis strategy of core–shell Co-N-C@surfactants materials. Reproduced with permission.[208] Copyright 2019. c) Schematic illustration of synthetic approach and proposed mechanism for formation of active sites. Reproduced with permission.[222] Copyright 2018, Springer Nature. d) Synthetic approach to synthesize MOF-derived Fe-N-C catalysts for ORR. Reproduced with permission.[209] Copyright 2018, Wiley.

use of conventional and low-cost metal salts (halides, nitrates, sulfates) due to their small size.

The single Cu-atom supported on porous N-doped carbon could also be prepared by using the MOF-precursor. ZIF-8 with a unique and flexible structural network offered an outstanding base for the formation of atomically dispersed active sites.[220,221] Further, Li et al.[222] reported a simple gas migration approach via direct emission of (Cu-SACs) atoms from the bulk metals and subsequently trapped on the surface of porous N-doped carbon with the aid of ammonia gas (Figure 8c). It was claimed that uniform dispersion of isolated Cu-atoms could be achieved via consuming graphene oxide (Cu-SAs/N-G) with 1.26 wt% Cu-loading from NH_3-carbonized ZIF-8, and the morphology of ZIF-8 was well maintained after pyrolysis. In nature, Cu is used for oxygen reduction catalysis from bacteria to humans.[223,224] Despite the good ORR performance,[225–227] there are few studies reported on Cu-N-C as fuel cell cathode.[228]

The mixed ligand strategy is also widely applied for MOF-derived electrocatalysts for ORR. To construct mixed-ligand MOFs, the type of second ligand can be categorized as: i) metal-free ligands and ii) metallated ligands. The metallated ligands are formed by coordinating metals with some special ligands such as porphyrins; noticeably the space between the neighboring metallated ligands can be tuned by altering the ratios of mixed ligands.[209,229,230] Using this method, Jiao et al.[209] reported a hierarchically porous single Fe atom catalyst (designated as FeSA-N-C) via pyrolysis of porphyrinic Fe_x-PCN-222 precursor using Fe:PCN with molar ratio of 2:1, followed by acid leaching step to eradicate ZrO_2, which resulted in a mesoporous structure with well-distributed micropores and an integrated hierarchical framework (Figure 8d). The predesigned mixed ligand MOF occupied enough distance which inhibits the immigration of metal atoms to agglomerate, and thus atomically dispersed Fe-N_x active sites can be formed.

In summary, MOFs are emerging precursors to produce a variety of electrocatalysts by fine-tuning the structures. Further, MOFs also have flexible textural properties to accommodate the incoming guest molecules, which provide an opportunity to incorporate the required functionality in MOF-derived catalysts. Further, the porosity can also be tuned by using soft- and hard templates in the MOF network during synthesis. These templates may be the external sacrificial agents (such as polymers) or non-sacrificial agents (SiO_2), which can be removed after pyrolysis.[200]

MOF-Derived Dual Atom Catalysts (DACs): The recent progress in MOF-derived SACs showed that the variation in intrinsic activity is directly linked to the nature of metal center (Fe, Co, Mn, etc.), and the existence of different reaction pathways on each metal. Despite the SACs, dual-atom catalysts (DACs) are getting more attractions due to their improved ORR performance.[78,153,158,231] The integration of synergistic interaction of different species DACs showed promising performance and can be categorized into two groups: i) homonuclear DACs, ii) heteronuclear DACs.[232,233]

MOFs are also employed to modify the synthesis of DACs, for example, Fe_2-N-C (homonuclear DACs) was synthesized by one-step encapsulation of $Fe_2(CO)_9$ into the pores of ZIF-8 following the in situ pyrolysis method. During the controlled pyrolysis, the $Fe_2(CO)_9$ molecules in the multiplex core–shell structure were converted into Fe_2 dual-atoms dispersed/attached on the ZIF-8 derived N-doped carbon. Despite the facile strategy to optimize DACs for ORR, the toxicity and cost of carbonyl compounds should be considered. How to precisely fabricate the heteronuclear DACs is a big question in catalysis. In the search of suitable materials, fortunately, MOFs can provide a suitable platform to synthesize DACs via controlled pyrolysis.

The DACs can be prepared with multiple-metal species (heteronuclear DACs) by using MOFs as precursors with multi-metallic nodes. In this regard, the Zn-species in Zn-based MOFs provide the assistance to inhibit the agglomeration of the active site.[234,235] Agreeing to the above method, Venegas et al. used the bimetallic MOF (Zn/Co MOF) as a host to accommodate the iron-based guest species, following the controlled pyrolysis, the hollow N-doped carbon framework with atomically distributed Fe-Co DACs were obtained (**Figure 9**a).[158] Through the pyrolysis, the iron also served as a catalyst to form the holes leading to the hollow structures with DACs, which performed good for ORR ($E_{1/2}$ of 0.863 V vs RHE) and high peak power density (505 mW cm^{-2} at 0.42 V) in the H_2/air fuel cell. Further, the $Fe(acac)_3$ molecules were also encapsulated in the skeleton of ZnCo-ZIF, after the pyrolysis of hybrid structure $FeCoN_x$/C catalyst with $FeCoN_5$-OH moieties were obtained.[231] The integration of different metal sources was also used for the preparation of MOF-derived DACs, e.g., FeNi-DACs.[236] Despite the ZIFs, other MOFs are also used for the preparation of MOF-derived DACs; for example, MET-6 and PCN-224 were used for the fabrication of CoFe@C DACs and $FeCo_2$-NC DACs, respectively.[192,237] Furthermore, atomically dispersed active sites with high metal-loading (density of active sites) are formed by optimizing the ratio of metal contents and heteroatom source or other templates.[238–241] For example, atomically dispersed dual Co-Ni sites encapsulated in N-doped hollow carbon (CoNi-SAs/NC) were obtained through annealing of dopamine coated MOF (Figure 9b).[242] The CoNi-SAs/NC as an ORR electrocatalyst demonstrated excellent activity with E_{onset} of 0.88 V and $E_{1/2}$ of 0.76 V, revealing that catalytically active sites were exposed when the catalyst was changed from nano-sized metallic agglomerates to isolated metal single atoms.[242] Shah et al.[198] precisely applied a multistep heating strategy to produce mesoporous N-doped carbon nanostructures with Mn-/Co-N_x dual moieties from mixed-metal zeolitic imidazolate frameworks (Figure 9c). The unique structure, with dual-metallic active sites, not only offers a high electrochemical performance for ORR ($E_{1/2}$ = 0.83 V vs RHE in acid media), but also enhances the durability of the catalyst after 20 000 cycles with 97% of retention and very low H_2O_2 production (<5%) in 0.1 M $HClO_4$. This is because MOF crystals may contain several metal species, making it likely that alternative energy resources might implement two or more independent atomic sites anchored on carbon materials.

The analysis of recent literature on the MOF-derived DACs revealed the infancy of this field and further research is urgently required for the mature application. The diatomic synergistic effect would be the base for future developments. Further, instead of DACs in the mixed mode, the paired metal DACs would be advantageous for advanced electrocatalysis via microenvironment modulations.

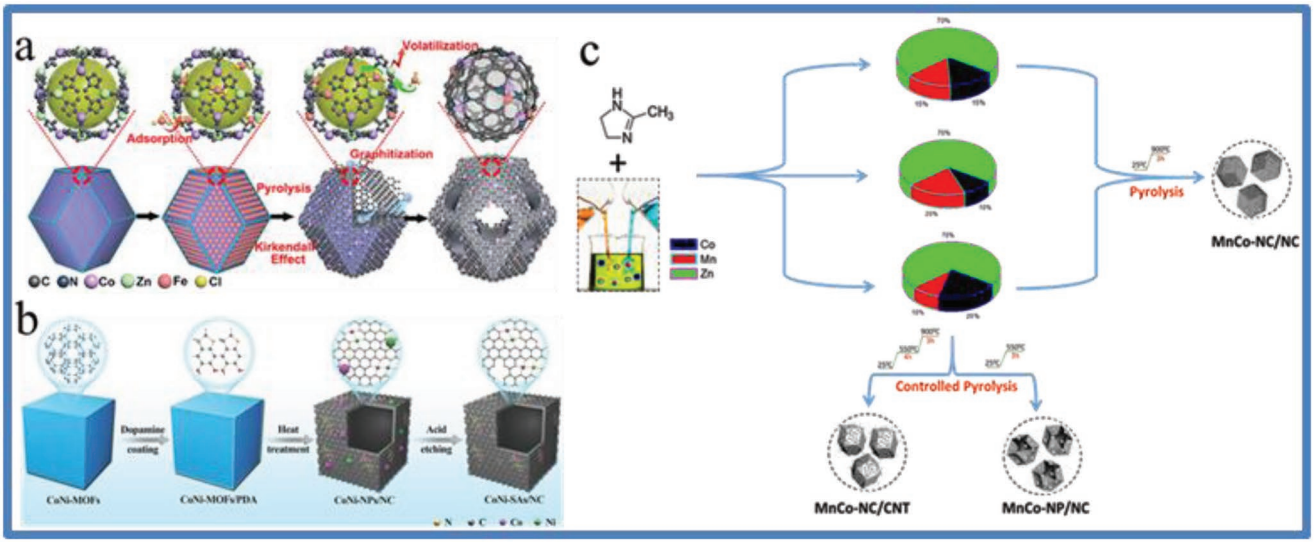

Figure 9. Schematic illustration of MOF-derived electrocatalysts with dual-metal active sites by using different strategies: a) Synthesis of Fe, Co/N-C. Reproduced with permission.[158] Copyright 2017, RSC. b) Formation of CoNi-SAs.NC. Reproduced with permission.[242] Copyright 2019, Wiley. c) Synthesis of mesoporous N-doped carbon nanostructures with Mn-/Co-N_x dual moieties. Reproduced with permission.[198] Copyright 2021, ACS.

3.4.2. Electronic Modification of MOFs Derived M-N-C Catalysts

The modulations in the microenvironment of MOF-derived atomically dispersed active sites is an emerging strategy to enhance the catalytic performance. This functional modification can be carried out via creating a defect in the carbon support and/or introducing the multiheteroatom dopants. These defects/dopants are considered to be responsible for altering the O–O bond cleavage pathways on the concerned active site. For example, edge-hosted M-N_4 (M-N_{2+2}) showed better ORR performance than that of bulk-hosted M-N_4. Further, the CN_x active sites may also affect the electronic distribution of carbon surrounding the M-N_4 active site leading to improved ORR performance. Similarly, other dopants (S, P) can also synergistically enhance the performance of metallic active sites. For example, Chen et al.[243] used the ZIF-8@polymer composite to prepare Fe-SACs anchored on the tri-doped (N, P, S) hollow carbon structures. The electronic tuning of the Fe-active sites results in improved ORR performance in the acidic electrolyte ($E_{1/2}$ = 0.791 V) and also in H_2-air fuel cell, with high methanol tolerance. Recently, we reported that P-doping could increase the catalytic properties of the Fe-N-C catalyst with antipoisoning ability against SO_x, NO_x, and PO_x. The Fe-N-C was fabricated by pyrolysis of a zeolite-imidazole-framework-8-coated Fe-doped Prussian blue analog (ZIF-8@Fe-PBA), which is obtained by carefully controlled growth of ZIF-8 on Fe-PBA cubes. The Fe-N-C comprises a unique 3D morphology of CNTs (carbon nanotubes) surrounded by a porous hierarchical polyhedron, denoted as 3D-Fe-N-C. Then, a further P-doping step was carried out by the second pyrolysis of phytic acid-coated Fe-N-C catalysts (denoted 3D-Fe-PNC). The further P-doping step greatly enhanced the catalytic performance due to the synergistic effect of P and N that creates more and stable active sites for ORR. The 3D-Fe-PNC exhibited excellent ORR activity with a positive shift of half-wave potential (70 mV) as compared to that of 3D-Fe-NC in acidic solution.

These studies suggested that the electronic configuration of MOF-based electroctalysts could be modified by the addition of an external source of heteroatom doping. The modification of electronic structure and/or microenvironment of MOF-based catalysts is an important and emerging field, required much attention for further exploration.[199]

4. Proton Exchange Membrane Fuel Cells

Membrane electrode fuel cells are capable to effectively generate electrical energy relatively at a low temperature of <90 °C via transforming chemical energy of hydrogen and oxygen, thus stands as the best clean-energy device in terms of ecological and economic perspectives.[3,44] Recently, PEMFCs are considered as ideal applicants for various automotive and portable devices with fewer limiting factors. The hydrogen and oxygen (in the air) are normally supplied to the anode and cathode of the fuel cell, respectively, and simultaneously, HOR and ORR occur as shown in **Figure 10**.

As stated in the introduction part, the ORR has more sluggish kinetics; hence, we have reviewed the performance of M-N-C electrocatalysts for PEMFCs in detail with reference to ORR. Currently, Fe-N-C catalysts are considered as viable record alternatives of Pt/C catalyst to achieve high-performance O_2 electrochemical reduction reaction during fuel cell operation.[46] The cathode prepared from Fe-N-C catalyst (Fe_2-Z8-C) showed high-power densities of 1.14 and 1.11 W cm^{-2} at 2.5, and 2.0 bar for H_2/O_2 MEA, as well as the highest value of 280 mW cm^{-2},[245] achieved at 0.8 V which surpasses the US 2020 DOE (Department of Energy) target (250 mW cm^{-2}).[246] Another research report also revealed that S-, N-dual doping improved the performance of fuel cell and Fe/N/S-MC (1:1:1) electrocatalyst demonstrated significantly improved performance with the highest power density of ≈386 mW cm^{-2} at ≈385 mA cm^{-2}, while operating at 0.6 V. The enhanced

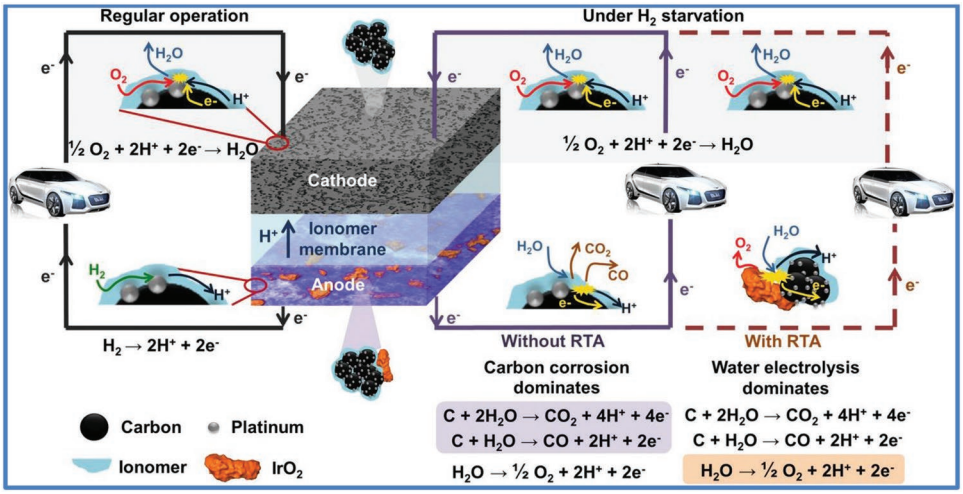

Figure 10. A presentation of fuel cell operations under normal and hydrogen starvation conditions, RTA (reversal tolerant electrode) a highly active catalyst (IrO_2, RuO_2) for oxygen evolution reaction to avoid the carbon corrosion. Reproduced with permission.[244] Copyright 2016, Elsevier.

performance of the PEMFC using Fe/N/S-MC(1:1:1) as a cathode catalyst may be ascribed to the Fe/N-containing catalytic sites surrounded by nitrogen atoms, co-doped by sulfur, and a mesoporous nanostructure.[247] Choi et al.[176] presented a surfactant-assisted methodology by thermal treatment of precursor prepared from g-C_3N_4 and Fe-loaded water-soluble surfactant F127 for synthesizing Fe-SAC. In order to monitor its practical application, the authors have fabricated a H_2-O_2 PEMFC, which delivered a power density of 823 mW cm^{-2} and a current density of 0.85/3.34 A cm^{-2} at potentials 0.6 /0.2 V, respectively. The high performance ascribed to the atomically dispersed Fe-single atoms stabilized with Fe-pyrrolic-N_4 structure and N-doped carbon nanosheets.[176] Yang et al.[248] reported Fe-SACs on porous NC matrix (Fe-SAs/N-C) through the versatile molecule-confined carbonization approach based on the wet-chemical procedure with 3.5 wt% of metal loading on N-doped carbon framework. The Fe-SAs/N-C catalyst showed open-circuit voltage of 0.89 V and 0.83 V, and power densities of 680 and 350 mW cm^{-2} for H_2/O_2 and H_2/air fuel cell operations. The improved performance of the electrocatalyst is mainly attributed to the reaction mechanism involving individual atomic Fe-N_x active sites than C-N_x.

Recent studies also showed the improved ORR performance of Co-based (Co-N-C) catalysts and stability at the MEA level.[249] For instance, Co-doped MOFs derived single Co-atom coordinated with nitrogen atoms displayed high ORR performance. The results obtained from AC electron microscopy fused with X-ray absorption spectroscopy proved the existence of Co-N_4 coordination in the catalyst. The fuel cell operation further verified that catalyst activity and stability are attributed to the existence of uniformly dispersed CoN_4 active sites packed in 3D porous MOF-derived carbon, without any inactive Co NPs.[249] He et al.[208] studied the Co-N-C@F127 catalyst fabricated on the MEA surface with 4.0 mg cm^{-2} of catalyst loading. At 0.8 V, the cell's open-circuit voltage was 0.92 V, while the current density was 30 mA cm^{-2} at 0.8 V. Meanwhile, at 0.4 V, the current density was 2.2 A cm^{-2}. Notably, the greater performance of the cathode was also achieved during 100% of relative humidity (RH) at high voltage (40.7 V) compared to Fe-N-C-based electrocatalysts. Nevertheless, the Co-N-C@F127 electrocatalyst exhibited comparable output with a high power density of 0.87 W cm^{-2} at medium voltages (0.5–0.7 V) for PEMFC operation. Moreover, the Co-N-C@F127 cathode also showed improved performance than Fe-N-C catalyst at a comparatively low RH (60%), giving a clue that overflowing of water is a severe problem of cathode owing to the micropore feature of catalyst. The performance of the fuel cell was further monitored under H_2/air condition at 1.0 bar pressure. The polarization profiles observed at 100% RH condition indicated a substantial loss in mass transportation, which may be ascribed to the significant issue of water flooding. However, the Co-N-C@127 showed increased activity at 60% of RH under all the voltages applied. The durability of the Co-N-C@F127 catalyst in the MEA was further evaluated for 100 h at a cell voltage of 0.7 V using H_2 and air at 1.0 bar and two different RHs which indicated the significant initial performance loss.[208] Gang et al.[219] described the fine-tuning of well-defined ZIF precursors by varying the Co-content and pyrolysis temperature. When 20Co-NC-1100 was employed as cathode with catalyst loading of 4 mg cm^{-2} for H_2/O_2 fuel cell, a maximum peak power density of 0.56 W cm^{-2} was observed, as compared to PANI-Co-KJ and PANI-Fe-KJ cathodes that performed less than 0.3 W cm^{-2}.[219] Thus, the precisely controlled metal content in precursor by overall chemical doping procedure, which established a worthy understanding of structural–synthesis–property correlations. Li et al.[250] reported a two-step reaction protocol by using Mn-doped ZIF-8 as a precursor with increased density of Mn sites (>3 wt% by ICP). A H_2/O_2 acidic fuel cell equipped with 20Mn-NC-second delivered the higher power density of 460 mW cm^{-2}. The 20Mn-NC-second exhibited a superior activity as compared to previously reported Fe-NC-based electrocatalysts (derived from PANI in 2010); the 20Fe-NC-second also presented inferior activity.[250]

In line with single-metal catalysts, the dual-atom electrocatalysts are also studied for PEMFCs and showed competing results with Pt-based counterparts. For example, a hollow carbon-derived framework with porphyrin-like dual Fe-Co sites was fabricated by Li et al.[155] using Zn/Co binary metal MOFs

as a base while Fe-ions as doped species. The authors claimed that various transformations occurred during the heat treatment in which Zn^{2+} ion vaporized because of the lower boiling point of ≈1173 K and the Fe^{3+} species reduced by as-transformed carbon, lead to geometric structure modification. Furthermore, Fe species motivate the decomposition of M-I-M (metal-imidazole-metal) bonding and generate voids in MOF assembly, which established bonding with adjacent Co-sites to form dual Co, Fe sites. Furthermore, a H_2/air fuel cell with (FeCo)/N-C cathode performed a power density close to 505 mW cm^{-2} at 0.42 V, exhibiting long stability for 100 h.[155] Yang et al.[251] prepared atomic Co/Zn double-sites embedded on N-doped carbon nanofibers (Co/Zn-NCNF) by electrospinning and post-heat treatments. The power density of 0.603 W cm^{-2} was measured in a H_2/O_2 fuel cell with Co/Zn-NCNF, maintained at ≈0.65 V of long-term stability even after 150 h. The DFT simulations explored that Co/Zn-NCNF comprised of the $N_2CoN_2ZnN_2$ configuration as main active site, contradictory to typical Co-N_4 or Zn-N_4 sites; thus during ORR-pathway, provide a tendency of lowering the dissociative barrier of *OOH intermediate. It is further found that the ORR performance was mainly inclined towards proton transfer and O_2 diffusion at lower potential range, suggesting a $4e^-$ pathway followed by Co/Zn-NCNF, while Co-NCNF and Zn-NCNF are likely to obey a $2e^-$ pathway.

Moreover, a bimetallic (HC-5Co95Zn) catalyst was investigated by the Tsiakaras group with a peak power density of 412 mW cm^{-2}, and this superb PEMFC performance of HC-5Co95Zn can be assigned to the role of dual Co, Zn sites coordination and the unique porous feature of HC-5Co95Zn.[29] Moreover, Wang and co-workers[155] studied a dual metal (Fe, Co)/N-C hollow carbon-derived catalyst with high performance for single fuel cell operation under both H_2/O_2 and H_2/air conditions. The (Fe, Co)/N-C electrocatalyst showed the highest peak power density of ≈0.85 and 0.98 W cm^{-2} for H_2/O_2 fuel cell at a partial pressure of 0.1 and 0.2 MPa. Further, the authors reported that this ADMC with dual Fe, Co sites displayed long-term stability performance carried out for 100 h during cyclic voltammetry test with 50 000 cycles for H_2/air single-cell operations. This research report also revealed that O_2 mass transport problems may be due to the use of pure O_2 as the oxidant for H_2/O_2 single cell with catalyst loading of ≈0.77 mg cm^{-2} (Fe, Co)/N-C at the cathode and 0.1 mg cm^{-2} (Pt/C) at the anode. Further, the current density > 550 mA cm^{-2} at a cell voltage of 0.6 V and a peak power density of 505 mW cm^{-2} at 0.42 V were achieved.[155]

These findings significantly revealed the importance of dual Fe, Co sites during ORR-pathway. Further, DFT results were carried out to estimate the potential surface energy during ORR pathway, which verified the successful dissociation of O–O bonding on the Fe-Co site (**Figure 11**e). It was observed that the (Fe, Co)/N-C catalyst displayed the far lower value (0.25 and 0.02 eV) of separation block for O_2 and OOH into O and OH, as compared to single Co SAs/N-C or Fe SAs/N-C site. The fast cleavage of O–O bonds occurred because Fe-Co single-site possesses high O_2 adsorption and enough activation of O–O bonds from 1.23 to 1.40 Å in gas phase. Further, it was found that the rate-limiting step is the hydrogenation of the adsorbed OH to H_2O, which has an activation barrier of 0.26 eV, compared to the O–O bond breakage on Fe/N-C (0.65 eV) and Pt-based catalysts (≈0.80 eV). The OH on dual sites in these samples became modifying ligands, which fit with the DFT findings. To produce high activity for ORR and high selectivity for four-electron reduction, the (Fe, Co)/N-C dual-site can reduce the barrier of O–O bond cleavage.[155,252]

Nevertheless, the reported Fe-N-C electrocatalyst displayed the highest peak power density during fuel cell operation only with the higher catalyst loading as compared with Pt/C. Apart from that, kinetic activity per volume of 300 A cm^{-3} @0.8 V iR-free is another main objective for MEAs consuming non-Pt catalysts as per DOE plans.[11,246] Here, the volumetric

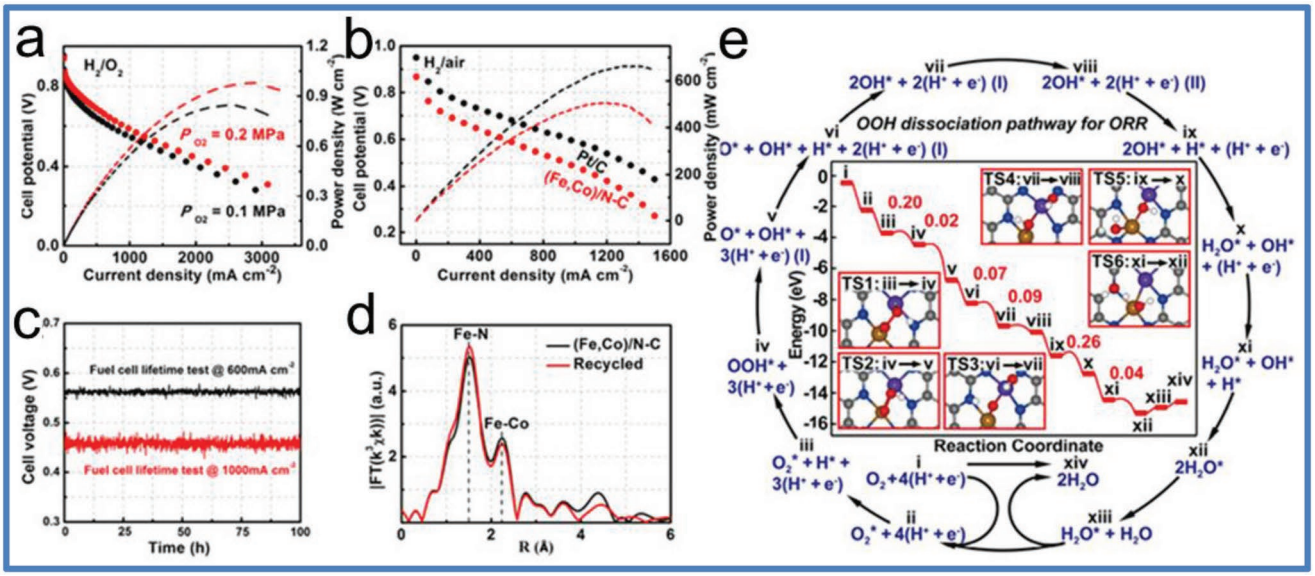

Figure 11. a) H_2/O_2 fuel cell polarization curves. b) H_2/air fuel cell polarization curves. c) Stability of (Fe,Co)/N-C in a H_2/air fuel cell. d) Fe K-edge EXAFS fitting curves of (Fe,Co)/N-C and (Fe,Co)/N-C after stability performance. e) The DFT study of intermediate's energies and transition states during ORR mechanism at (Fe,Co)/N-C. Reproduced with permission.[155] Copyright 2017, ACS.

performance of ORR was related to catalytic activity as barriers for mass transportation were linked with electrode thicknesses; that's why more thickness of MEA leads to inferior mass transportation and causes a decline in power density.[46] With current state-of-the-art Fe-N-C catalysts, the volumetric current densities remain much below from DOE's objective. More details may be provided by considering that higher carbonization temperatures (700 °C or above) lead to a greater degree of hydrophobicity for Fe-N-C catalysts, but porous Fe-N-C catalysts serve to increase the surface areas and to promote mass transport. Furthermore, because of the higher density of the bulk, these catalysts will be thicker than Pt/C, with the same loading amount.[253] Hence, it is challenging to fabricate NPMC catalyst for achieving or surpassing the performance of benchmark Pt/C electrocatalyst without compromising the thickness (**Table 1**).

5. Durability and Degradation of M-N-C Catalysts

The challenge of nonprecious catalysts (NPC) for ORR has been remained the main focus in literature reports, even though so far, these catalysts could not compete with the Pt-containing catalysts.[263–267] Inspired by nature (chlorophyll, cytochromes, and hemes), the primary focus of NPC remained the performance enhancement of M-N-C catalysts.[21,268] The metal-coordinated with four N atoms, macrocyclic compounds are not cost-effective for the synthesis and also unstable in acidic electrolytes; however, the synthesis of analogous M-N_x active sites through pyrolysis of metal and C/N sources is a possible solution both for cost and stability.[21,87,131,138,181,268,269] Several N/C sources including ammonia, acetonitrile, aniline, pyrrole, cyanamide, etc. have been used to generate M-N_x type active sites.[29,177,181,186,268–272]

The most active metal is iron, even though some cobalt-based catalysts also showed similar activity. But the so-called Fenton reaction via in situ production of H_2O_2 declines the capability of iron-based catalysts for long time stability operations. For producing an active catalyst and enhanced stability, the optimal synthesis methodology includes thermal treatment such as pyrolysis at a temperature between 750 and 950 °C.[29,43,55,84,113,185] At lower pyrolysis temperatures, the subsequent low ORR activity gives lack of active site creation, and higher pyrolysis temperatures gave lower than optimal activity owing to diminishing catalyst surface area.[113] It has been hypothesized that the degradation rate of PEM fuel cells with M-N-C cathodes is related to the presence of micropores with diameters less than 2 nm, as these micropores have an enormous surface area and a large microporous surface area which tends to provide both improved initial performance and a quicker degradation rate.[45] The sources of N-dopants have been tailored to increase activity: heteroatomic aromatic compounds further improve graphitization, and sources like cyanamide, formamide are considered for boosting the performance through pore-forming or isolation of metallic sites.[47,78] Moreover, ZIFs normally add Zn ions, which serve to heighten the surface area after pyrolysis by evaporating and creating pores, hence helping to maximize the total number of metals (Fe, Co, and Mn) sites. Despite these improvements, still, a big challenge of durability relies. Nevertheless, some better results are found in current accelerated stability tests (AST) in three-electrode system. For instance, He et al. studied a new atomically distributed Co-N-C@F127 catalyst comprised of considerable CoN_{2+2} sites, being active and thermodynamically suitable

Table 1. The Fuel cell performance based on single /dual doped catalysts.

Catalyst	Active site	Open circuit potential [V]	Power density [mW cm^{-2}]	Stability	Refs.
C-FeHZ8@g-C_3N_4-950	Fe-N_4	0.98 (O_2)	628 (O_2)	8 h	[254]
Fe SAs/NPS-HC	Fe-N_4	0.96 (air)	333 (air)	–	[252]
Fe SAs/N-C	Fe-N_4	0.89 (O_2)/0.83 (air)	680 (O_2)/350 (air)	–	[248]
FeSA-G	Fe-N	–	325(O_2)	100 h	[255]
1.5Fe-ZIF	Fe-N_4	0.98 (O_2)/ 0.95 (air)	660 (O_2)/360 (air)	100 h	[256]
Fe-C-N_{950}	–	0.80 (O_2)	680 (O_2)	–	[257]
FeN_4/HOPC-c-1000	Fe-N_4	0.99 (O_2)/ 0.91 (air)	660 (O_2)/420 (air)	100 h	[258]
TP1@Z8(SiO_2)-650-C	Fe-N_4	0.91 (air)	420 (air)	–	[259]
Co-N-C@F127	Co-N_4, Co-N_{2+2}	0.92 (O_2)	870 (O_2)	100 h	[260]
CoNC-ArNH_3	Co-N_4	0.88 (air)	440 (O_2)/221 (air)	20 h	[128]
20Co-NC-1100	Co-N_4	0.95 (O_2)/0.89 (air)	560(O_2)/280 (air)	100 h	[219]
Co@SACo-N-C	Co-N_x	0.91 (O_2)/0.91 (air)	420(O_2)/230 (air)	10 h	[261]
20-Mn-NC-second	Mn-N_4	0.95(O_2)	460 (O_2)	100 h	[250]
Ce/Fe-NCNW	Fe-N_4-O	1.02(O_2)	496 (O_2)	–	[262]
(FeCo)/N-C	(Fe-Co)N_6	–	980 (O_2)	100 h	[155]
FeNi-N_6	FeNi-N_6	0.82(O_2)	216 (O_2)	–	[236]
Zn/CoN-C	(Zn-Co)N_6	–	705 (O_2)	8 h	[155]
Co/Zn-NCNF	(Zn-Co)N_6	0.884(O_2)	603(O_2)	150 h	[251]

for the four-electron ORR corridor with very low production of H_2O_2. The Co-N-C@F127 catalyst displays an extraordinary ORR activity with improved stability in the acidic medium up to 100 h of continuous operation.[208] The stability test of single cobalt catalyst (Co-N-C) derived from bimetallic (Zn/Co) MOF, accomplished both potential cycling (0.6–1.0 V, 50 mV s^{-1}) and chronoamperometry test operated at 0.7 V in O_2-saturated 0.5 M H_2SO_4. One of the most stable catalysts in the market that able to maintain its integrity with just a 30 mV drop in $E_{1/2}$ after 10000 cycles, as opposed to an 80 mV drop for a PANI-derived Fe-N-C catalyst after 5000 cycles. In addition, chronoamperometry operated at a high potential of 0.7 V for the duration of 100 hours maintained excellent initial activity retention, with an 83% retention of initial activity. Following the stability test, the catalyst was studied with HAADF-STEM analysis and was seen to preserve its 3D carbon architecture after 10 000 cycles, indicating sufficient stability of the catalyst. Additionally, the Co atoms were still distinctly discernible and could be seen distributed throughout the carbon planes boundaries. The atomic-scale visualization of the EELS in the atomic scale demonstrated the co-occurrence of Co and N, therefore supporting the idea that the catalyst's ORR stability is linked to the coordination of atomic Co and N sites.[249] Choi et al.[273] studied that Fe-N_xC_y moieties are active for 4 e^- ORR pathway with very low production of H_2O_2. They also studied the peroxide reduction reaction (PRR) and clarified the relation between Fe nanoparticles and PRR. The catalyst consists of various relative contents of Fe-N_xC_y moieties and Fe particles covered in N-doped carbon layers (0–100%) which demonstrated that both types of sites are active even though in average level, toward H_2O_2 reduction. For enriching the ORR-pathway, Fe-N_xC_y moieties are more selective than Fe NPs in N-doped carbon.[273] Shah and co-workers also studied that Fe-N_x active for PRR and decreases the peroxide production (less than 3%). The AST test (10 000 cycles) in 0.1 M $HClO_4$ demonstrated the greater stability with a little change in half-wave potential.[25] On the same lines, Zhang and co-workers[206] also reported the best performing Fe-ZIF derived single Fe atom (Fe-N_4) catalyst, which produced a negligible H_2O_2 yield (less than 1%) and showing 4e^- reduction pathway. The AST cycling test (0.6 to 1.0 V in O_2-saturated 0.5 M H_2SO_4) on Fe-ZIF catalyst (50 nm) indicated a greatly improved stability with a slight deviation of 20 mV in E_{onset} after 10 000 cycles. The greater decomposition of Pt/C was observed because of the dissolution/aggregation of Pt nanoparticles on supports.[206]

5.1. Current Durability Status of PEMFCs

Improved performance of the PGM-free electrocatalyst fuel cell has been obtained by controlling the pore structure of the catalyst. Macro/mesopores help in the transportation of products and reactants from/to the NPC active sites hosted on the micropores.[46,274] A lot of processes have been developed to get this hierarchical pore structure, such as mesoporous templates,[275–277] MOFs,[278] N-precursors acting as formers.[279] Nonetheless, some research studies showed the strength of electrocatalyst under fuel cell testing conditions. Choi's group presented a study of performance loss during fuel cell operation by fabricating the electrocatalysts derived from the polyaniline and phenanthroline as pore-forming agent.[280] This study reveals that approximately 25% decline in current density was obtained after constant voltage (0.4 V) for 4 h. Zhang and co-workers studied ZIF-8 derived catalyst at 0.6 V for 15 h and also observed an abrupt decline in activity.[281] However, Serov's group prepared electrocatalyst through sacrificial support strategy, which demonstrated strong durability (100 h) at constant voltage of 0.65 V.[276] Similarly, He and co-workers[208] also presented highly stable catalysts at 0.7 V, the Co-N-C@F127 performed good during fuel cell (H_2/air) operation for 100 h at 1.9 bar pressure. However, the substantial initial performance loss was observed at a relatively high voltage (i.e., 0.7 V) which is still far better than Fe-free cathodes and other PGM-free electrocatalysts. This decrease in performance may be attributed to the surficial oxidation of catalyst along with the cathodic three-phase degradation. Presently, the main target is to prepare a PGM-free cathode for long-term stable operation carried out at relatively high voltages. Wu et al. reported a Fe-Co electrocatalyst demonstrating high stability for 700 h at 0.4 V.[282] Several deprivation mechanisms had been hypothesized with numerous degradation factors, such as radical (hydroperoxyl) attack/generation,[283–285] demetalation,[286–288] poisoning of active sites,[289] corrosion,[176] and flooding of micropores,[280,281] however, the major performance failure occurred during the operation of fuel cells.

5.2. Proposed Degradation Mechanisms

The degradation mechanism is proposed on the same rational design relative to PGM-based electrocatalysts, which consist of two main classifications; 1) atomic-scale degradation of active sites and 2) macro and mesoscale degradation affecting the catalyst layer structure. A further illustration of the degradation mechanism of PGM-free ORR catalysts is exemplified in **Figure 12**.[55] By considering the example of Fe-N_4 active sites, the zig-zag edge structure formed with *OH ligand. The first dissolution of metal center, called "demetalation" altered the active sites and leading to the activity loss; following the N-C degradation which altered the microenvironment of the active sites, resulting in the active site poisoning and reduced binding capacity of O_2 at active sites (left column). In the parallel process, carbon corrosion reduces the electrical conductivity/contact, loss of porous structure and mass transfer problems and finally removing the active sites (right column).

5.2.1. Atomic-Scale Degradation

Although, a particular environment of the NPC active sites designed through pyrolysis still remains the topic of strong discussion, nonetheless, carbon-entrenched M-N_xC_y assemblies were interrelated to greater ORR performance.[94,126] Practically, it is a challenging task to precisely prepare M-N_x structures. Although current synthetic processes produce several M-N-C structures but few are found to be spectators.[176,290] Hence, it is important to recognize the active site moieties to exactly recognize the degradation mechanism. Gupta et al. first established

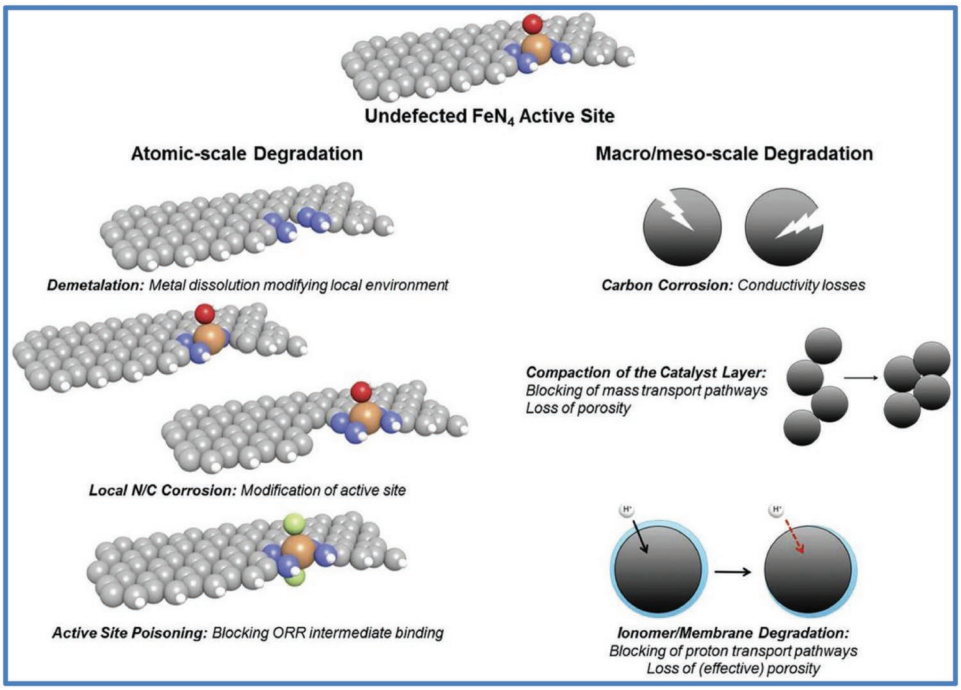

Figure 12. Proposed mechanism of degradation during ORR performance for PGM-free electrocatalysts. Reproduced with permission.[55] Copyright 2019, Wiley.

a relationship between the performance loss and leaching of active sites.[268] The substantial loss in performance of Co-based catalyst was detected and attributed to the high solubility of cobalt species in acidic media. After that, Lalande and Fauber's group studied the effect of heat treatment on the stabilization and activity of the Co and Fe based non-PGM catalysts.[291,292] As a result, high activity was found in the pyrolysis range of 500–700 °C, where the N_4-metal chelates were the main source. The catalyst produced at high temperature (900–1000 °C) exhibited good stability. The discovery of graphitic layers around the metal centers and their protective qualities were uncovered, and researchers concluded that these protective layers sheltered the metal active sites from leaching. A detailed study has recently been conducted to understand the demetalation mechanism by Choi et al.[176,288] A study team used operando spectroscopic methods, ICP-MS and DEMS, to measure the extent of Fe demetalation after 2000 and 5000 cycles at 0.1–0.4, 0.6–0.9, and 1.2–1.5 V at temperatures 20 °C, 50 °C, and 70 °C, respectively. Two types of demetalation processes were observed; 1) lower potential demetalation (less than 0.70 V vs RHE), and 2) higher potential demetalation (more than 0.9 V vs RHE). First demetalation type had no severe effect on the ORR activity, while at a potential higher than 0.9 V versus RHE had substantial loss of activity.[176] These types of demetalations were named as; 1) ineffective demetalation, and 2) effective demetalation and concluded that ineffective demetalation leached out Fe species, i.e., demetalation of inactive Fe species and effective demetalation may be ascribed to the destruction of active Fe-N_xC_y moieties as a result of carbon corrosion. In the presence of a catalyst, it has been reported that for the removal of inactive species even after the preliminary acid treatment, there is a chance of iron loss in the Fe-N-C catalysts. But this loss of iron can be the result of carbon oxidation by high overpotentials and/or oxidative attack of peroxide or simple demetalation in the acidic medium.[283,293,294] The leaching of inactive Fe species will not give any impact on the stability of the Fe-N-C catalysts but could be detrimental to the PEMFC system. In another study, to show the removal of the inactive iron species from the Fe-N-C catalysts, a team of researchers devised and successfully implemented procedures.[295] These processes include: i) preparation of Fe-N-C catalyst without Fe particles, and ii) removal of exposed Fe particles through post-synthetic procedure which includes external potentiostat or an internal reducing agent ($SnCl_2$).

The fuel cell operation includes more complex degradation mechanisms. Recently, Chenitz et al.[287] proposed: i) a double exponential performance loss (a rapid one followed by a much slower one), and ii) the rapid performance loss is due to a site demetalation process. This fast site demetalation was very recently confirmed by Jaouen et al.[296] who detected by Mossbauer spectroscopy and reported two types of sites S1 and S2 in a Fe-based catalyst, further found that the site S1 was demetallating, while S2 was stable in their catalyst. Choi et al.[288] proposed that the macro-scale degradation processes tend to lower the performance, for example, hydroperoxyl radical generation and oxidation of catalyst surface.

5.2.2. Macroscale Degradation

Carbon corrosion is considered as a major cause for meso- and macroscale loss in performance. Further, the corrosion can also lead to the dissolution of active sites, structural conductivity failure, with the removal of additional active sites from

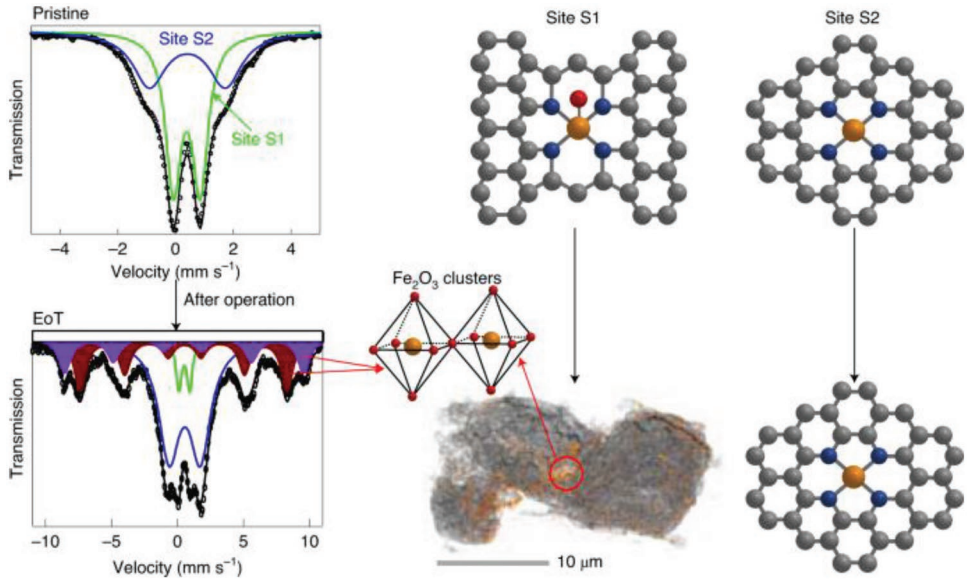

Figure 13. Degradation of Fe-N-C active sites (S1, S2) during the fuel cell operation. Reproduced with permission.[296] Copyright 2020, Springer Nature.

the boundary of triple phase, which is necessary for ORR. Furthermore, porosity reduction due to the carbon corrosion, and thus compaction of the catalyst layers will further lead to a decrease in the available and exposed active catalytic sites which ultimately cause transport issues. Several reports have been published in which the mechanisms of carbon corrosion are studied as carbon support of PGM PEMFCs.[297,298] A considerable amount of H_2O_2 can be produced on the carbonaceous support which may tend to increase the corrosion process at a lower potential, whereas carbon defects can be corroded at a higher potentials. Such types of effects have been shown to be aggravated with increased in the humidity and temperature. While carbon corrosion considered as a main culprit for activity loss of the PGM-free materials, herein two important factors to better understand the stability performance between PGM-free and PGM catalysts are: 1) the PGM-free type catalysts are more graphitized as these are usually synthesized at comparatively high temperature up to 1100 °C, as a result, less heterogeneous carbon structures can be obtained as compared to carbon black used as a support for PGM systems, and 2) the absence of Pt, as Pt is considered to be responsible for the activation of corrosion mechanism of Pt/C type electrocatalysts.[297,299] Recently published report by Zhang et al.[281] suggests that the electro-oxidation of carbon matrix considerably increased the surface oxidation, which as a result increases the hydrophilicity of overall catalyst's surface causing micropore flooding, thus, significant loss in the performance of the catalysts was observed.[281] However, in a more systematic approach reported by Choi et al.,[280] a slight increase in the wetting of the catalyst's layer was noted by faster AST operation, but the wetting cannot be exclusively considered liable for the overall activity loss. The activity losses were more prominent in the kinetic regions, where they are believed due to the degradation of active sites caused by increased hydrophilicity oxidation of Fe-N_xC_y.[280] Another important problem with such types of catalysts can be understood in the fuel cell process which is the probability of Fenton-type side reactions releasing hydroperoxyl radicals and degrading catalysts, membrane, ionomer. Some of the published researches suggest that the exposure of a catalyst to the H_2O_2 can lead to a minimal loss of PGM-free catalytic active sites, whereas the main cause of decreasing activity is surface oxidation of electrocatalyst.[281,283,285] However, further studies are required for better understanding the generation of H_2O_2 toward the catalytic performance in the fuel cell. Kumar et al.[300] investigated the degradation mechanism of Fe-N-C catalyst via AST testing in the presence of Ar- and O_2-saturated electrolytes in acidic media. The spectroscopic results showed the carbon corrosion and formation of Fe-oxide after AST in O_2-saturated and confirmed unpredicted carbon corrosion belonged to reactive oxygen species produced between H_2O_2 and Fe sites via Fenton reactions. From the above discussion in the section, it can be concluded that the mentioned two or more degradation mechanisms at both atomic- and macroscale level, such as demetalation and carbon corrosion can concurrently occur within the cathode layer of catalyst. Recently, Li et al.[296] used in situ, operando and end-of-test (EoT) spectroscopies to study the degradation of Fe-N-C catalysts during PEMFC operation. In situ and ex situ[57] Fe Mössbauer spectroscopy revealed that Fe-N-C catalysts initially comprising two distinct FeN_x sites (S1 and S2) degrade via the transformation of S1 into iron oxides while the structure and number of S2 were unmodified (**Figure 13**). Structure-activity correlations drawn from end-of-test[57] Fe Mössbauer spectroscopy reveal that both sites initially contribute to the oxygen reduction reaction activity, but only S2 substantially contributes after 50 h of operation.

Moreover, one degradation process primarily imitates the secondary degradation mechanism. For example, demetalation involved in the hydroperoxyl radical generation ultimately leads to the degradation of subsequent membrane/ionomer. A wider scope of fuel cell catalytic activation mechanisms is recommended to further understand the degradation processes.

5.3. Development of Techniques to Investigate Degradation Mechanisms

Different poisons have been investigated as probes to overcome the active site challenges. For example, the idea of heme-like structure (a metal centered) in an active site structure can be successfully[111] and unsuccessfully[110] poisoned by using CO as a probing agent at room temperature and at lower temperature respectively. The active sites in the catalysts can be calculated using a correlation of probe molecules with the actual loss in determining the catalytic activity after poisoning. By the comparative study of initial and final performance of catalyst via molecular probes, which can help to solve the vulnerable active sites loss during the catalytic activity. These efforts are only fruitful by understanding the actual poisoning mechanism of catalysts and the selective binding of probe molecules on the active sites. Recently, Malko et al. reported Fe-N-C catalysts, which were poisoned and then recovered in terms of performance by using radicals as probes such as NO_2^- and NO.[105] In another effort, the binding of NO to Fe^{2+} was successfully reported by Zelenay et al. and Kneebone et al. with an increase in the coordination number which was also detected in Fe-specific nuclear resonance vibrational spectroscopy (NRVS) measurements.[114]

To understand the key mechanism of degradation on macroscale level such as ionomer degradation and carbon corrosion, different morphological analysis techniques are commonly employed before and after the probing test such as, X-ray computed tomography (XCT),[301] electron microscopy/tomography,[302,303] stained ionomers using nano-CT,[304] and F^- mapping.[305] Mössbauer spectroscopy is also used to study the demetalation of catalysts,[296,306–308] for example, Xie et al.[306] demonstrated extensive degradation mechanism by using XAS and Mössbauer spectroscopy. In another study, in situ Fe K-edge absorption spectra were recorded during the continuous operation of the fuel cell and the observed changes in spectra suggested the demetalation process.[309]

Moreover, unlike in PGM materials, the PGM-free catalysts required other characterization techniques, including the imaging and the analytical, to decouple the generation of CO_2 at high potential. CO_2 is generated from ionomer and membrane decomposition because of harmful hydroperoxyl radical formation during catalytic operations. For example, CO_2 emissions can be measured by using non-dispersive infrared spectroscopy (NDIR) in a coupled mode with F^- and Fe emissions from ion-exchange chromatography and inductively coupled plasma measurements which can help in defining the more active carbon corrosion mechanism and degrading materials (ionomer vs catalyst). Additionally, in situ, water imaging within the catalyst layer via neutron radiography will be able to clarify the effect of the wettability of the carbon during catalytic operations.[310]

5.4. Modeling of Possible Degradation Mechanisms

Using quantum chemical simulations, the experimental efforts can be improved and alleviate the performance loss in PGM-free electrocatalysts. These types of methodologies generate atomic-scale structure, which is experimentally tough to produce heterogeneous electrocatalysts (PGM-free M-N-C type).[311] The understanding of the probe molecules binding to various atomic-scale structures is essential in order to recognize the specificity of the probe molecules.

When the theoretical predictions were modified with regard to the proposed active site structure (that could happen with carbon corroded or surficial oxidation), the new theoretical predictions changed the proposed active site structure and affected the catalytic performance. The kinetics of bond breakage in the expected degradation can also be tested to understand the mechanism of most susceptible removal of atoms in a given structure.[312] Furthermore, a mesoscale simulation of the catalyst layer may offer invaluable insight into the possible change in the porosity and, therefore, the change in the catalyst activity caused by the fuel cell parameters.[313,314] By combining these approaches would greatly help in understanding the true degradation mechanisms and interpretation of performance loss in PGM-free electrocatalysts.

5.5. Catalytic Poisoning

Catalytic poisoning is one of the most important areas with respect to the performance loss of catalyst. The small amount of poisonous species can result in a drastic performance loss. Therefore, considering its drastic effects on catalytic performance, the poisoning of catalysts would be discussed in a separate section here.

Although PGM-free electrocatalysts have been considered as superior performers with a number of poisons as compared to PGM catalysts.[315,316] Though, the poisoning probability of active sites is still high as already reported in several researches.[109,289,317,318] In a study, it is proposed by Herranz et al.[289] that the poisoning of active site can be risen by the surface nitrogen protonation and decreased in the anion binding during ORR activity. It was perceived that under low pH catalytic conditions Fe-N-C catalysts with active $Fe-N_4$ cites, the poisoning can occur by surface nitrogen protonation and which is then not involved in $Fe-N_x$ coordinated structures. Some strong electrostatic connections with anions were poisoned, and the $Fe-N_4$ active site was blocked as a consequence. As a result of adsorbates, it is possible to poison active sites in an indirect manner.[319] When any adsorbate is present near the active site, it affects the binding conditions for ORR intermediates, either by interfering with the steric arrangement of the active site or by changing the local electronic structure of the site. At the cathode of air/H_2 PEMFCs, oxygen is provided by the surrounding atmosphere.[27] The gas filters are crucial to fence the air pollutants; as a result, these PEMFCs need the additional expense and have poor overall energy efficiency.[320,321] Deng and co-workers observed that the cell voltage of Fe/Fe_3C@Fe-N-C at ORR catalysts in PEMFC tests was stable with 10 ppm SO_2 in the air inlet, whereas the cell voltage of commercially available Pt/C was dropped about 40% in 1 h.[322] Among other air pollutants, CO is the most poisonous to the noble-metal electrode and must be attention-seeking for researchers. It was authenticated lately by Zhang and co-workers that adsorption of CO and oxidation were very subtle to active site structures[323]

Using DFT probing and calculation, they have simulated various Fe-N containing active sites including Fe-N_4 porphyrin-like CNT (T-FeN_4), Fe-N_4 porphyrin-like graphene (G-FeN_4), Fe-N_3 pyridine-like CNT (T-FeN_3), and Fe-N_2 nanoribbon (R-FeN_2). They found that the CO adsorption was more prominent at T-FeN_4 and G-FeN_4 sites, as compared to O_2, but the oxidation to CO_2 barely occurred.[323] In another report, Zhang and co-workers reported that all sites with nitrogen-doped carbon (CN_x) showed less CO adsorption and more O_2 adsorption.[109] From the results of DFT calculation, it was revealed that the CO binding energy at Fe-N-C sites was almost similar to that at Pt (111) but was weaker than that of the binding energy of O_2 at Fe-N-C sites, which suggested that the Fe-N-C electrocatalysts were more partially tolerant to CO. They concluded that the CO tolerance to Fe-N-C was much superior as compared to commercial Pt/C, but it was at the same time inferior to CN_x-type materials. These results were also concluded by electrochemical tests and diffuse reflectance infrared Fourier transform (DRIFT) spectroscopy.[109]

NO is another well-known air pollutant. Malko et al. reported an effective poisoning approach and then recovered performance of the Fe-N-C catalyst by utilizing molecular probes of NO_2^- and NO.[105] In another study, the binding of NO to Fe^{2+} was separately studied by Zelenay et al., and Kneebone et al. reported the noticeable increase in the coordination number by Fe-specific nuclear resonance vibrational spectroscopy (NRVS) characterizations.[114] Hence, this so-called probing material is actually a hidden enemy of the Fe-N-C-based catalysts.

Li and co-workers[324] observed that the Fe-N-C catalysts demonstrated high phosphate tolerance in 5.0 M H_3PO_4 due to the segregation of Fe nanoparticles from electrolyte using graphitic layers and finally sheltered through the adsorption PO_x. Holst-Olesen and co-workers reported the DFT calculation of anions such as ClO_4^-, SO_4^{2-}, PO_4^{3-}, Cl^- adsorption on Fe-N_4 moieties and observed that the binding energies of ClO_4^- and SO_4^{2-} were weaker as that of H_2O; therefore, $HClO_4$ and H_2SO_4 electrolyte caused a little effect on ORR activity.[325] On the other hand, the binding energies of PO_4^{3-} and Cl^- on Fe-N_4 effectively increase the barrier performance of the rate-limiting step, these sites were strong enough to alter the thermodynamic barrier.[324] The robust adsorption properties of PO_4^{3-} and Cl^- affected the ORR performance of Fe-N_4 species; however, the thermodynamic obstacle for the rate-limiting step in case of H_3PO_4 was depressed. Hence the ORR performance was enhanced; while the thermodynamic barrier performance of the rate-limiting step in HCl electrolyte was raised and inhibited the ORR activity. These ORR activities of Fe-N_4 moieties in different electrolytes were also analyzed by experiments.[326] Similarly, the influence of Cl^- on Fe-N_4 moieties reported by Hu et al.[327] According to these findings, the aerosol salts may harm the PEMFCs in the presence of highly concentrated Cl^-.

Najam et al. presented a breakthrough in the field of carbon-based high-performance catalysts with antipoisoning approach[23,27,328] and proposed first theory that "the addition of phosphorus atoms into M-N-C or N-C can improve both structural stability as well as antipoisoning performance" as shown in **Figure 14**. A strong antipoisoning effect in the environment of different anions, SO_x, NO_x, and PO_x, was observed for 3D-Fe-PNC. However, 3D-Fe-NC and Pt/C (20%) showed decrease catalytic activity in the presence of SO_x, PO_x, and PO_x. Moreover, 3D Fe-PNC also showed good stability in 1 M H_3PO_4 under varying temperature conditions from 25 to 50 °C. In contrast, a straight decline was observed by Pt/C (20%) and Fe-NC electrocatalysts under the same condition.[23] Furthermore, a new series of carbon material (PNC) co-doped with P, N were prepared using the mixtures of polydiaminopyridine (PDAP) and phytic acid followed by pyrolysis. The half-wave potential of 0.79 V was observed by PNC in 0.1 M $HClO_4$. The ORR activities of PNC were all steadily stable in the presence of SO_3^{2-} (50×10^{-3} M $NaHSO_3$), NO_2^- (50×10^{-3} M $NaNO_2$), and HPO_4^{2-} (50×10^{-3} M Na_2HPO_4), while the commercially available Pt/C was heavily poisoned under the same environment.[27] Wang's group[329] also observed a similar poisoning effect on commercial Pt and Pd-based electrocatalysts during ORR and proposed a new strategy to reduce the poisoning of Pd-based catalysts by alloying Pd with bimetals (PdBiCu) in the form of nanowires with ultrathin diameter. The PdBiCu nanowires showed the retention electrochemical ORR performance in the existence of SO_3^{2-}, NO_2^- and HPO_4^{2-}, whereas the commercial Pt/C and Pd/C were poisoned by decreasing the half-wave potential as well as mass activity.[329]

Hence, further studies are required to fully understand the role of heteroatoms in creating stable active sites in a non-noble metal catalyst during the ORR pathway using a simple and effective route.

6. Summary and Future Outlook

The high ORR performance for NPMCs has been attained through transition metal SACs and metal-nitrogen moieties coordinated with central Fe or Co atoms. Numerous materials are prepared through the carbonization of several precursors; however, the Fe-N_x/C-based catalysts are the supreme electrocatalysts. The synthesis of such metal–nitrogen complexes is the most challenging task due to the formation of side products during pyrolysis. These side products make it difficult to isolate the M-N_x /C active sites as a result, limit the ORR performance as well as reduce the probability to investigate the corresponding ORR mechanisms. Additionally, the generation of single atoms is normally ignored in the reported literature because the high yield of single atoms in M-N_x/C type materials remains challenging. Moreover, the MOF-based materials are considered as suitable precursors for the formation of SACs. However, novel synthesis techniques are required to increase the activity of M-N_x/C materials to further develop the ORR activity and stability as well. Furthermore, the stability of SACs is indeed to be enhanced in practical applications. Doping strategies are proposed to achieve improved stability via the generation of synergistic effects by improving catalytic ORR activity. One promising way is to partially substitute N-atom with other non-metal atoms (B, P, or S) into M-N_x/C type. As catalytic ORR performance and the M-N_x/C stability is greatly dependent on the central metallic sites as well as the coordinating environment, hence suitable modification of M-N_x/C structures is another favorable research route. Theoretical and experimental validation of results are required for understanding the mechanism of these SACs during ORR-pathway.

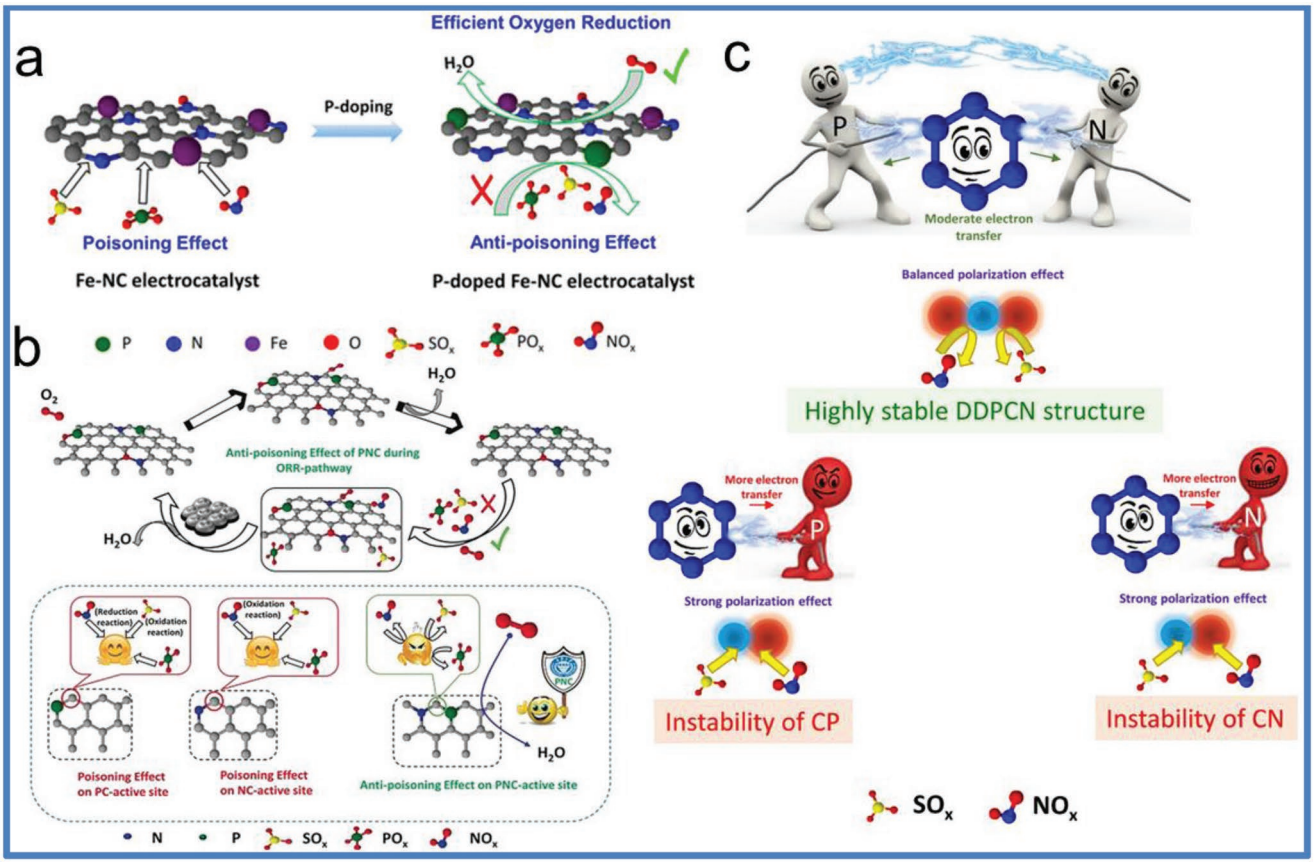

Figure 14. a) Poisoning and anti-poisoning effect of Fe-N-C and P-doped Fe-N-C actives sites, respectively. Reproduced with permission.[23] Copyright 2019, ACS. b) Graphical illustration of P-doping effect on NC performance against poisoning species. Reproduced with permission.[27] Copyright 2018, Wiley. c) Structural resistance of DDPCN, CN, and CP for the incoming small molecules. Reproduced with permission.[328] Copyright 2020, Elsevier.

The very next approach is the formation of highly dispersed diatomic transition metal-based catalysts. The alloying of two different metals in such a way that they can modify the properties of each other because of their interactions. Hence, the synthesis of active structures with two transition metal atoms of different elements bonds to each other. In these types of materials, the interaction between the central metal atoms and the coordinating environment provides more control toward ORR stability and catalytic activity.

The recent durability study discussed above reports the catalyst's degradation mechanism and the strategies to further understand the causes of performance decay in PGM-free electrocatalysts. In addition, it also highlighted the fundamental research gaps that must be filled for selective stability improvements. Some new characterization techniques are required to solve the intricacy of nonprecious metal catalysts and the mystery of the active site efficiency. Further theoretical models are also highly needed to further investigate the nature of the exposed active sites and their structure(s) in various situations. Moreover, in situ characterization analysis for MEA are required to establish/employ for understanding the degradation mechanisms. Already well-known probing strategies are needed to further improved for MEA studies to ensure the selective investigation of M-N_x active sites, not only to the MEA but also other elements, such as microporous layer (MPL), gas diffusion layer (GDL), or spectator species in the catalyst. The studies indicated that there is a lack of sole techniques to understand the in-depth degradation mechanism; therefore, various physical/chemical theoretical characterization methods should be studied together to understand the source of performance loss. Such techniques include XAS from which we can get the information of the metal center, oxidation state using XANES, the addition of coordination by extended XAS fine structure (EXAFS); in a combination of in situ XAS with electrochemical methods.[295] Fe-specific techniques such as Mössbauer spectroscopy and NVRS[330] would clarify the adjacent atoms/ligands and the changes in Fe metal center; and XPS provides the promising determination of chemical nature of key elements (C, N, and Fe).

Currently, Fe-based electrocatalysts are regarded as highly active ORR catalysts among other PGM-free electrocatalysts. Though, at the same time, progress in research is extensively carried out to prepare Fe-free or PGM-free materials in order to minimize the risk toward performance loss due to Fe-demetalation and Fenton reactions. The macroscale degradation mechanism will be suitable for Fe-free electrocatalysts, whereas the atomic-scale degradation mechanism depends upon the nature of metal, and therefore demetalation may be linked with redox potential window, which varies with different transition metals.

As a final point, there is no developed protocol available to monitor the aging performance of PGM-free catalysts such as potentiostatic hold, potential cycling, fuel cell conditions, etc. The real-time durability experiments are not only time taking but also consist of exhausted resources. Consequently, if the degradation mechanism of PGM-free catalysts can be coupled during fuel cell working, then the degradation rate for PGM-free catalysts would be tested by using the precise "stressors" to enable ASTs progress, as previously employed in the case of PGM electrocatalysts. Different conditions for each degradation mechanism are needed to be devised. The development of efficient non-precious metal catalysts is dependent on the degradation mitigation and improved understanding of the degradation mechanism. The most important aspect for practical application of this technology is "catalytic poisoning", hence; more studies are required to develop some protocols to assess the poisoning mechanism. Further, it is required to improve the anti-poisoning ability of current state-of-art catalysts. The so-called probing agents for the identification of active sites are the major source of catalytic poisoning in the real application.

Acknowledgements

This work was financially supported by the National Natural Science Foundation of China (21972111). This publication was supported by RUDN University Strategic Academic Leadership Program (R.L.). This publication has been supported by RUDN University Strategic Academic Leadership Program (R. Luque). R. Luque gratefully acknowledges funding for Open Access charges to Universidad de Córdoba/CBUA.

Conflict of Interest

The authors declare no conflict of interest.

Keywords

catalytic poisoning, durability, electrocatalysts, fuel cells, metal organic frameworks (MOFs), oxygen reduction reaction (ORR), single-atom active sites (SACs)

Received: October 15, 2021
Revised: December 31, 2021
Published online: March 25, 2022

[1] M. S. Dresselhaus, I. L. Thomas, *Nature* **2001**, *414*, 332.
[2] B. C. Steele, A. Heinzel, *Nature* **2001**, *414*, 345.
[3] S. Zaman, L. Huang, A. I. Douka, H. Yang, B. You, B. Y. Xia, *Angew. Chem., Int. Ed.* **2021**, *60*, 17832.
[4] M. S. Javed, N. Shaheen, A. Idrees, C. Hu, R. Raza, *Int. J. Hydrogen Energy* **2017**, *42*, 10416.
[5] M. S. Javed, R. Raza, Z. Ahsan, M. S. Rafique, S. Shahzadi, S. F. Shaukat, N. Shaheen, M. S. Khalid, H. Chengou, B. Zhu, *Int. J. Hydrogen Energy* **2016**, *41*, 3072.
[6] S. S. A. Shah, T. Najam, M. S. Javed, M. S. Bashir, M. A. Nazir, N. A. Khan, A. u. Rehman, M. A. Subhan, M. M. Rahman, *Chem. Rec.* **2022**, https://doi.org/10.1002/tcr.202100280.
[7] K. Wang, H. X. Chen, X. F. Zhang, Y. X. Tong, S. Q. Song, P. Tsiakaras, Y. Wang, *Appl. Catal., B* **2020**, *264*, 118468.
[8] R. F. Wu, P. Tsiakaras, P. K. Shen, *Appl. Catal., B* **2019**, *251*, 49.
[9] L. Du, V. Prabhakaran, X. Xie, S. Park, Y. Wang, Y. Shao, *Adv. Mater.* **2021**, *33*, 1908232.
[10] Z. Xia, S. Wang, L. Jiang, H. Sun, S. Liu, X. Fu, B. Zhang, D. Sheng Su, J. Wang, G. Sun, *Sci. Rep.* **2015**, *5*, 16100.
[11] H. A. Gasteiger, S. S. Kocha, B. Sompalli, F. T. Wagner, *Appl. Catal., B* **2005**, *56*, 9.
[12] A. Navaee, A. Salimi, S. Soltanian, P. Servati, *J. Power Sources* **2015**, *277*, 268.
[13] Q. Wang, S. Chen, F. Shi, K. Chen, Y. Nie, Y. Wang, R. Wu, J. Li, Y. Zhang, W. Ding, Y. Li, L. Li, Z. Wei, *Adv. Mater.* **2016**, *28*, 10673.
[14] T. Najam, S. S. A. Shah, S. Ibraheem, X. Cai, E. Hussain, S. Suleman, M. S. Javed, P. Tsiakaras, *Energy Storage Mater.* **2022**, *45*, 504.
[15] C. Chen, Y. Kang, Z. Huo, Z. Zhu, W. Huang, H. L. Xin, J. D. Snyder, D. Li, J. A. Herron, M. Mavrikakis, M. Chi, K. L. More, Y. Li, N. M. Markovic, G. A. Somorjai, P. Yang, V. R. Stamenkovic, *Science* **2014**, *343*, 1339.
[16] M. Li, Z. Zhao, T. Cheng, A. Fortunelli, C. Y. Chen, R. Yu, Q. Zhang, L. Gu, B. V. Merinov, Z. Lin, E. Zhu, T. Yu, Q. Jia, J. Guo, L. Zhang, W. A. Goddard3rd , Y. Huang, X. Duan, *Science* **2016**, *354*, 1414.
[17] J. Lu, L. Luo, S. Yin, S. W. Hasan, P. Tsiakaras, *ACS Sustainable Chem. Eng.* **2019**, *7*, 16209.
[18] L. Luo, H. S. Abbo, S. J. J. Titinchi, P. Tsiakaras, S. B. Yin, *Int. J. Hydrogen Energy* **2019**, *44*, 6582.
[19] L. Tang, B. Han, K. Persson, C. Friesen, T. He, K. Sieradzki, G. Ceder, *J. Am. Chem. Soc.* **2010**, *132*, 596.
[20] B. H. Han, C. E. Carlton, A. Kongkanand, R. S. Kukreja, B. R. Theobald, L. Gan, R. O'Malley, P. Strasser, F. T. Wagner, Y. Shao-Horn, *Energy Environ. Sci.* **2015**, *8*, 258.
[21] A. Kumar, Y. Zhang, W. Liu, X. M. Sun, *Coord. Chem. Rev.* **2020**, *402*, 213047.
[22] F. Xiao, G. L. Xu, C. J. Sun, M. J. Xu, W. Wen, Q. Wang, M. Gu, S. Q. Zhu, Y. Y. Li, Z. D. Wei, X. Q. Pan, J. A. Wang, K. Amine, M. H. Shao, *Nano Energy* **2019**, *61*, 60.
[23] T. Najam, S. S. A. Shah, W. Ding, Z. D. Wei, *J. Phys. Chem. C* **2019**, *123*, 16796.
[24] T. Najam, S. S. A. Shah, W. Ding, J. H. Deng, Z. D. Wei, *J. Power Sources* **2019**, *438*, 226919.
[25] S. S. A. Shah, T. Najam, C. Cheng, L. Peng, R. Xiang, L. Zhang, J. Deng, W. Ding, Z. Wei, *Chemistry* **2018**, *24*, 10630.
[26] S. S. Ahmad Shah, T. Najam, C. Cheng, S. Chen, R. Xiang, L. Peng, L. Lu, W. Ding, Z. Wei, *Electrochim. Acta* **2018**, *272*, 169.
[27] T. Najam, S. S. A. Shah, W. Ding, J. Jiang, L. Jia, W. Yao, L. Li, Z. Wei, *Angew. Chem., Int. Ed.* **2018**, *57*, 15101.
[28] S. S. A. Shah, L. S. Peng, T. Najam, C. Cheng, G. P. Wu, Y. Nie, W. Ding, X. Q. Qi, S. G. Chen, Z. D. Wei, *Electrochim. Acta* **2017**, *251*, 498.
[29] Z. Meng, S. Cai, R. Wang, H. Tang, S. Song, P. Tsiakaras, *Appl. Catal., B* **2019**, *244*, 120.
[30] S. S. A. Shah, T. Najam, M. K. Aslam, M. Ashfaq, M. M. Rahman, K. Wang, P. Tsiakaras, S. Q. Song, Y. Wang, *Appl. Catal., B* **2020**, *268*, 118570.
[31] T. Najam, M. Wang, M. S. Javed, S. Ibraheem, Z. Song, M. M. Ahmed, A. U. Rehman, X. Cai, S. S. A. Shah, *J. Colloid Interface Sci.* **2020**, *578*, 89.
[32] T. Najam, X. K. Cai, M. K. Aslam, M. K. Tufail, S. S. A. Shah, *Int. J. Hydrogen Energy* **2020**, *45*, 12903.
[33] T. Najam, S. S. A. Shah, W. Ding, Z. Ling, L. Li, Z. D. Wei, *Electrochim. Acta* **2019**, *327*, 134939.
[34] S. S. A. Shah, T. Najam, M. S. Bashir, L. Peng, M. A. Nazir, M. S. Javed, *Energy Storage Mater.* **2022**, *45*, 301.
[35] T. Najam, S. S. A. Shah, L. Peng, M. S. Javed, M. Imran, M.-Q. Zhao, P. Tsiakaras, *Coord. Chem. Rev.* **2022**, *454*, 214339.

[36] M. Yi, Y. Hua, K. Wang, Y. Wang, S. Song, P. Tsiakaras, *Electrochim. Acta* **2018**, *260*, 264.
[37] L. Jiao, H.-L. Jiang, *Chem* **2019**, *5*, 786.
[38] E. Luo, H. Zhang, X. Wang, L. Gao, L. Gong, T. Zhao, Z. Jin, J. Ge, Z. Jiang, C. Liu, W. Xing, *Angew. Chem., Int. Ed.* **2019**, *58*, 12469.
[39] F. Luo, A. Roy, L. Silvioli, D. A. Cullen, A. Zitolo, M. T. Sougrati, I. C. Oguz, T. Mineva, D. Teschner, S. Wagner, J. Wen, F. Dionigi, U. I. Kramm, J. Rossmeisl, F. Jaouen, P. Strasser, *Nat. Mater.* **2020**, *19*, 1215.
[40] S. C. Cai, Z. H. Meng, H. L. Tang, Y. Wang, P. Tsiakaras, *Appl. Catal., B* **2017**, *217*, 477.
[41] Y. Q. Hua, T. T. Jiang, K. Wang, M. M. Wu, S. Q. Song, Y. Wang, P. Tsiakaras, *Appl. Catal., B* **2016**, *194*, 202.
[42] D. Banham, T. Kishimoto, Y. Zhou, T. Sato, K. Bai, J. I. Ozaki, Y. Imashiro, S. Ye, *Sci. Adv.* **2018**, *4*, eaar7180.
[43] E. Proietti, F. Jaouen, M. Lefevre, N. Larouche, J. Tian, J. Herranz, J. P. Dodelet, *Nat. Commun.* **2011**, *2*, 416.
[44] F. Xiao, Y. C. Wang, Z. P. Wu, G. Chen, F. Yang, S. Zhu, K. Siddharth, Z. Kong, A. Lu, J. C. Li, C. J. Zhong, Z. Y. Zhou, M. Shao, *Adv. Mater.* **2021**, *33*, 2006292.
[45] M. Shao, Q. Chang, J.-P. Dodelet, R. Chenitz, *Chem. Rev.* **2016**, *116*, 3594.
[46] M. Lefevre, E. Proietti, F. Jaouen, J. P. Dodelet, *Science* **2009**, *324*, 71.
[47] H. T. Chung, D. A. Cullen, D. Higgins, B. T. Sneed, E. F. Holby, K. L. More, P. Zelenay, *Science* **2017**, *357*, 479.
[48] S. Liu, Z. Li, C. Wang, W. Tao, M. Huang, M. Zuo, Y. Yang, K. Yang, L. Zhang, S. Chen, P. Xu, Q. Chen, *Nat. Commun.* **2020**, *11*, 938.
[49] Z. Li, W. Wang, M. Zhou, B. He, W. Ren, L. Chen, W. Xu, Z. Hou, Y. Chen, *J. Energy Chem.* **2021**, *54*, 310.
[50] J. Masa, W. Xia, M. Muhler, W. Schuhmann, *Angew. Chem., Int. Ed.* **2015**, *54*, 10102.
[51] S. Shahgaldi, J. Hamelin, *Carbon* **2015**, *94*, 705.
[52] D. Higgins, P. Zamani, A. P. Yu, Z. W. Chen, *Energy Environ. Sci.* **2016**, *9*, 357.
[53] K. Yuan, D. Lutzenkirchen-Hecht, L. Li, L. Shuai, Y. Li, R. Cao, M. Qiu, X. Zhuang, M. K. H. Leung, Y. Chen, U. Scherf, *J. Am. Chem. Soc.* **2020**, *142*, 2404.
[54] L. Du, L. X. Xing, G. X. Zhang, S. H. Sun, *Carbon* **2020**, *156*, 77.
[55] U. Martinez, S. Komini Babu, E. F. Holby, H. T. Chung, X. Yin, P. Zelenay, *Adv. Mater.* **2019**, *31*, 1806545.
[56] Z. L. Wang, D. Xu, J. J. Xu, X. B. Zhang, *Chem. Soc. Rev.* **2014**, *43*, 7746.
[57] M. Shen, C. Wei, K. Ai, L. Lu, *Nano Res.* **2017**, *10*, 1449.
[58] Q. Jia, N. Ramaswamy, H. Hafiz, U. Tylus, K. Strickland, G. Wu, B. Barbiellini, A. Bansil, E. F. Holby, P. Zelenay, S. Mukerjee, *ACS Nano* **2015**, *9*, 12496.
[59] J. H. Zagal, M. T. Koper, *Angew. Chem., Int. Ed.* **2016**, *55*, 14510.
[60] S. Kattel, P. Atanassov, B. Kiefer, *Phys. Chem. Chem. Phys.* **2013**, *15*, 148.
[61] S. Kattel, P. Atanassov, B. Kiefer, *J. Phys. Chem. C* **2012**, *116*, 8161.
[62] F. Calle-Vallejo, J. I. Martínez, J. Rossmeisl, *Phys. Chem. Chem. Phys.* **2011**, *13*, 15639.
[63] H. Tributsch, U. I. Koslowski, I. Dorbandt, *Electrochim. Acta* **2008**, *53*, 2198.
[64] K. X. Liu, S. Kattel, V. Mao, G. F. Wang, *J. Phys. Chem. C* **2016**, *120*, 1586.
[65] S. Kattel, G. Wang, *J. Mater. Chem. A* **2013**, *1*, 10790.
[66] K. Liu, S. Kattel, V. Mao, G. Wang, *J. Phys. Chem. C* **2016**, *120*, 1586.
[67] Y. Wu, C. Li, W. Liu, H. Li, Y. Gong, L. Niu, X. Liu, C. Sun, S. Xu, *Nanoscale* **2019**, *11*, 5064.
[68] C. Deng, R. He, W. Shen, M. Li, T. Zhang, *Phys. Chem. Chem. Phys.* **2019**, *21*, 6900.
[69] S. Kattel, G. Wang, *J. Phys. Chem. Lett.* **2014**, *5*, 452.
[70] Z. S. Lu, G. L. Xu, C. Z. He, T. X. Wang, L. Yang, Z. X. Yang, D. W. Ma, *Carbon* **2015**, *84*, 500.
[71] H. L. Fei, J. C. Dong, Y. X. Feng, C. S. Allen, C. Z. Wan, B. Volosskiy, M. F. Li, Z. P. Zhao, Y. L. Wang, H. T. Sun, P. F. An, W. X. Chen, Z. Y. Guo, C. Lee, D. L. Chen, I. Shakir, M. J. Liu, T. D. Hu, Y. D. Li, A. I. Kirkland, X. F. Duan, Y. Huang, *Nat. Catal.* **2018**, *1*, 63.
[72] A. Zitolo, V. Goellner, V. Armel, M. T. Sougrati, T. Mineva, L. Stievano, E. Fonda, F. Jaouen, *Nat. Mater.* **2015**, *14*, 937.
[73] H. Fei, J. Dong, M. J. Arellano-Jimenez, G. Ye, N. D. Kim, E. L. Samuel, Z. Peng, Z. Zhu, F. Qin, J. Bao, M. J. Yacaman, P. M. Ajayan, D. Chen, J. M. Tour, *Nat. Commun.* **2015**, *6*, 8668.
[74] A. G. Saputro, H. Kasai, *Phys. Chem. Chem. Phys.* **2015**, *17*, 3059.
[75] S. Kattel, P. Atanassov, B. Kiefer, *Phys. Chem. Chem. Phys.* **2014**, *16*, 13800.
[76] R. Venegas, F. J. Recio, C. Zuniga, M. Viera, M. P. Oyarzun, N. Silva, K. Neira, J. F. Marco, J. H. Zagal, F. Tasca, *Phys. Chem. Chem. Phys.* **2017**, *19*, 20441.
[77] X. X. Sun, K. Li, C. Yin, Y. Wang, M. G. Jiao, F. He, X. W. Bai, H. Tang, Z. J. Wu, *Carbon* **2016**, *108*, 541.
[78] G. Zhang, Y. Jia, C. Zhang, X. Xiong, K. Sun, R. Chen, W. Chen, Y. Kuang, L. Zheng, H. Tang, W. Liu, J. Liu, X. Sun, W.-F. Lin, H. Dai, *Energy Environ. Sci.* **2019**, *12*, 1317.
[79] C. Lin, X. P. Li, S. S. Shinde, D. H. Kim, X. K. Song, H. J. Zhang, J. H. Lee, *ACS Appl. Energy Mater.* **2019**, *2*, 1747.
[80] Y. Li, H. Wang, C. Priest, S. Li, P. Xu, G. Wu, *Adv. Mater.* **2021**, *33*, 2000381.
[81] X. N. Li, C. S. Cao, S. F. Hung, Y. R. Lu, W. Z. Cai, A. I. Rykov, S. Miao, S. B. Xi, H. B. Yang, Z. H. Hu, J. H. Wang, J. Y. Zhao, E. E. Alp, W. Xu, T. S. Chan, H. M. Chen, Q. H. Xiong, H. Xiao, Y. Q. Huang, J. Li, T. Zhang, B. Liu, *Chem* **2020**, *6*, 3440.
[82] A. N. Marianov, Y. J. Jiang, *ACS Sustainable Chem. Eng.* **2019**, *7*, 3838.
[83] K. X. Liu, Z. Qiao, S. Hwang, Z. Y. Liu, H. G. Zhang, D. Su, H. Xu, G. Wu, G. F. Wang, *Appl. Catal., B* **2019**, *243*, 195.
[84] U. Martinez, E. F. Holby, S. K. Babu, K. Artyushkova, L. Lin, S. Choudhury, G. M. Purdy, P. Zelenay, *J. Electrochem. Soc.* **2019**, *166*, F3136.
[85] W. Orellana, *Chem. Phys. Lett.* **2012**, *541*, 81.
[86] K. Naito, H. Iezaki, T. Yasui, K. Takada, *J. Electrochem. Soc.* **2018**, *165*, H455.
[87] A. A. Gewirth, J. A. Varnell, A. M. DiAscro, *Chem. Rev.* **2018**, *118*, 2313.
[88] Q. Deng, J. Zhao, T. Wu, G. Chen, H. A. Hansen, T. Vegge, *J. Catal.* **2019**, *370*, 378.
[89] E. F. Holby, C. D. Taylor, *Appl. Phys. Lett.* **2012**, *101*, 064102.
[90] Y. Li, W. Zhou, H. Wang, L. Xie, Y. Liang, F. Wei, J. C. Idrobo, S. J. Pennycook, H. Dai, *Nat. Nanotechnol.* **2012**, *7*, 394.
[91] M. J. Workman, A. Serov, L.-k. Tsui, P. Atanassov, K. Artyushkova, *ACS Energy Lett.* **2017**, *2*, 1489.
[92] L. F. Zhai, S. Y. Kong, H. Y. Zhang, W. J. Tian, M. Sun, H. Q. Sun, S. B. Wang, *Chem. Eng. Sci.* **2019**, *194*, 45.
[93] J. Li, S. Ghoshal, W. Liang, M.-T. Sougrati, F. Jaouen, B. Halevi, S. McKinney, G. McCool, C. Ma, X. Yuan, Z.-F. Ma, S. Mukerjee, Q. Jia, *Energy Environ. Sci.* **2016**, *9*, 2418.
[94] Q. Jia, N. Ramaswamy, U. Tylus, K. Strickland, J. Li, A. Serov, K. Artyushkova, P. Atanassov, J. Anibal, C. Gumeci, S. C. Barton, M.-T. Sougrati, F. Jaouen, B. Halevi, S. Mukerjee, *Nano Energy* **2016**, *29*, 65.
[95] M. A. Montes-Moran, D. Suarez, J. A. Menendez, E. Fuente, *Carbon* **2004**, *42*, 1219.
[96] N. Ramaswamy, U. Tylus, Q. Jia, S. Mukerjee, *J. Am. Chem. Soc.* **2013**, *135*, 15443.
[97] Y. He, Q. Shi, W. Shan, X. Li, A. J. Kropf, E. C. Wegener, J. Wright, S. Karakalos, D. Su, D. A. Cullen, G. Wang, D. J. Myers, G. Wu, *Angew. Chem., Int. Ed.* **2021**, *60*, 9516.
[98] U. Tylus, Q. Jia, K. Strickland, N. Ramaswamy, A. Serov, P. Atanassov, S. Mukerjee, *J. Phys. Chem. C* **2014**, *118*, 8999.

[99] A. Zitolo, N. Ranjbar-Sahraie, T. Mineva, J. Li, Q. Jia, S. Stamatin, G. F. Harrington, S. M. Lyth, P. Krtil, S. Mukerjee, E. Fonda, F. Jaouen, *Nat. Commun.* **2017**, *8*, 957.
[100] J. Li, A. Alsudairi, Z.-F. Ma, S. Mukerjee, Q. Jia, *J. Am. Chem. Soc.* **2017**, *139*, 1384.
[101] L. Osmieri, A. H. A. Monteverde Videla, P. Ocón, S. Specchia, *J. Phys. Chem. C* **2017**, *121*, 17796.
[102] S. Kozuch, J. M. L. Martin, *ACS Catal.* **2012**, *2*, 2787.
[103] C. Cui, L. Gan, M. Heggen, S. Rudi, P. Strasser, *Nat. Mater.* **2013**, *12*, 765.
[104] J. Mahmood, F. Li, S. M. Jung, M. S. Okyay, I. Ahmad, S. J. Kim, N. Park, H. Y. Jeong, J. B. Baek, *Nat. Nanotechnol.* **2017**, *12*, 441.
[105] D. Malko, A. Kucernak, T. Lopes, *Nat. Commun.* **2016**, *7*, 13285.
[106] U. I. Kramm, I. Herrmann-Geppert, J. Behrends, K. Lips, S. Fiechter, P. Bogdanoff, *J. Am. Chem. Soc.* **2016**, *138*, 635.
[107] M. H. Shao, J. H. Odell, S. I. Choi, Y. N. Xia, *Electrochem. Commun.* **2013**, *31*, 46.
[108] D. F. van der Vliet, C. Wang, D. Li, A. P. Paulikas, J. Greeley, R. B. Rankin, D. Strmcnik, D. Tripkovic, N. M. Markovic, V. R. Stamenkovic, *Angew. Chem., Int. Ed.* **2012**, *51*, 3139.
[109] Q. Zhang, K. Mamtani, D. Jain, U. Ozkan, A. Asthagiri, *J. Phys. Chem. C* **2016**, *120*, 15173.
[110] L. Birry, J. H. Zagal, J.-P. Dodelet, *Electrochem. Commun.* **2010**, *12*, 628.
[111] N. R. Sahraie, U. I. Kramm, J. Steinberg, Y. Zhang, A. Thomas, T. Reier, J. P. Paraknowitsch, P. Strasser, *Nat. Commun.* **2015**, *6*, 8618.
[112] N. D. Leonard, S. Wagner, F. Luo, J. Steinberg, W. Ju, N. Weidler, H. Wang, U. I. Kramm, P. Strasser, *ACS Catal.* **2018**, *8*, 1640.
[113] S. T. Thompson, A. R. Wilson, P. Zelenay, D. J. Myers, K. L. More, K. C. Neyerlin, D. Papageorgopoulos, *Solid State Ionics* **2018**, *319*, 68.
[114] J. L. Kneebone, S. L. Daifuku, J. A. Kehl, G. Wu, H. T. Chung, M. Y. Hu, E. E. Alp, K. L. More, P. Zelenay, E. F. Holby, M. L. Neidig, *J. Phys. Chem. C* **2017**, *121*, 16283.
[115] U. I. Kramm, J. Herranz, N. Larouche, T. M. Arruda, M. Lefèvre, F. Jaouen, P. Bogdanoff, S. Fiechter, I. Abs-Wurmbach, S. Mukerjee, J.-P. Dodelet, *Phys. Chem. Chem. Phys.* **2012**, *14*, 11673.
[116] U. I. Kramm, M. Lefèvre, N. Larouche, D. Schmeisser, J.-P. Dodelet, *J. Am. Chem. Soc.* **2014**, *136*, 978.
[117] M. S. Thorum, J. M. Hankett, A. A. Gewirth, *J. Phys. Chem. Lett.* **2011**, *2*, 295.
[118] G. Bae, H. Kim, H. Choi, P. Jeong, D. H. Kim, H. C. Kwon, K. S. Lee, M. Choi, H. S. Oh, F. Jaouen, C. H. Choi, *JACS Au* **2021**, *1*, 586.
[119] G. X. Zhang, X. H. Yang, M. Dubois, M. Herraiz, R. Chenitz, M. Lefevre, M. Cherif, F. Vidal, V. P. Glibin, S. H. Sun, J. P. Dodelet, *Energy Environ. Sci.* **2019**, *12*, 3015.
[120] M. L. Xiao, H. Zhang, Y. T. Chen, J. B. Zhu, L. Q. Gao, Z. Jin, J. J. Ge, Z. Jiang, S. L. Chen, C. P. Liu, W. Xing, *Nano Energy* **2018**, *46*, 396.
[121] Z. Duan, G. Wang, *Phys. Chem. Chem. Phys.* **2011**, *13*, 20178.
[122] J. K. Nørskov, J. Rossmeisl, A. Logadottir, L. Lindqvist, J. R. Kitchin, T. Bligaard, H. Jónsson, *J. Phys. Chem. B* **2004**, *108*, 17886.
[123] U. Tylus, Q. Jia, K. Strickland, N. Ramaswamy, A. Serov, P. Atanassov, S. Mukerjee, *J. Phys. Chem. C* **2014**, *118*, 8999.
[124] M. Xiao, J. Zhu, L. Ma, Z. Jin, J. Ge, X. Deng, Y. Hou, Q. He, J. Li, Q. Jia, S. Mukerjee, R. Yang, Z. Jiang, D. Su, C. Liu, W. Xing, *ACS Catal.* **2018**, *8*, 2824.
[125] Y. Wang, Y. J. Tang, K. Zhou, *J. Am. Chem. Soc.* **2019**, *141*, 14115.
[126] E. F. Holby, G. Wu, P. Zelenay, C. D. Taylor, *J. Phys. Chem. C* **2014**, *118*, 14388.
[127] S. H. Noh, D. H. Kwak, M. H. Seo, T. Ohsaka, B. Han, *Electrochim. Acta* **2014**, *140*, 225.
[128] L. Y. Chen, X. F. Liu, L. R. Zheng, Y. C. Li, X. Guo, X. Wan, Q. T. Liu, J. X. Shang, J. L. Shui, *Appl. Catal., B* **2019**, *256*, 117849.
[129] S. Bruller, H. W. Liang, U. I. Kramm, J. W. Krumpfer, X. L. Feng, K. Mullen, *J. Mater. Chem. A* **2015**, *3*, 23799.
[130] X. L. Zhang, Z. S. Lu, Z. X. Yang, *Int. J. Hydrogen Energy* **2016**, *41*, 21212.
[131] A. Kulkarni, S. Siahrostami, A. Patel, J. K. Nørskov, *Chem. Rev.* **2018**, *118*, 2302.
[132] X. Wang, A. Vasileff, Y. Jiao, Y. Zheng, S. Z. Qiao, *Adv. Mater.* **2019**, *31*, 1803625.
[133] Y. Q. Wang, Y. Q. Zou, L. Tao, Y. Y. Wang, G. Huang, S. Q. Du, S. Wang, *Nano Res.* **2019**, *12*, 2055.
[134] L. Zhang, J. Niu, L. Dai, Z. Xia, *Langmuir* **2012**, *28*, 7542.
[135] Y. Zheng, Y. Jiao, S. Z. Qiao, *Adv. Mater.* **2015**, *27*, 5372.
[136] Y. Wang, H. Yuan, Y. F. Li, Z. F. Chen, *Nanoscale* **2015**, *7*, 11633.
[137] M. H. Seo, D. Higgins, G. P. Jiang, S. M. Choi, B. Han, Z. W. Chen, *J. Mater. Chem. A* **2014**, *2*, 19707.
[138] L. Liu, A. Corma, *Chem. Rev.* **2018**, *118*, 4981.
[139] P. Yin, T. Yao, Y. Wu, L. Zheng, Y. Lin, W. Liu, H. Ju, J. Zhu, X. Hong, Z. Deng, G. Zhou, S. Wei, Y. Li, *Angew. Chem., Int. Ed.* **2016**, *55*, 10800.
[140] S. L. Zhao, J. Yang, M. Han, X. M. Wang, Y. Lin, R. Yang, D. D. Xu, N. E. Shi, Q. Wang, M. J. Yang, Z. H. Dai, J. C. Bao, *Appl. Catal., B* **2020**, *260*, 118207.
[141] M. F. Qiao, Y. Wang, L. Li, G. Z. Hu, G. A. Zou, X. Mamat, Y. M. Dong, X. Hu, *Rare Met.* **2020**, *39*, 824.
[142] H. J. Shen, E. Gracia-Espino, J. Y. Ma, H. D. Tang, X. Mamat, T. Wagberg, G. Z. Hu, S. J. Guo, *Nano Energy* **2017**, *35*, 9.
[143] C. Zhu, Q. Shi, B. Z. Xu, S. Fu, G. Wan, C. Yang, S. Yao, J. Song, H. Zhou, D. Du, S. P. Beckman, D. Su, Y. Lin, *Adv. Energy Mater.* **2018**, *8*, 1801956.
[144] H. Xu, D. Cheng, D. Cao, X. C. Zeng, *Nat. Catal.* **2018**, *1*, 339.
[145] A. Titov, P. Zapol, P. Kral, D. J. Liu, H. Iddir, K. Baishya, L. A. Curtiss, *J. Phys. Chem. C* **2009**, *113*, 21629.
[146] K. X. Liu, G. Wu, G. F. Wang, *J. Phys. Chem. C* **2017**, *121*, 11319.
[147] S. Yasuda, A. Furuya, Y. Uchibori, J. Kim, K. Murakoshi, *Adv. Funct. Mater.* **2016**, *26*, 738.
[148] Z. Miao, X. Wang, M. C. Tsai, Q. Jin, J. Liang, F. Ma, T. Wang, S. Zheng, B. J. Hwang, Y. Huang, S. Guo, Q. Li, *Adv. Energy Mater.* **2018**, *8*, 1801226.
[149] P. Song, Y. Wang, J. Pan, W. L. Xu, L. Zhuang, *J. Power Sources* **2015**, *300*, 279.
[150] F. Jaouen, S. Marcotte, J. P. Dodelet, G. Lindbergh, *J. Phys. Chem. B* **2003**, *107*, 1376.
[151] M. Lefèvre, J. P. Dodelet, P. Bertrand, *J. Phys. Chem. B* **2002**, *106*, 8705.
[152] Z. Lu, B. Wang, Y. Hu, W. Liu, Y. Zhao, R. Yang, Z. Li, J. Luo, B. Chi, Z. Jiang, M. Li, S. Mu, S. Liao, J. Zhang, X. Sun, *Angew. Chem., Int. Ed.* **2019**, *58*, 2622.
[153] D. Zhang, W. Chen, Z. Li, Y. Chen, L. Zheng, Y. Gong, Q. Li, R. Shen, Y. Han, W. C. Cheong, L. Gu, Y. Li, *Chem. Commun.* **2018**, *54*, 4274.
[154] Z. H. Li, H. Y. He, H. B. Cao, S. M. Sun, W. L. Diao, D. L. Gao, P. L. Lu, S. S. Zhang, Z. Guo, M. J. Li, R. J. Liu, D. H. Ren, C. M. Liu, Y. Zhang, Z. Yang, J. K. Jiang, G. J. Zhang, *Appl. Catal., B* **2019**, *240*, 112.
[155] J. Wang, Z. Huang, W. Liu, C. Chang, H. Tang, Z. Li, W. Chen, C. Jia, T. Yao, S. Wei, Y. Wu, Y. Li, *J. Am. Chem. Soc.* **2017**, *139*, 17281.
[156] P. Chen, T. Zhou, L. Xing, K. Xu, Y. Tong, H. Xie, L. Zhang, W. Yan, W. Chu, C. Wu, Y. Xie, *Angew. Chem., Int. Ed.* **2017**, *56*, 610.
[157] J. Sun, Y. H. Fang, Z. P. Liu, *Phys. Chem. Chem. Phys.* **2014**, *16*, 13733.
[158] R. Venegas, F. J. Recio, J. Riquelme, K. Neira, J. F. Marco, I. Ponce, J. H. Zagal, F. Tasca, *J. Mater. Chem. A* **2017**, *5*, 12054.

[159] J. Riquelme, K. Neira, J. F. Marco, P. Hermosilla-Ibanez, W. Orellana, J. H. Zagal, F. Tasca, *Electrochim. Acta* **2018**, *265*, 547.
[160] J. Chlistunoff, J. M. Sansinena, *J. Phys. Chem. C* **2014**, *118*, 19139.
[161] Y. Lin, P. Liu, E. Velasco, G. Yao, Z. Tian, L. Zhang, L. Chen, *Adv. Mater.* **2019**, *31*, 1808193.
[162] D. X. Liu, B. Wang, H. G. Li, S. F. Huang, M. M. Liu, J. Wang, Q. J. Wang, J. J. Zhang, Y. F. Zhao, *Nano Energy* **2019**, *58*, 277.
[163] D.-H. Kwak, S.-B. Han, Y.-W. Lee, H.-S. Park, I.-A. Choi, K.-B. Ma, M.-C. Kim, S.-J. Kim, D.-H. Kim, J.-I. Sohn, K.-W. Park, *Appl. Catal., B* **2017**, *203*, 889.
[164] Q. Lai, L. Zheng, Y. Liang, J. He, J. Zhao, J. Chen, *ACS Catal.* **2017**, *7*, 1655.
[165] Q. Wang, Z. Y. Zhou, Y. J. Lai, Y. You, J. G. Liu, X. L. Wu, E. Terefe, C. Chen, L. Song, M. Rauf, N. Tian, S. G. Sun, *J. Am. Chem. Soc.* **2014**, *136*, 10882.
[166] A. Muthukrishnan, Y. Nabae, T. Okajima, T. Ohsaka, *ACS Catal.* **2015**, *5*, 5194.
[167] J. C. Li, P. X. Hou, S. Y. Zhao, C. Liu, D. M. Tang, M. Cheng, F. Zhang, H. M. Cheng, *Energy Environ. Sci.* **2016**, *9*, 3079.
[168] H. W. Liang, W. Wei, Z. S. Wu, X. Feng, K. Mullen, *J. Am. Chem. Soc.* **2013**, *135*, 16002.
[169] A. Kong, B. Dong, X. Zhu, Y. Kong, J. Zhang, Y. Shan, *Chemistry* **2013**, *19*, 16170.
[170] Y. J. Sa, D. J. Seo, J. Woo, J. T. Lim, J. Y. Cheon, S. Y. Yang, J. M. Lee, D. Kang, T. J. Shin, H. S. Shin, H. Y. Jeong, C. S. Kim, M. G. Kim, T. Y. Kim, S. H. Joo, *J. Am. Chem. Soc.* **2016**, *138*, 15046.
[171] X. F. Zhu, X. Tan, K. H. Wu, C. L. Chiang, Y. C. Lin, Y. G. Lin, D. W. Wang, S. Smith, X. Y. Lu, R. Amal, *J. Mater. Chem. A* **2019**, *7*, 14732.
[172] X. Wan, R. Wu, J. Deng, Y. Nie, S. Chen, W. Ding, X. Huang, Z. Wei, *J. Mater. Chem. A* **2018**, *6*, 3386.
[173] L. Yang, D. Cheng, H. Xu, X. Zeng, X. Wan, J. Shui, Z. Xiang, D. Cao, *Proc. Natl. Acad. Sci. USA* **2018**, *115*, 6626.
[174] F. Jaouen, J. Herranz, M. Lefevre, J. P. Dodelet, U. I. Kramm, I. Herrmann, P. Bogdanoff, J. Maruyama, T. Nagaoka, A. Garsuch, J. R. Dahn, T. Olson, S. Pylypenko, P. Atanassov, E. A. Ustinov, *ACS Appl. Mater. Interfaces* **2009**, *1*, 1623.
[175] J. Kim, J. Lee, Y. Choi, C. Jo, *Carbon* **2014**, *75*, 95.
[176] C. H. Choi, C. Baldizzone, J.-P. Grote, A. K. Schuppert, F. Jaouen, K. J. J. Mayrhofer, *Angew. Chem., Int. Ed.* **2015**, *54*, 12753.
[177] W. Ding, L. Li, K. Xiong, Y. Wang, W. Li, Y. Nie, S. Chen, X. Qi, Z. Wei, *J. Am. Chem. Soc.* **2015**, *137*, 5414.
[178] W. Wang, W. H. Chen, P. Y. Miao, J. Luo, Z. D. Wei, S. L. Chen, *ACS Catal.* **2017**, *7*, 6144.
[179] J. Li, S. G. Chen, W. Li, R. Wu, S. Ibraheem, J. Li, W. Ding, L. Li, Z. D. Wei, *J. Mater. Chem. A* **2018**, *6*, 15504.
[180] A. Serov, K. Artyushkova, P. Atanassov, *Adv. Energy Mater.* **2014**, *4*, 1301735.
[181] Y. Nie, Z. Wei, *ChemCatChem* **2019**, *11*, 5885.
[182] X. G. Fu, F. M. Hassan, P. Zamani, G. P. Jiang, D. C. Higgins, J. Y. Choi, X. L. Wang, P. Xu, Y. R. Liu, Z. W. Chen, *Nano Energy* **2017**, *42*, 249.
[183] J. H. Shu, Q. J. Niu, N. N. Wang, J. Nie, G. P. Ma, *Appl. Surf. Sci.* **2019**, *485*, 520.
[184] X. H. Yang, Y. C. Wang, G. X. Zhang, L. Du, L. J. Yang, M. Markiewicz, J. Y. Choi, R. Chenitz, S. H. Sun, *Appl. Catal., B* **2020**, *264*, 118523.
[185] R. Wu, Y. J. Song, X. Huang, S. G. Chen, S. Ibraheem, J. H. Deng, J. Li, X. Q. Qi, Z. D. Wei, *J. Power Sources* **2018**, *401*, 287.
[186] R. Wu, X. Wan, J. Deng, X. Huang, S. Chen, W. Ding, L. Li, Q. Liao, Z. Wei, *Chem. Commun.* **2019**, *55*, 9023.
[187] W. Li, W. Ding, J. X. Jiang, Q. He, S. C. Tao, W. L. Wang, J. Li, Z. D. Wei, *J. Mater. Chem. A* **2018**, *6*, 878.
[188] H. F. Wang, L. Chen, H. Pang, S. Kaskel, Q. Xu, *Chem. Soc. Rev.* **2020**, *49*, 1414.
[189] R. Zhao, Z. Liang, S. Gao, C. Yang, B. Zhu, J. Zhao, C. Qu, R. Zou, Q. Xu, *Angew. Chem., Int. Ed.* **2019**, *58*, 1975.
[190] X. Zhang, J. Han, J. Guo, Z. Tang, *Small Struct.* **2021**, *2*, 2000141.
[191] W. Cao, Y. Tang, Y. Cui, G. Qian, *Small Struct.* **2020**, *1*, 2000019.
[192] L. Yang, X. Zeng, W. Wang, D. Cao, *Adv. Funct. Mater.* **2018**, *28*, 1704537.
[193] S. S. A. Shah, T. Najam, M. K. Aslam, M. Ashfaq, M. M. Rahman, K. Wang, P. Tsiakaras, S. Song, Y. Wang, *Appl. Catal., B* **2019**, *268*, 118570.
[194] J. D. Xiao, H. L. Jiang, *Acc. Chem. Res.* **2019**, *52*, 356.
[195] M. Ding, R. W. Flaig, H. L. Jiang, O. M. Yaghi, *Chem. Soc. Rev.* **2019**, *48*, 2783.
[196] L. Jiao, Y. Wang, H. L. Jiang, Q. Xu, *Adv. Mater.* **2018**, *30*, 1703663.
[197] Y.-Z. Chen, R. Zhang, L. Jiao, H.-L. Jiang, *Coord. Chem. Rev.* **2018**, *362*, 1.
[198] S. S. A. Shah, T. Najam, M. S. Javed, M. M. Rahman, P. Tsiakaras, *ACS Appl. Mater. Interfaces* **2021**, *13*, 23191.
[199] L. Jiao, J. Wang, H.-L. Jiang, *Acc. Mater. Res.* **2021**, *2*, 327.
[200] L. Jiao, R. Zhang, G. Wan, W. Yang, X. Wan, H. Zhou, J. Shui, S. H. Yu, H. L. Jiang, *Nat. Commun.* **2020**, *11*, 2831.
[201] M. Ding, X. Cai, H. L. Jiang, *Chem. Sci.* **2019**, *10*, 10209.
[202] L. Li, J. He, Y. Wang, X. Lv, X. Gu, P. Dai, D. Liu, X. Zhao, *J. Mater. Chem. A* **2019**, *7*, 1964.
[203] Q. Ren, H. Wang, X. F. Lu, Y. X. Tong, G. R. Li, *Adv. Sci.* **2018**, *5*, 1700515.
[204] H. Yang, R. Shi, L. Shang, T. Zhang, *Small Struct.* **2021**, *2*, 2100007.
[205] J. Yang, W. Li, D. Wang, Y. Li, *Small Struct.* **2020**, *2*, 2000051.
[206] H. Zhang, S. Hwang, M. Wang, Z. Feng, S. Karakalos, L. Luo, Z. Qiao, X. Xie, C. Wang, D. Su, Y. Shao, G. Wu, *J. Am. Chem. Soc.* **2017**, *139*, 14143.
[207] Y. Chen, S. Ji, Y. Wang, J. Dong, W. Chen, Z. Li, R. Shen, L. Zheng, Z. Zhuang, D. Wang, Y. Li, *Angew. Chem., Int. Ed.* **2017**, *56*, 6937.
[208] Y. H. He, S. Hwang, D. A. Cullen, M. A. Uddin, L. Langhorst, B. Y. Li, S. Karakalos, A. J. Kropf, E. C. Wegener, J. Sokolowski, M. J. Chen, D. Myers, D. Su, K. L. More, G. F. Wang, S. Litster, G. Wu, *Energy Environ. Sci.* **2019**, *12*, 250.
[209] L. Jiao, G. Wan, R. Zhang, H. Zhou, S. H. Yu, H. L. Jiang, *Angew. Chem., Int. Ed.* **2018**, *57*, 8525.
[210] Y. Ye, H. Li, F. Cai, C. Yan, R. Si, S. Miao, Y. Li, G. Wang, X. Bao, *ACS Catal.* **2017**, *7*, 7638.
[211] M. M. Wu, K. Wang, M. Yi, Y. X. Tong, Y. Wang, S. Q. Song, *ACS Catal.* **2017**, *7*, 6082.
[212] Y. Z. Chen, C. Wang, Z. Y. Wu, Y. Xiong, Q. Xu, S. H. Yu, H. L. Jiang, *Adv. Mater.* **2015**, *27*, 5010.
[213] C. Yan, H. Li, Y. Ye, H. Wu, F. Cai, R. Si, J. Xiao, S. Miao, S. Xie, F. Yang, Y. Li, G. Wang, X. Bao, *Energy Environ. Sci.* **2018**, *11*, 1204.
[214] X. X. Wang, D. A. Cullen, Y. T. Pan, S. Hwang, M. Wang, Z. Feng, J. Wang, M. H. Engelhard, H. Zhang, Y. He, Y. Shao, D. Su, K. L. More, J. S. Spendelow, G. Wu, *Adv. Mater.* **2018**, *30*, 1706758.
[215] L. Shang, H. Yu, X. Huang, T. Bian, R. Shi, Y. Zhao, G. I. Waterhouse, L. Z. Wu, C. H. Tung, T. Zhang, *Adv. Mater.* **2016**, *28*, 1668.
[216] B. You, N. Jiang, M. Sheng, W. S. Drisdell, J. Yano, Y. Sun, *ACS Catal.* **2015**, *5*, 7068.
[217] X. Wu, G. Meng, W. X. Liu, T. Li, Q. Yang, X. M. Sun, J. F. Liu, *Nano Res.* **2018**, *11*, 163.
[218] J. Z. Li, M. J. Chen, D. A. Cullen, S. Hwang, M. Y. Wang, B. Y. Li, K. X. Liu, S. Karakalos, M. Lucero, H. G. Zhang, C. Lei, H. Xu, G. E. Sterbinsky, Z. X. Feng, D. Su, K. L. More, G. F. Wang, Z. B. Wang, G. Wu, *Nat. Catal.* **2018**, *1*, 935.
[219] Z. Geng, Y. Liu, X. Kong, P. Li, K. Li, Z. Liu, J. Du, M. Shu, R. Si, J. Zeng, *Adv. Mater.* **2018**, *30*, 1803498.
[220] Q. Yang, C. C. Yang, C. H. Lin, H. L. Jiang, *Angew. Chem., Int. Ed.* **2019**, *58*, 3511.

[221] Y. Zhang, L. Jiao, W. Yang, C. Xie, H. L. Jiang, *Angew. Chem., Int. Ed.* **2021**, *60*, 7607.
[222] Y. T. Qu, Z. J. Li, W. X. Chen, Y. Lin, T. W. Yuan, Z. K. Yang, C. M. Zhao, J. Wang, C. Zhao, X. Wang, F. Y. Zhou, Z. B. Zhuang, Y. Wu, Y. D. Li, *Nat. Catal.* **2018**, *1*, 781.
[223] A. Namslauer, P. Brzezinski, *FEBS Lett.* **2004**, *567*, 103.
[224] V. R. Kaila, M. I. Verkhovsky, M. Wikstrom, *Chem. Rev.* **2010**, *110*, 7062.
[225] F. Li, G. F. Han, H. J. Noh, S. J. Kim, Y. L. Lu, H. Y. Jeong, Z. P. Fu, J. B. Baek, *Energy Environ. Sci.* **2018**, *11*, 2263.
[226] H. Wu, H. Li, X. Zhao, Q. Liu, J. Wang, J. Xiao, S. Xie, R. Si, F. Yang, S. Miao, X. Guo, G. Wang, X. Bao, *Energy Environ. Sci.* **2016**, *9*, 3736.
[227] G. K. Han, Y. Zheng, X. Zhang, Z. Q. Wang, Y. Gong, C. Y. Du, M. N. Banis, Y. M. Yiu, T. K. Sham, L. Gu, Y. R. Sun, Y. J. Wang, J. P. Wang, Y. Z. Gao, G. P. Yin, X. L. Sun, *Nano Energy* **2019**, *66*, 104088.
[228] L. T. Cui, L. R. Cui, Z. J. Li, J. Zhang, H. N. Wang, S. F. Lu, Y. Xiang, *J. Mater. Chem. A* **2019**, *7*, 16690.
[229] H. Tao, C. Choi, L.-X. Ding, Z. Jiang, Z. Han, M. Jia, Q. Fan, Y. Gao, H. Wang, A. W. Robertson, S. Hong, Y. Jung, S. Liu, Z. Sun, *Chem* **2019**, *5*, 204.
[230] W. Chen, J. Pei, C.-T. He, J. Wan, H. Ren, Y. Wang, J. Dong, K. Wu, W.-C. Cheong, J. Mao, X. Zheng, W. Yan, Z. Zhuang, C. Chen, Q. Peng, D. Wang, Y. Li, *Adv. Mater.* **2018**, *30*, 1800396.
[231] M. Xiao, Y. Chen, J. Zhu, H. Zhang, X. Zhao, L. Gao, X. Wang, J. Zhao, J. Ge, Z. Jiang, S. Chen, C. Liu, W. Xing, *J. Am. Chem. Soc.* **2019**, *141*, 17763.
[232] J. Jiao, R. Lin, S. Liu, W.-C. Cheong, C. Zhang, Z. Chen, Y. Pan, J. Tang, K. Wu, S.-F. Hung, H. M. Chen, L. Zheng, Q. Lu, X. Yang, B. Xu, H. Xiao, J. Li, D. Wang, Q. Peng, C. Chen, Y. Li, *Nat. Chem.* **2019**, *11*, 222.
[233] D.-D. Ma, Q.-L. Zhu, *Coord. Chem. Rev.* **2020**, *422*, 213483.
[234] H. Yang, X. Chen, W.-T. Chen, Q. Wang, N. C. Cuello, A. Nafady, A. M. Al-Enizi, G. I. N. Waterhouse, G. A. Goenaga, T. A. Zawodzinski, P. E. Kruger, J. E. Clements, J. Zhang, H. Tian, S. G. Telfer, S. Ma, *ACS Nano* **2019**, *13*, 8087.
[235] J. Wang, W. Liu, G. Luo, Z. Li, C. Zhao, H. Zhang, M. Zhu, Q. Xu, X. Wang, C. Zhao, Y. Qu, Z. Yang, T. Yao, Y. Li, Y. Lin, Y. Wu, Y. Li, *Energy Environ. Sci.* **2018**, *11*, 3375.
[236] Y. Zhou, W. Yang, W. Utetiwabo, Y.-m. Lian, X. Yin, L. Zhou, P. Yu, R. Chen, S. Sun, *J. Phys. Chem. Lett.* **2020**, *11*, 1404.
[237] X. Fang, L. Jiao, S.-H. Yu, H.-L. Jiang, *ChemSusChem* **2017**, *10*, 3019.
[238] H. J. Lee, W. Cho, M. Oh, *Chem. Commun.* **2012**, *48*, 221.
[239] Y. Shan, L. Chen, H. Pang, Q. Xu, *Small Struct.* **2020**, *2*, 2000078.
[240] Y. He, S. Yang, Y. Fu, F. Wang, J. Ma, G. Wang, G. Chen, M. Wang, R. Dong, P. Zhang, X. Feng, *Small Struct.* **2020**, *2*, 2000095.
[241] P. Wu, Y. Shen, H. Li, W. Shi, L. Zhang, T. Pan, W. Pei, W. Zhang, F. Huo, *Small Struct.* **2021**, *2*, 2000119.
[242] X. Han, X. Ling, D. Yu, D. Xie, L. Li, S. Peng, C. Zhong, N. Zhao, Y. Deng, W. Hu, *Adv. Mater.* **2019**, *31*, 1905622.
[243] Y. Chen, S. Ji, S. Zhao, W. Chen, J. Dong, W. C. Cheong, R. Shen, X. Wen, L. Zheng, A. I. Rykov, S. Cai, H. Tang, Z. Zhuang, C. Chen, Q. Peng, D. Wang, Y. Li, *Nat. Commun.* **2018**, *9*, 5422.
[244] B. K. Hong, P. Mandal, J. G. Oh, S. Litster, *J. Power Sources* **2016**, *328*, 280.
[245] Q. Liu, X. Liu, L. Zheng, J. Shui, *Angew. Chem., Int. Ed.* **2018**, *57*, 1204.
[246] J. S. Spendelow, D. C. Papageorgopoulos, *Fuel Cells* **2011**, *11*, 775.
[247] D. H. Kwak, S. B. Han, Y. W. Lee, H. S. Park, I. A. Choi, K. B. Ma, M. C. Kim, S. J. Kim, D. H. Kim, J. I. Sohn, K. W. Park, *Appl. Catal., B* **2017**, *203*, 889.
[248] Z. Yang, Y. Wang, M. Zhu, Z. Li, W. Chen, W. Wei, T. Yuan, Y. Qu, Q. Xu, C. Zhao, X. Wang, P. Li, Y. Li, Y. Wu, Y. Li, *ACS Catal.* **2019**, *9*, 2158.
[249] W. X. Xia, C. D. A. , P. Yung-Tin, H. Sooyeon, W. Maoyu, F. Zhenxing, W. Jingyun, E. M. H. , Z. Hanguang, H. Yanghua, S. Yuyan, S. Dong, M. K. L. , S. J. S. , W. Gang, *Adv. Mater.* **2018**, *30*, 1706758.
[250] J. Li, M. Chen, D. A. Cullen, S. Hwang, M. Wang, B. Li, K. Liu, S. Karakalos, M. Lucero, H. Zhang, C. Lei, H. Xu, G. E. Sterbinsky, Z. Feng, D. Su, K. L. More, G. Wang, Z. Wang, G. Wu, *Nat. Catal.* **2018**, *1*, 935.
[251] J. Zang, F. Wang, Q. Cheng, G. Wang, L. Ma, C. Chen, L. Yang, Z. Zou, D. Xie, H. Yang, *J. Mater. Chem. A* **2020**, *8*, 3686.
[252] R. Hu, Y. Li, Q. Zeng, J. Shang, *Appl. Surf. Sci.* **2020**, *525*, 146588.
[253] Y. C. Wang, Y. J. Lai, L. Song, Z. Y. Zhou, J. G. Liu, Q. Wang, X. D. Yang, C. Chen, W. Shi, Y. P. Zheng, M. Rauf, S. G. Sun, *Angew. Chem., Int. Ed.* **2015**, *54*, 9907.
[254] Y. Deng, B. Chi, X. Tian, Z. Cui, E. Liu, Q. Jia, W. Fan, G. Wang, D. Dang, M. Li, K. Zang, J. Luo, Y. Hu, S. Liao, X. Sun, S. Mukerjee, *J. Mater. Chem. A* **2019**, *7*, 5020.
[255] Y. Cheng, S. He, S. Lu, J.-P. Veder, B. Johannessen, L. Thomsen, M. Saunders, T. Becker, R. De Marco, Q. Li, S.-z. Yang, S. P. Jiang, *Adv. Sci.* **2019**, *6*, 1802066.
[256] H. Zhang, H. T. Chung, D. A. Cullen, S. Wagner, U. I. Kramm, K. L. More, P. Zelenay, G. Wu, *Energy Environ. Sci.* **2019**, *12*, 2548.
[257] T. Al-Zoubi, Y. Zhou, X. Yin, B. Janicek, C. Sun, C. E. Schulz, X. Zhang, A. A. Gewirth, P. Huang, P. Zelenay, H. Yang, *J. Am. Chem. Soc.* **2020**, *142*, 5477.
[258] M. Qiao, Y. Wang, Q. Wang, G. Hu, X. Mamat, S. Zhang, S. Wang, *Angew. Chem., Int. Ed.* **2020**, *59*, 2688.
[259] X. Wan, X. Liu, Y. Li, R. Yu, L. Zheng, W. Yan, H. Wang, M. Xu, J. Shui, *Nat. Catal.* **2019**, *2*, 259.
[260] Y. He, S. Hwang, D. A. Cullen, M. A. Uddin, L. Langhorst, B. Li, S. Karakalos, A. J. Kropf, E. C. Wegener, J. Sokolowski, M. Chen, D. Myers, D. Su, K. L. More, G. Wang, S. Litster, G. Wu, *Energy Environ. Sci.* **2019**, *12*, 250.
[261] Q. Cheng, S. Han, K. Mao, C. Chen, L. Yang, Z. Zou, M. Gu, Z. Hu, H. Yang, *Nano Energy* **2018**, *52*, 485.
[262] J.-C. Li, S. Maurya, Y. S. Kim, T. Li, L. Wang, Q. Shi, D. Liu, S. Feng, Y. Lin, M. Shao, *ACS Catal.* **2020**, *10*, 2452.
[263] Z. W. Chen, D. Higgins, A. P. Yu, L. Zhang, J. J. Zhang, *Energy Environ. Sci.* **2011**, *4*, 3167.
[264] D. Xia, C. Yu, Y. Zhao, Y. Wei, H. Wu, Y. Kang, J. Li, L. Gan, F. Kang, *Chem. Sci.* **2021**, *12*, 11576.
[265] X. Wan, X. Liu, J. Shui, *Prog. Nat. Sci.: Mater. Int.* **2020**, *30*, 721.
[266] J. Liu, X. Wan, S. Liu, X. Liu, L. Zheng, R. Yu, J. Shui, *Adv. Mater.* **2021**, *33*, 2103600.
[267] X. Zeng, J. Shui, X. Liu, Q. Liu, Y. Li, J. Shang, L. Zheng, R. Yu, *Adv. Energy Mater.* **2018**, *8*, 1701345.
[268] S. Gupta, D. Tryk, I. Bae, W. Aldred, E. Yeager, *J. Appl. Electrochem.* **1989**, *19*, 19.
[269] F. Charreteur, S. Ruggeri, F. Jaouen, J. P. Dodelet, *Electrochim. Acta* **2008**, *53*, 6881.
[270] C. Zhang, W. Zhang, W. Zheng, *ChemCatChem* **2019**, *11*, 655.
[271] R. Wu, S. G. Chen, Y. L. Zhang, Y. Wang, Y. Nie, W. Ding, X. Q. Qi, Z. D. Wei, *J. Mater. Chem. A* **2016**, *4*, 2433.
[272] Y. Nie, L. Li, Z. Wei, *Chem. Soc. Rev.* **2015**, *44*, 2168.
[273] C. H. Choi, W. S. Choi, O. Kasian, A. K. Mechler, M. T. Sougrati, S. Bruller, K. Strickland, Q. Jia, S. Mukerjee, K. J. J. Mayrhofer, F. Jaouen, *Angew. Chem., Int. Ed.* **2017**, *56*, 8809.
[274] F. Jaouen, M. Lefevre, J. P. Dodelet, M. Cai, *J. Phys. Chem. B* **2006**, *110*, 5553.
[275] H.-W. Liang, W. Wei, Z.-S. Wu, X. Feng, K. Müllen, *J. Am. Chem. Soc.* **2013**, *135*, 16002.
[276] A. Serov, M. J. Workman, K. Artyushkova, P. Atanassov, G. McCool, S. McKinney, H. Romero, B. Halevi, T. Stephenson, *J. Power Sources* **2016**, *327*, 557.

[277] A. Serov, A. D. Shum, X. H. Xiao, V. De Andrade, K. Artyushkova, I. V. Zenyuk, P. Atanassov, *Appl. Catal., B* **2018**, *237*, 1139.
[278] V. Armel, S. Hindocha, F. Salles, S. Bennett, D. Jones, F. Jaouen, *J. Am. Chem. Soc.* **2017**, *139*, 453.
[279] X. Fu, P. Zamani, J. Y. Choi, F. M. Hassan, G. Jiang, D. C. Higgins, Y. Zhang, M. A. Hoque, Z. Chen, *Adv. Mater.* **2017**, *29*, 1604456.
[280] J.-Y. Choi, L. Yang, T. Kishimoto, X. Fu, S. Ye, Z. Chen, D. Banham, *Energy Environ. Sci.* **2017**, *10*, 296.
[281] G. Zhang, R. Chenitz, M. Lefèvre, S. Sun, J.-P. Dodelet, *Nano Energy* **2016**, *29*, 111.
[282] G. Wu, K. L. More, C. M. Johnston, P. Zelenay, *Science* **2011**, *332*, 443.
[283] M. Lefevre, J. P. Dodelet, *Electrochim. Acta* **2003**, *48*, 2749.
[284] U. Martinez, S. K. Babu, E. F. Holby, P. Zelenay, *Curr. Opin. Electrochem.* **2018**, *9*, 224.
[285] V. Goellner, V. Armel, A. Zitolo, E. Fonda, F. Jaouen, *J. Electrochem. Soc.* **2015**, *162*, H403.
[286] B. Wang, *J. Power Sources* **2005**, *152*, 1.
[287] R. Chenitz, U. I. Kramm, M. Lefèvre, V. Glibin, G. Zhang, S. Sun, J.-P. Dodelet, *Energy Environ. Sci.* **2018**, *11*, 365.
[288] C. H. Choi, C. Baldizzone, G. Polymeros, E. Pizzutilo, O. Kasian, A. K. Schuppert, N. R. Sahraie, M. T. Sougrati, K. J. J. Mayrhofer, F. Jaouen, *ACS Catal.* **2016**, *6*, 3136.
[289] J. Herranz, F. Jaouen, M. Lefevre, U. I. Kramm, E. Proietti, J. P. Dodelet, P. Bogdanoff, S. Fiechter, I. Abs-Wurmbach, P. Bertrand, T. M. Arruda, S. Mukerjee, *J. Phys. Chem. C* **2011**, *115*, 16087.
[290] M. Ferrandon, X. Wang, A. J. Kropf, D. J. Myers, G. Wu, C. M. Johnston, P. Zelenay, *Electrochim. Acta* **2013**, *110*, 282.
[291] G. Faubert, G. Lalande, R. Cote, D. Guay, J. P. Dodelet, L. T. Weng, P. Bertrand, G. Denes, *Electrochim. Acta* **1996**, *41*, 1689.
[292] G. Lalande, R. Cote, G. Tamizhmani, D. Guay, J. P. Dodelet, L. Dignardbailey, L. T. Weng, P. Bertrand, *Electrochim. Acta* **1995**, *40*, 2635.
[293] H. Schulenburg, S. Stankov, V. Schünemann, J. Radnik, I. Dorbandt, S. Fiechter, P. Bogdanoff, H. Tributsch, *J. Phys. Chem. B* **2003**, *107*, 9034.
[294] C. H. Choi, C. Baldizzone, J. P. Grote, A. K. Schuppert, F. Jaouen, K. J. Mayrhofer, *Angew. Chem., Int. Ed.* **2015**, *54*, 12753.
[295] C. Zuniga, C. Candia-Onfray, R. Venegas, K. Munoz, J. Urra, M. Sanchez-Arenillas, J. F. Marco, J. H. Zagal, F. J. Recio, *Electrochem. Commun.* **2019**, *102*, 78.
[296] J. Li, M. T. Sougrati, A. Zitolo, J. M. Ablett, I. C. Oğuz, T. Mineva, I. Matanovic, P. Atanassov, Y. Huang, I. Zenyuk, A. Di Cicco, K. Kumar, L. Dubau, F. Maillard, G. Dražić, F. Jaouen, *Nat. Catal.* **2020**, *4*, 10.
[297] S. Maass, F. Finsterwalder, G. Frank, R. Hartmann, C. Merten, *J. Power Sources* **2008**, *176*, 444.
[298] Y. M. Yi, G. Weinberg, M. Prenzel, M. Greiner, S. Heumann, S. Becker, R. Schlogl, *Catal. Today* **2017**, *295*, 32.
[299] S. S. Zhang, X. Z. Yuan, J. N. C. Hin, H. J. Wang, K. A. Friedrich, M. Schulze, *J. Power Sources* **2009**, *194*, 588.
[300] K. Kumar, L. Dubau, M. Mermoux, J. Li, A. Zitolo, J. Nelayah, F. Jaouen, F. Maillard, *Angew. Chem., Int. Ed.* **2020**, *59*, 3235.
[301] R. T. White, A. Wu, M. Najm, F. P. Orfino, M. Dutta, E. Kjeang, *J. Power Sources* **2017**, *350*, 94.
[302] B. T. Sneed, D. A. Cullen, K. S. Reeves, O. E. Dyck, D. A. Langlois, R. Mukundan, R. L. Borup, K. L. More, *ACS Appl. Mater. Interfaces* **2017**, *9*, 29839.
[303] S. Stariha, K. Artyushkova, M. J. Workman, A. Serov, S. Mckinney, B. Halevi, P. Atanassov, *J. Power Sources* **2016**, *326*, 43.
[304] S. Komini Babu, H. T. Chung, P. Zelenay, S. Litster, *ACS Appl. Mater. Interfaces* **2016**, *8*, 32764.
[305] K. Artyushkova, M. J. Workman, I. Matanovic, M. J. Dzara, C. Ngo, S. Pylypenko, A. Serov, P. Atanassov, *ACS Appl. Energy Mater.* **2017**, *1*, 68.
[306] X. Xie, C. He, B. Li, Y. He, D. A. Cullen, E. C. Wegener, A. J. Kropf, U. Martinez, Y. Cheng, M. H. Engelhard, M. E. Bowden, M. Song, T. Lemmon, X. S. Li, Z. Nie, J. Liu, D. J. Myers, P. Zelenay, G. Wang, G. Wu, V. Ramani, Y. Shao, *Nat. Catal.* **2020**, *3*, 1044.
[307] T. Mineva, I. Matanovic, P. Atanassov, M.-T. Sougrati, L. Stievano, M. Clémancey, A. Kochem, J.-M. Latour, F. Jaouen, *ACS Catal.* **2019**, *9*, 9359.
[308] V. Goellner, C. Baldizzone, A. Schuppert, M. T. Sougrati, K. Mayrhofer, F. Jaouen, *Phys. Chem. Chem. Phys.* **2014**, *16*, 18454.
[309] Y. Nabae, Q. Yuan, S. Nagata, K. Kusaba, T. Aoki, N. Takao, T. Itoh, M. Arao, H. Imai, K. Higashi, T. Sakata, T. Uruga, Y. Iwasawa, *J. Electrochem. Soc.* **2021**, *168*, 014513.
[310] D. S. Hussey, J. M. LaManna, E. Baltic, D. L. Jacobson, S. Stariha, D. Spernjak, R. Mukundan, R. L. Borup, *ECS Trans.* **2017**, *80*, 385.
[311] E. F. Holby, P. Zelenay, *Nano Energy* **2016**, *29*, 54.
[312] E. F. Holby, *Fuel Cells* **2016**, *16*, 669.
[313] L. Chen, G. Wu, E. F. Holby, P. Zelenay, W. Q. Tao, Q. J. Kang, *Electrochim. Acta* **2015**, *158*, 175.
[314] S. K. Babu, H. T. Chung, P. Zelenay, S. Litster, *J. Electrochem. Soc.* **2017**, *164*, F1037.
[315] D. Malko, T. Lopes, E. Symianakis, A. R. Kucernak, *J. Mater. Chem. A* **2016**, *4*, 142.
[316] T. Reshetenko, A. Serov, K. Artyushkova, I. Matanovic, S. Stariha, P. Atanassov, *J. Power Sources* **2016**, *324*, 556.
[317] Q. Li, G. Wan, H. Zhao, L. Pan, N. Wang, W. Zhao, X. Zhou, X. Cui, H. Chen, *ChemSusChem* **2017**, *10*, 499.
[318] D. Singh, K. Mamtani, C. R. Bruening, J. T. Miller, U. S. Ozkan, *ACS Catal.* **2014**, *4*, 3454.
[319] M. Busch, N. B. Halck, U. I. Kramm, S. Siahrostami, P. Krtil, J. Rossmeisl, *Nano Energy* **2016**, *29*, 126.
[320] Y. Zhai, G. Bender, S. Dorn, R. Rocheleau, *J. Electrochem. Soc.* **2010**, *157*, B20.
[321] J. St-Pierre, Y. F. Zhai, M. Angelo, *Int. J. Hydrogen Energy* **2012**, *37*, 6784.
[322] D. Deng, L. Yu, X. Chen, G. Wang, L. Jin, X. Pan, J. Deng, G. Sun, X. Bao, *Angew. Chem., Int. Ed.* **2013**, *52*, 371.
[323] P. Zhang, X. F. Chen, J. S. Lian, Q. Jiang, *J. Phys. Chem. C* **2012**, *116*, 17572.
[324] Q. Li, G. Wu, D. A. Cullen, K. L. More, N. H. Mack, H. T. Chung, P. Zelenay, *ACS Catal.* **2014**, *4*, 3193.
[325] K. Holst-Olesen, M. Reda, H. A. Hansen, T. Vegge, M. Arenz, *ACS Catal.* **2018**, *8*, 7104.
[326] M. Zhou, Y. Yu, K. Hu, M. V. Mirkin, *J. Am. Chem. Soc.* **2015**, *137*, 6517.
[327] Y. Hu, J. O. Jensen, C. Pan, L. N. Cleemann, I. Shypunov, Q. Li, *Appl. Catal., B* **2018**, *234*, 357.
[328] T. Najam, S. S. A. Shah, H. Ali, Z. Q. Song, H. H. Sun, Z. C. Peng, X. K. Cai, *Carbon* **2020**, *164*, 12.
[329] H. Ali, H. Lin, Q. Lu, X. Wang, *J. Phys. Chem. C* **2021**, *125*, 14646.
[330] Q. Zuo, P. Zhao, W. Luo, G. Cheng, *Nanoscale* **2016**, *8*, 14271.

Syed Shoaib Ahmad Shah received his M.Sc., M.Phil degrees in Chemistry from Islamia University of Bahawalpur (IUB) and Ph.D. (2015–2018) from Chongqing University under the supervision of Prof. Wei Zidong. He worked as assistant professor (August 2018–December 2019) at the Institute of Chemistry, IUB. He has been a CAS-President Postdoc Fellow in Department of Chemistry, University of Science and Technology of China with Prof. Jiang Hai-Long (2019–2021). Currently, he is working as postdoc researcher with Prof Shu-Juan Bao at School of Materials and Energy, Southwest University. He has published more than 85 SCI articles focusing on metal-organic frameworks derived carbon materials for energy conversion and storage devices.

Tayyaba Najam earned her Bachelor (B.S) in Chemistry and M.Phil (Chemistry) from University of Wah and the Islamia University of Bahawalpur (Pakistan) respectively. She received her Ph.D. (2019) from Chongqing University, China, under the supervision of Prof. Wei Zidong. She did her postdoctoral research work (2019-2021) at Institute for Advanced Study, Shenzhen University, China. Currently, she is working as "Associate Researcher" at College of Chemistry and Environmental Engineering, Shenzhen University, China. Her research interests are: i) design and synthesis of nanostructured materials for Fuel cells (ORR), ii) zinc–air battery (ORR and OER), iii) water-splitting (OER and HER), and iv) supercapacitors.

Muhammad Sohail Bashir received B.Sc. (2011) and M.Sc. (2014) degree in Chemical Engineering from University of Gujrat and University of Engineering and Technology of Lahore, Pakistan. After serving as Lecturer (2014–2016) at The University of Faisalabad, Pakistan, he moved to China and received his Ph.D. degree (2020) in Chemical Engineering and Technology from University of Jinan, under the supervision of Prof. Xiang Zheng Kong. Currently, he is serving as postdoctoral fellow in Prof. Chen Changle group at University of Science and Technology of China (USTC). His research interests focus on flow chemistry, polymer synthesis, porous materials, catalysis, and environmental remediation.

Muhammad Sufyan Javed received his B.S. (2012) and M.Sc. (2014) from COMSATS University Islamabad, Lahore Campus and involved in fuel cells research (Prof. Rizwan Raza). He received his Ph.D. (2017) in Condensed Matter Physics under the supervision of Prof. Chenguo Hu. He did his postdoctoral research work at Department of Physics, Jinan University, China; under the supervision of Prof. Wenjie Mai. Currently, he is working as young research professor at School of Physical Science and Technology, Lanzhou University, China. He has published more than 150 peer-reviewed research articles. His research interests include synthesis of porous materials, 2D materials, MXenes for energy conversion and storage devices, especially supercapacitors and multi-ion batteries.

Aziz-ur Rehman is currently working as head of Analytical Chemistry section, in Institute of Chemistry, The Islamia University of Bahawalpur, Pakistan. He did his doctorate degree (Ph.D.) from Department of Chemistry, Quaid Azam University, Islamabad Pakistan and postdoc CAS-president fellowship from Changchun Institute of applied chemistry, China. His research interest is the synthesis, applications of nanoparticles and their composites in various fields like water purification, catalysis, and energy storage. He supervised 9 Ph.D. and 70 M.phil. students so far, and have 75 peer reviewed published articles in well-known international journals.

Rafael Luque (Ph.D. in 2005 from Universidad de Cordoba, Spain) has significant experience in biomass and waste valorization practices to materials, fuels, and chemicals as well as nanoscale chemistry (600+ publications, h-index 89, >34 000 citations, 7 patents, >10 edited books). Prof. Luque is editor-in-chief of Molecular Catalysis and is serving on the advisory/editorial Board of over 10 Q1 RSC, Wiley, ACS, and Elsevier Journals. Prof. Luque was named 2018, 2019, 2020 and recently 2021 highly cited researcher (Clarivate Analytics), being director of the Center for Molecular Design and Synthesis at RUDN University in Moscow, Russia, distinguished chair professor from Xi'an Jiaotong University as well as distinguished scientist from the Department of Chemistry at King Saud University (Saudi Arabia) under the DSFP Program.

Shu-Juan Bao is currently working at the School of Materials and Energy, Southwest University. She received her Ph.D. degree in Physical Chemistry from Lanzhou University in 2006. As postdoctoral, she has worked at Nanyang Technological University for two years and as a visiting scholar at the Texas University at Austin for one year. Her research interests mainly focus on the interface catalytic process of electrochemical reaction and bio-sensing. She has published over 200 SCI academic papers and these published papers have been cited more than 6000 times, with the highest citation for a single paper being 388 times.